Stratigraphy and pyrite geochemistry of the Lower–Upper Ordovician in the Lerhamn and Fågelsång-3 drill cores, Scania, Sweden

Fisnik Balija

Dissertations in geology at Lund University,
Master's thesis, no 530
(45 hp/ECTS credits)

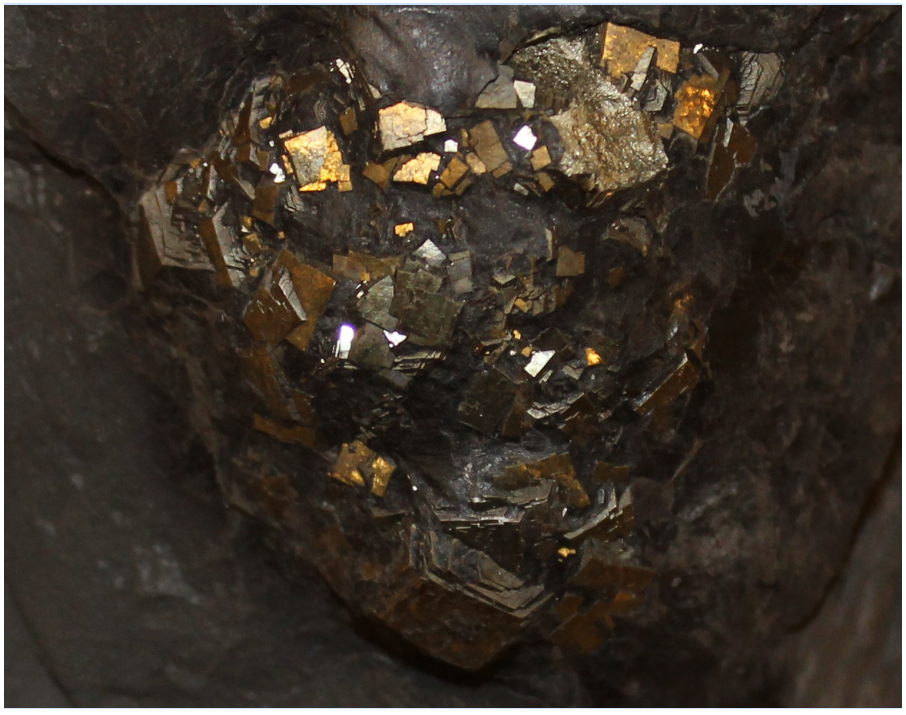

Department of Geology
Lund University
2018

Stratigraphy and pyrite geochemistry of the Lower–Upper Ordovician in the Lerhamn and Fågelsång-3 drill cores, Scania, Sweden

Master's thesis

Fisnik Balija

Department of Geology
Lund University
2018

Contents

Cover Picture: Pyrite with well shaped crystals at a drilling depth of 48.19 m in the Lerhamn drill core. Photo: Joaen Stamsnijder.

Stratigraphy and pyrite geochemistry of the Lower–Upper Ordovician in the Lerhamn and Fågelsång-3 drill cores, Scania, Sweden

FISNIK BALIJA

Balija, F., 2018: Stratigraphy and pyrite geochemistry of the Lower–Upper Ordovician in the Lerhamn and Fågelsång-3 drill cores, Scania, Sweden. *Dissertations in Geology at Lund University*, No. 530, 37 pp. 45 hp (45 ECTS credits).

Abstract: Arsenic is a very toxic element present in rocks, soils, and natural groundwater, and known to cause serious health effects. Neurological damage is known in humans to occur at concentrations as low as 100 μg/L, while 1–3 mg/kg of body weight As is a lethal dose. Exposure to As may lead to e.g. cellular injury and DNA damage, a number of diseases and disorders and several types of cancer. High concentrations of As can be produced in the presence of sulfide minerals, such as pyrite (FeS_2). Diagenetic pyrite is commonly found in shale and formed at high rates during the Ordovician Period, favored by low C/S ratios. In addition to As, pyrite is also known to incorporate heavy metals. A pilot study at Lund University, using XRF-analysis, have shown an As-anomaly with elevated concentrations in an Ordovician shale from a drill core obtained in the Lerhamn area, northwestern Scania, southern Sweden. In this follow-up study a deeper geochemical analysis with focus on pyrite from the Lerhamn drill core is done using LA-ICP-MS, for high precision and accurate results. A second drill core (Fågelsång-3) retrieved from Ordovician shales in the Fågelsång area, south-west Scania, is also investigated for a comparison of the result. In addition to As a number of heavy metals are also of interest. The analytical results confirm high concentrations of As, including some of the heavy metals (V, Cr, Co, Mo, Cd, Sb, W, Hg, Pb), in both drill cores. However, a single significant As-anomaly is only observed in the Lerhamn drill core peaking at around 40 m depth. The average As concentration is approximately 736 ppm in the Lerhamn drill core and 268 ppm in the Fågelsång-3 drill core, with highest values ranging up to 17660 ppm and 2295 ppm, respectively. This study concludes that the relatively high As concentrations in the Lerhamn and Fågelsång shale is of no concern in its present location. However, there is a potential risk for local As-contamination of the environment if shale/pyrite with high As concentrations, in particular from Lerhamn, is exposed to surface conditions. The pyrite would readily oxidize, and As and heavy metals be released.

Keywords: Ordovician, shale, drill cores, arsenic, pyrite, heavy metals, Lerhamn, Fågelsång, Scania, Sweden.

Supervisors: Prof. Leif Johansson & Prof. Per Ahlberg
Co-supervisor: Dr. Tomas Naeraa

Subject: Bedrock Geology

Fisnik Balija, Department of Geology, Lund University, Sölvegatan 12, SE-223 62 Lund, Sweden.
E-mail: fisnik.balija@gmail.com

Stratigrafi och pyritgeokemi i undre–övre ordovicium i Lerhamns- och Fågelsång-3-borrkärnan från Skåne, Sverige

FISNIK BALIJA

Balija, F., 2018: Stratigrafi och pyritgeokemi i undre–övre ordovicium i Lerhamns- och Fågelsång-3-borrkärnan från Skåne, Sverige. *Examensarbeten i geologi vid Lunds universitet*, Nr. 530, 37 sid. 45 hp.

Sammanfattning: Arsenik är ett mycket giftigt ämne som finns i berg, mark och grundvatten, och är känt för att orsaka allvarliga hälsoeffekter. Neurologiska skador hos människan inträffar vid koncentrationer så låga som 100 µg/L, medan 1–3 mg/kg kroppsvikt As är en dödlig dos. Exponering för As kan leda till bland annat cell- och DNA-skador, ett antal sjukdomar och störningar samt olika typer av cancer. Höga As-koncentrationer kan uppstå i närvaro av sulfidmineral, såsom pyrit (FeS_2). Diagenetisk pyrit finns vanligen i skiffer och bildades i stor omfattning under ordovicium, till följd av låga C/S-förhållanden. Förutom As så är pyrit även känt för att innehålla tungmetaller. En pilotstudie vid Lunds universitet visade med hjälp av XRF-analys en As-anomali med förhöjda koncentrationer i en ordovicisk skiffer från Lerhamnsborrningen i nordvästra Skåne. I denna uppföljningsstudie görs en mer detaljerad geokemisk analys med fokus på pyrit från Lerhamnsborrkärnan med hjälp av LA-ICP-MS, för högre precision och noggrannare resultat. En annan borrkärna (Fågelsång-3) med ordoviciska skiffrar från Fågelsångsområdet i sydvästra Skåne, används för en jämförelse av resultat. Förutom As så är även ett antal tungmetaller av intresse. Analyserna bekräftar höga koncentrationer av As och även höga halter av några tungmetaller (V, Cr, Co, Mo, Cd, Sb, W, Hg, Pb) i pyrit i båda borrkärnorna. Dock så observeras en tydlig As-anomali endast i Lerhamnsborrkärnan, med mycket höga halter omkring 40 m djup. Den genomsnittliga As-koncentrationen är ca 736 ppm i Lerhamnsborrkärnan och 268 ppm i Fågelsång-3-borrkärnan, med maximala värden på 17660 ppm respektive 2295 ppm. Det föreligger emellertid inga risker så länge dessa skifferlagerföljder inte utsätts för erosion och vittring. Däremot finns det en potentiell risk för lokal As-förorening av miljön om skiffer/pyrit med höga As-koncentrationer, särskilt från Lerhamn, exploateras och pyriten utsätts för oxidation. Pyriten skulle då brytas ned och As och tungmetaller frigöras.

Nyckelord: Ordovicium, skiffer, borrkärnor, arsenik, pyrit, tungmetaller, Lerhamn, Fågelsång, Skåne, Sverige.

Handledare: Prof. Leif Johansson & Prof. Per Ahlberg
Biträdande handledare: Dr. Tomas Naeraa

Ämnesinriktning: Berggrundsgeologi

Fisnik Balija, Geologiska institutionen, Lunds universitet, Sölvegatan 12, SE-223 62 Lund, Sverige.
E-post: fisnik.balija@gmail.com

1 Introduction

The Ordovician Period (485.4–443.8 Ma) lasted for about 42 million years and was a turning point in Earth history, moving from late Cambrian warm climate to progressively cooler conditions through the Ordovician (Munnecke et al., 2010; Cooper & Sadler, 2012). During this period one of the greatest evolutionary radiations in the history of marine life occurred, known as 'The Great Ordovician Biodiversification Event' or GOBE (Munnecke et al., 2010; Cooper & Sadler, 2012; Servais & Harper, 2018). The massive thrive of marine animals came to an end at the mass extinction associated with a glacial period during the latest Ordovician, causing a major faunal turnover (Munnecke et al., 2010; Cooper & Sadler, 2012).

The tectonic activity was extensive during the Ordovician and characterized by rapid plate movements and high rates of continental seafloor spreading giving rise to tall mid-ocean ridges (Munnecke et al., 2010; Cooper & Sadler, 2012; Holland, 2017). Sea level peaked in the Early and Late Ordovician, with a substantial dip during Middle Ordovician, and estimated to have been approximately 225 m above present day during its maximum (early Katian) (Haq & Schutter, 2008; Holland, 2017). Many cratons were submerged under vast, shallow epicontinental seas formed during sea level high stands (Barnes, 2004; Munnecke et al., 2010; Holland, 2017).

The Ordovician climate was highly affected by widespread volcanic activity releasing high levels of CO_2 to the atmosphere (Munnecke et al., 2010; Holland, 2017). A global rise in atmospheric CO_2, 14–16 times higher than today, resulted in a green-house state during the Early Ordovician to early Katian (Cooper & Sadler, 2012; Holland, 2017). Another potentially more influential gas for the green-house climate was water vapor. The movement of landmasses in combination with warm climatic conditions led to a reduced and more sluggish ocean circulation, with poor upwelling and nutrient supply (Barnes, 2004; Mango & Ryan, 2015; Holland, 2017). Together with low O_2 levels, 50% of today's atmospheric level, this resulted in widespread anoxia in the deep marine environments during Ordovician (Barnes, 2004; Cooper & Sadler, 2012; Mango & Ryan, 2015; Holland, 2017).

Anoxia in the marine environment promotes the formation of siliciclastic rocks such as black shales (Holland, 2017). Black shales were abundant globally, favored by the ocean and climatic conditions, during Ordovician and accumulated predominantly in the deepwater settings of epicontinental seas (Mango & Ryan, 2015; Holland, 2017). The deposition of black, organic-rich sediments were higher during the earliest Ordovician and decreased in later periods as a result of increasing O_2 levels (Nielsen, 2004). Diagenetic minerals like pyrite (FeS_2) is commonly found in shale and formed at high rates during this period (Berner & Raiswell, 1983; Schieber, 2011). Due to low C/S ratios (weight ratio of organic carbon to pyrite S), more pyrite were buried per unit of organic carbon and thus favoring the widespread formation of pyrite during Ordovician times (Berner, 1984). Pyrite is known to incorporate different trace-elements like As and heavy metals such as Mn, Mo, Cd, Hg, Pb etc. However, As in particular may accumulate in high concentrations in pyrite (Berner et al., 2013). Sedimentary rocks formed during O_2-depleted conditions are more likely to contain As-bearing pyrite compared to times with O_2 promoted environments (Mango & Ryan, 2015).

Arsenic is a very toxic element and occurs commonly as arsenite (As(III)) or arsenate (As(V)) (Snow et al., 2003). Exposure to As can cause serious health effects at low concentrations leading to e.g. cellular injury and DNA damage, a number of diseases and disorders and several types of cancer (Hu et al., 2003; Selinus et al., 2010; Mukherjee, 2011; Cullen & Reimer, 2016; Livsmedelsverket, 2017; Persson, 2017). Arsenic poisoning has therefore led to a cause for concern by the World Health Organization (WHO), who regulates the provisional guideline value for As (Selinus et al., 2010).

A pilot study conducted by Professor Leif Johansson at Lund University showed high As concentrations in an Ordovician shale from a drill core obtained in the Lerhamn area in northwestern Scania, southern Sweden (Fig, 1). The analysis was done using a handheld X-ray fluorescence (XRF) analyzer.

This study aims to conduct a deeper geochemical analysis with focus on pyrites from the Lerhamn drill core. In addition to As a number of heavy metals are also of interest. By using the LA-ICP-MS laboratory at Lund University, high precision and accurate results can be obtained. Further, pyrite extracted from a second drill core from Ordovician shales in the Fågelsång area is also investigated for a comparison of the results.

The main objectives of this study are:

- To describe the stratigraphy of two Ordovician drill cores from Lerhamn and Fågelsång.
- To analyze the concentration of As and heavy metals in pyrite in the Lerhamn and Fågelsång-3 drill cores.
- If high concentrations of As are also present in the Fågelsång-3 drill core, is there a correlation between the Ordovician successions in the Lerhamn and Fågelsång-3 drill cores?
- If high-As rocks are exposed for weathering what are then the potential risks and health effects of As?

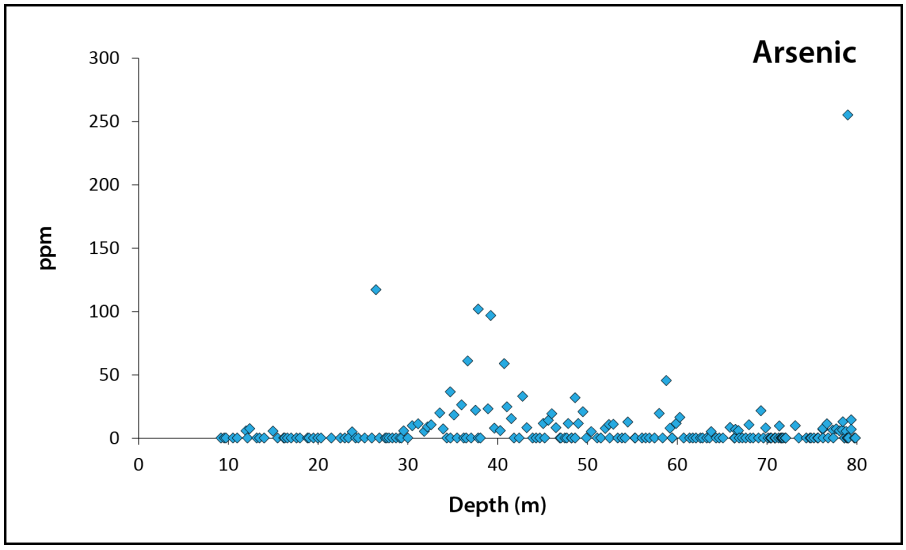

Fig. 1. Diagram showing the arsenic concentration from the XRF-analysis of the shale from the Lerhamn drill core. An As-anomaly with high concentrations can be observed between 30–45 m depth.

2 Shale

Shale is a fine-grained detrital sedimentary rock formed by consolidation of clay and silt (mud). It is characterized by finely laminated structure and dominated by clay minerals and quartz. In sediment starved settings, shales can also consist of (<50%) microbial induced early diagenetic cements, such as calcite ($CaCO_3$), dolomite ($CaMg(CO_3)_2$), ferroan carbonates, silica, iron sulfides and authigenic clays. Terminal electron acceptors (ex. O_2, nitrate, Fe(III), Mn(IV), sulfate, CO_2) are important for the microbial breakdown process of buried organic matter, and decreases downwards from the sediment-water surface. Other common components are organic matter and biogenic debris (Schieber, 2011).

Carbonates are found in many fine-grained sedimentary rocks, including shale. If the amount of carbonate is below 50%, the terms shale and mudstone are used, however, if it exceeds that it is more common to use the terms marl, micrite, limestone and dolostone (Schieber, 2011). Phosphatic concretions ranging from less than a millimeter to more than 100 millimeters may form if enough phosphatic, ex. skeletal, material accumulates, leading to abundance in phosphorous which is necessary in the initial mud (Shen et al., 2000). Pyrite, calcite or dolomite is common diagenetic minerals found in shale (Stow, 2005; Tucker, 2011). During compaction, the early diagenetic minerals are preserved in the shale as a result of rapid and systematic ejection of pore waters and decrease in porosity (Schieber, 2011).

Preservation of organic carbon results in a darker color, becoming very dark grey or black with increasing content of carbon. Shales were formed in a wide range of environments, including river flood-plain, lake, low-energy shoreline, lagoon, delta, outer-marine shelf and deep-ocean basin settings (Stow, 2005; Tucker, 2011).

For simplicity, grey shale has herein been sub-divided after a darkness index (DI) due to color variation. The darkness index ranges from 1–4, where 4 is almost black (cf. Figs. 11, 14).

3 Arsenic

3.1 Properties of arsenic

Arsenic is a chemical element with the atomic number 33 and an atomic mass of 75u. In the periodic table As is found in group 15 (Nitrogen family), and is a metalloid (Wenzel, 2013). A metalloid is neither a metal nor a nonmetal, but share same properties of these in terms of electrical and heat conductivity (Selinus, 2010).

Arsenic is monoisotopic, meaning it has only one stable isotope, where ^{75}As is the only stable and naturally occurring isotope (Henke, 2009; Burford et al., 2011). It has a number of valence states, however, the most common states are –3, 0, +3 and +5 (Henke, 2009). Elemental As occur as three main allotropes; grey As (the rhombohedral β-As, most common), yellow As (consists of As_4, the most toxic and unstable) and the black amorphous form (Burford et al., 2011; Pichon, 2013). The yellow form of As resembles the white phosphorus form, which shares the same properties, and decomposes when exposed to light (Pichon, 2013). Both forms, yellow and black, require high temperature or pressure conditions for stability (Burford et al., 2011).

Arsenic exists in various inorganic and organic forms, these include the elemental forms and its compounds: organoarsenicals, arsenides, arsenosulfides, arsenites and arsenates (Henke, 2009). Furthermore, As atoms form covalent bonds, these strong bonds give solid samples of elemental As physical properties

that tend to be brittle, nonductile and insoluble in water (Henke & Hutchison, 2009).

3.2 Geochemistry of arsenic

In natural waters As occurs mostly as +3 and +5 ions, forming inorganic arsenite (inorganic As(III)) and arsenate (inorganic As(V)) through O_2 bonding in reducing and oxidizing environments, respectively (Henke & Hutchison, 2009). The oxidation state and chemical composition determines the toxicity of As (Del Razo et al., 2003). While both oxidation states of As are toxic, the inorganic and organic form of the trivalent As is more mobile and by far more toxic (Del Razo et al., 2003; Price & Pichler, 2005).

Arsenite is found in groundwaters and hydrothermal waters where O_2 levels are low. It exists as $H_3AsO_3^0$ (arsenous acid), $H_2AsO_3^-$ (dihydrogen arsenite), $HAsO_3^{2-}$ (hydrogen arsenite) and/or AsO_3^{3-} (arsenite) depending on pH, but can also form thioarsenic compounds in sulfide-rich and anoxic waters by substitution of O_2 with S (Fig. 2; Henke & Hutchison, 2009).

Arsenate is generally present where we have O_2-rich conditions and is found in groundwaters as well as in surface waters. It exists, depending on the pH, as $H_3AsO_4^0$ (arsenate acid), $H_2AsO_4^-$ (dihydrogen arsenate), $HAsO_4^{2-}$ (hydrogen arsenate) and/or AsO_4^{3-} (arsenate). Furthermore, arsenate forms the equivalent of thioarsenic, namely thioarsenate, in sulfide-rich and anoxic groundwaters and hydrothermal waters (Fig. 2; Henke & Hutchison, 2009).

In reducing environments reductants oxidize and donate electrons to As, whose valence state during reduction can decrease to as low as –3. Common reductants are hydrogen sulfide (H_2S). Arsenate reduction is rapid, particularly in acidic conditions, in the presence of H_2S, and organic carbon (Henke & Hutchison, 2009). Microorganisms are important during reduction processes, for example arsenate-reducing bacteria such as *Pseudomonas flourescens* and *Anabaena oscillaroides* (Cullen & Reimer, 1989). In natural environments arsenate-reducing bacteria help to reduce arsenate to arsenite, and arsenite to arsine or dimethylarsine ($(CH_3)_2AsH$) (Henke & Hutchison, 2009).

During oxidation the process is reversed, oxidants receive electrons from As. The valence state of As during oxidation can increase to as high as +5 by loss of valence electrons. In oxidizing environments As may oxidize to arsenite and arsenite to arsenate. Oxidants like Fe(III) species, nitrate (NO_3^-) or Mn(III,VI) (oxy)(hydr)oxide compounds, sometimes even in the absence of O_2, significantly increase the oxidation rate of arsenite. In natural waters arsenite oxidizes slowly from air and pure O_2 (Henke & Hutchison, 2009). Other factors such as microorganisms or natural organic matter (NOM) may help to catalyze the process (Redman et al., 2002; Stollenwerk, 2003).

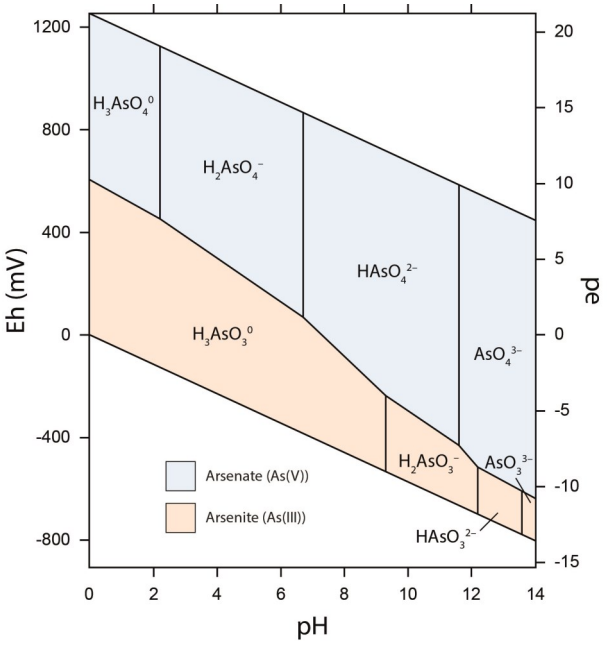

Fig. 2. Eh-pH diagram for arsenite and arsenate (at 25°C and 1 bar pressure). Modified from Smedley & Kinniburgh (2002).

Arsenite is found to be more metastable in aerobic environments whereas arsenate preferentially reduces rapidly in anaerobic environments (Stollenwerk, 2003).

3.3 Mineralogy of arsenic

In the sediments, soils and crustal rocks less than 10 As minerals are common from the over 320 that are known. If we disregard scorodite ($FeAsO_4 \cdot 2H_2O$), then As oxides or As sulfides are the most encountered As minerals (Foster, 2003; Henke & Hutchison, 2009). Arsenic minerals are classified into five groups, as previously mentioned, these are: elemental, arsenides, arsenosulfides, arsenites and arsenates (Henke & Hutchison, 2009). In Table 2.5 in Henke & Hutchison (2009) the authors have listed relatively common As-bearing minerals, to mention a few we have arsenolite (As_2O_3, arsenite), arsenolamprite (As^0, elemental), arsenopyrite (FeAsS, arsenosulfide), niccolite (NiAs, arsenide), orpiment (As_2S_3, arsenosulfide), scorodite etc. Arsenopyrite is the most widely spread, occurring in hydrothermal deposits, intrusive igneous rocks and metamorphic rocks, but can also be a result of microbial precipitates (Welch et al., 2000; Henke & Hutchison, 2009; Cullen & Reimer, 2016).

Arsenic-bearing minerals have a far more complex structure than the formula used to describe them. We have, for instance, substitution between As and elements such as S (partial substitute), Co, Ni and other metals within individual specimen changing its chemical composition. Furthermore, arsenian minerals are one example of specimens of minerals that yield little or no As, but may contain several weight percent (wt %) of As by partially substituting for S, Sb (less

common) and sometimes arsenate for phosphate (PO_4^{3-}) (Henke & Hutchison, 2009). Minerals like galena (PbS), sphalerite ((Zn,Fe)S), chalcopyrite ($CuFeS_2$), marcasite (FeS_2) and pyrite are examples of As-bearing sulfides that may contain As concentrations of 1 wt% or higher. In pyrite the As concentration generally range between 0.02–0.5 wt% (200–5000 mg/kg), but may have concentrations up to 6.5 wt% (65 000 mg/kg) (Welch et al., 2000).

3.4 Geological occurrence of arsenic

Arsenic concentration in soils around the world are estimated between 0.005 and 0.0075% (50–75 mg/kg), with a common range of 0.0001–0.0055% (1–55 mg/kg). Contribution of large As concentrations found at regional or local scale is controlled by two main sources, geogenic anomalies (bedrock) or anthropogenic activities (Wenzel, 2013).

Arsenic in soils originate mainly from weathering of parent materials (bedrock), with higher concentrations found in shales, clays and phosphorites (phosphates) and lower concentrations more often found in sandstones, limestones and igneous rock (Table 1). Ores represents sources where extremely high concentrations of As can accumulate (Wenzel, 2013).

Groundwater is another input source that may add As to soils that are in contact or under irrigation by groundwater. This is often the case where the groundwater aquifer is in contact with sediments naturally rich in As or (mine) waste materials. Global background concentrations of As in groundwater are estimated between 0.5 and 0.9 µg/L. However, geogenic or anthropogenic activities can generate concentrations above 1000 µg/L, one–two thousand times the expected world background estimate (Table 1). Bangladesh and West Bengali, India, are two well-known cases of mass As poisoning related, not only to contaminated tube well waters, but also the accumulation of As in soils through irrigation of fields (ex. paddy soils) (Wenzel, 2013).

In addition to weathering and groundwater, another important source of As in the soil is through atmospheric deposition. Atmospheric deposition of As occurs via dry and wet deposition. Between 50–80% of the total As is present in soluble form, where highest concentrations are related to mining districts, metal smelters and urban areas. Very low concentrations are typical for remote areas (Table 1) (Wenzel, 2013). Volcanoes are responsible for a significant amount of natural As released from the lithosphere into the atmosphere (Signorelli, 1997). It is estimated that approximately $1.7 \cdot 10^4$ t/year is released globally

Table 1: Different source materials with its respective arsenic concentrations. Modified from Wenzel (2013).

Source	Unit	Estimate	Mean	Minimum	Maximum	Reference
Parent materials						
Igneous rocks	mg/kg		1.5–3.0	0.06	113	1
Granites, granodiorites	mg/kg	3				2
Limestone	mg/kg	1.5	1.7	0.1	20	1, 2
Sandstone	mg/kg	0.5–1.0	2	0.6	120	1, 2
Shales, schists	mg/kg	13				2
Shale and clay	mg/kg		14.5	0.3	490	1
Mafic (gabros, basalts)	mg/kg	0.7–1.0				2
Ultramafic	mg/kg	0.7				2
Phosphorite	mg/kg	21				3
Phosphates	mg/kg		22.6	0.4	188	1
Groundwater						
World background estimate	µg/L	0.5–0.9				4
World range estimate	µg/L	0.1–230				4
Atmospheric deposition						
Air						
Remote areas	ng/m^3			0.008	1	1, 5
Urban areas	ng/m^3			<d.l.	0.16	1
Contaminated areas	ng/m^3		15			5
Bulk (total) deposition						
Remote areas	ng/L			0.0009	80	5
Rural areas	ng/L			240	370	5
Urban areas	ng/L			900	12300	5

1. Jenkins (1980)
2. Koljonen (1992)
3. Boyle & Jonsson (1973)
4. Yang et al (2000)
5. Matschullat (2000)

(Matschullat, 2000). The As concentration in volcanic gases is controlled by the properties of the magma and surrounding rocks, as well as volatile element (Signorelli, 1997). Looking at the total bulk deposition, urban environments represents the highest values, with As concentrations up to 12300 ng/L, while remote areas represents the lowest values, down to 0.0009 ng/L (Table 1) (Wenzel, 2013).

3.5 Medical geology aspects on arsenic (Toxicology of arsenic)

Arsenic occurs mainly as arsenite or arsenate, but is also found as several methylated forms, which are less toxic species, for example monomethylarsonic acid (MMA) and dimethylarsinic acid (DMA) (Price & Pichler, 2005; Fendorf et al., 2010). The toxicity of As depends on the oxidation state and chemical composition, where arsenite is more mobile and by far the more toxic of the two (Del Razo et al., 2003; Abernathy et al., 2003; Price & Pichler, 2005; Hughes et al., 2009). Arsenate's toxicity is thought to arise mainly from its in vivo reduction to arsenite (Snow et al., 2003).

In high concentration arsenite is known to be weakly mutagenic in mammalian cells at single gene loci, while bacteria is not susceptible to mutations in the presence of arsenite (Rossman et al., 2003). Because of the toxicity of As, certain higher eukaryotic organisms, such as fungi, and some archaea and aerobic eubacteria have evolved mechanisms to convert arsenate to arsenite. The arsenite is then further methylated to MMA, DMA or trimethylarsine (TMA), which are less toxic species and readily removed from the cell (Fendorf et al., 2010). However, in marine organisms, arsenite causes reduction in growth at concentrations of less than 3 µg/L (Price & Pichler, 2005).

Arsenic and As-containing compounds are known human carcinogens and associated primarily with inorganic arsenite (Liu et al., 2003; Rossman et al., 2003; Wei et al., 2003; Selinus et al., 2010). Exposure can lead to many diverse ailments and is particularly harmful when exposed to early in life (ex. as a fetus or during childhood), some effects may first be expressed decades later (Cullen & Reimer, 2016). These effects involve acute and, of main concern, chronic As poisoning and are a major public health problem around the world (Liu et al., 2003; Rossman et al., 2003; Wei et al., 2003, Cullen & Reimer, 2016).

Exposure to As can lead to a number of health effects, including cardiovascular and peripheral vascular disease, inhibited growth, development anomalies, nervous system disorders, chronic cough, diabetes, hearing loss, portal fibrosis, hematologic disorders and several types of cancer (Mukherjee, 2011; Cullen & Reimer, 2016; Livsmedelsverket, 2017; Persson, 2017). Other health effects caused by As contaminated drinking water include skin diseases (pigmentation, lesions/keratosis and cancer) and incidences of cancer in lung, urinary bladder, liver, kidney, naval cavity and prostate (Abernathy et al., 2003; Rossman et al., 2003; Trouba et al., 2003; Wei et al., 2003; Cullen & Reimer, 2016). It is, however, still unknown how As induces cancer and more work is needed to get a better understanding of the mechanisms behind it (Wei et al., 2003). Aside from health effects, low doses of As may favor other carcinogens such as ultraviolet (UV) radiation and X-rays, by enhancing their mutagenicity and clastogenic effects (Rossman et al., 2003). Ironically, As trioxide (also known as the white oxide or the "assassin poison"; Selinus, 2010), which is an anhydrous form, is an effective and safe chemotherapeutic agent for treating cancer like acute promyelocytic leukemia (APL) (Liu et al., 2003).

Arsenic can enter the body through ingestion, inhalation and dermal contact (Selinus et al., 2010). However, ingestion of As contaminated drinking water is the major source of As exposure to humans and is caused by oxidation of As-bearing minerals which liberate As into the underground water or water aquifers (Tchounwou et al., 2015). Furthermore, its colorless, odorless and tasteless characteristics make it difficult to detect in drinking water (Cullen & Reimer, 2016). Typical symptoms of As poising are "garlic breath", skin sensitivity, depigmentation, dermatitis, keratitis, eyelid edema, gastrointestinal irritation, vomiting, diarrhea, bloody urine, anuria, shock, convulsions and coma (Hughes, 2002; Selinus et al., 2010; Mukherjee, 2011).

Neurological damage is known in humans and occurs at concentrations as low as 100 µg/L, while 1–3 mg/kg of body weight As is a lethal dose (Hughes, 2002; Price & Pichler, 2005). According to Livsmedelsverket (Swedish Food Administration) the maximum (permitted) value for As in drinking water is limited to 10 µg/L (Livsmedelsverket, 2017; Persson, 2017). Health based target value for As intake has been estimated and identified to 0.3 to 8 µg/kg of body weight for an increased risk of cancer of the lung, skin and bladder, but also skin lesions (EFSA, 2014; Livsmedelsverket, 2017).

4 Pyrite

4.1 Properties and structure of pyrite

Pyrite is an iron sulfide. It is mined for the extraction of S which is used, among other things, to produce sulfuric acid, one of the most important industrial chemicals (Rickard, 2015). It is recognized by its bright metallic luster and brass-yellowish color. Further, pyrite is a semiconductor, which means it can conduct electricity, but only partly (Mukherjee, 2011).

Pyrite commonly occurs in cubic or octahedral shape, but may also be found as pentagonal dodecahedrons, also known as pyritohedrons (Deer et al., 1992). In the cubic shape, the Fe atoms occupies the face-centers and corners of the cube, while the S atoms lie

in pairs centered at the cube's body-center and mid-points of the cube's edges (Fig. 3). In an octahedron the S atoms are in six fold coordination surrounding each Fe atom in the corners (Fig. 4; Mason & Berry, 1968; Vaughan & Craig, 1978, Deer et al., 1992). The packing arrangement of the cubic pyrite shape is called a face-centered arrangement, and is one of the densest packing arrangements. This makes pyrite fairly heavy with a density twice the average rock (Rickard, 2015).

According to Moh's relative scale of hardness we find pyrite to be a hard mineral. In fact some of the hardest sulfide minerals include the pyrite group, with pyrite at 6–6.5, sperrylite at 6–7 and laurite at 7.5 in hardness (Mason & Berry, 1968).

Pyrite reflects 53.5% (589 nm) of the white light and consistently shows anisotropy regardless of its cubic shape (Deer et al., 1992). Furthermore, pyrite exhibit metallic luster which is indicative of the presence of metallic bonding, a type of chemical bonding, within the crystal lattice (Mukherjee, 2011).

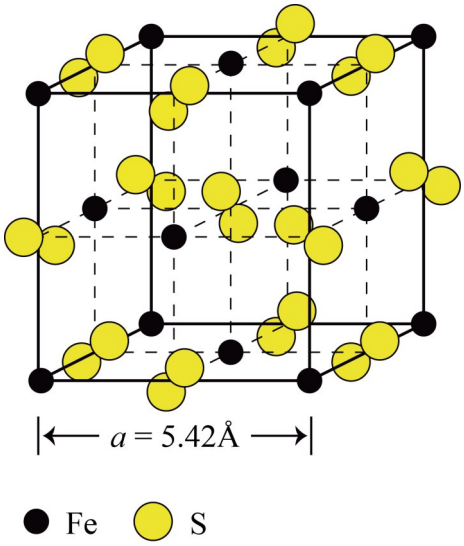

Fig. 3. The pyrite unit cell – cube shape. Modified from Deer et al. (1992).

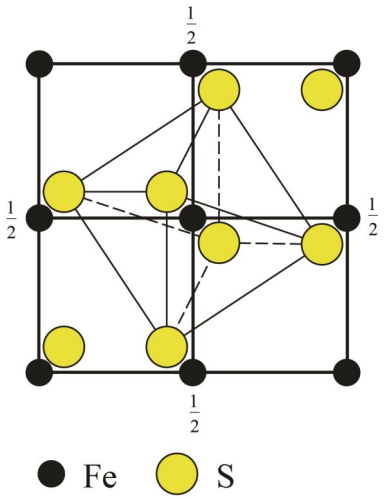

Fig. 4. The pyrite unit cell – octahedron shape. Modified from Deer et al. (1992).

In nature pseudomorphism may occur. One type of pseudomorphism is by alteration: a mineral forms by altering the internal structure and chemical composition of the existing mineral, but preserves the external form (Mukherjee, 2011). Hematite (Fe_2O_3), chalcocite (Cu_2S) and graphite are common minerals that form pseudomorphs after pyrite. Other examples of pseudomorphs after pyrite include pyrrhotite ($Fe_{1-x}S$), arsenopyrite (FeAsS), marcasite, fluorite (CaF_2), calcite ($CaCO_3$) and barite ($BaSO_4$) (Deer et al., 1992).

The mineral marcasite, also known as white iron pyrite, is a polymorph of pyrite (Deer et al., 1992; C.E.E., 2017). Marcasite share same chemical composition, FeS_2, and is very identical to pyrite, but differs in that it becomes darker upon oxidation, crystallizes with an orthorhombic structure and has a lighter color (C.E.E., 2017).

4.2 Chemistry of pyrite

During oxidation the S (and Fe) atoms react with O_2 to form sulfates (SO_4^{2-}) and eventually iron hydroxides ($Fe(OH)_3$) and their hydrates (Deer et al., 1992; Rickard, 2015). The oxidation process of pyrite may involve 15 or more steps, making it a very complex chemical process. The oxidation process is simplified into the following reaction (Welch et al., 2000):

$$FeS_2 + 15/4O_2 + 7/2H_2O \rightarrow Fe(OH)_3 + 2H_2SO_4$$

Furthermore, heavy metals such as Cu, Pb, As and Zn are some elements that can be present in pyrite in solid solutions, but in very low amounts (Deer et al., 1992).

Bacteria are known to catalyze reaction rates for sulfide mineral oxidation by five orders of magnitude compared to abiotic reaction rates. For example *Thiobacillus ferrooxidans* and *Leptospirillum ferrooxidans* catalyzes the reaction between O_2 and Fe(II) to form Fe(III) (Welch, 2000). Pyrite oxidation rates on the other hand can increase by several tens orders of magnitude in the presence of bacteria, and is much faster with Fe(III) than dissolved O_2 (Welch, 2000; Rickard, 2015).

High concentrations of As, exceeding 1000 µg/L, can be produced near or above the water table in the presence of sulfide minerals. Pyrite is known to have produced As concentrations well above 50 µg/L by oxidation of nitrate (Welch, 2000).

4.3 Geological occurrence of pyrite

Pyrite is the most abundant mineral among the sulfides (Vaughan & Craig, 1978). It is very widespread and occurs in large masses or as a primary or secondary mineral in veins of hydrothermal origin, in igneous rocks and in sedimentary (predominantly argillaceous and carbonaceous) rocks (Deer et al., 1992).

Pyrites are often found in sediments together with glauconite under reducing conditions forming diagenetically in muds on the sea floor, often in shallow water. In sedimentary and low-temperature hydrothermal deposits, pyrite is generally found with poor crystallization form. The term 'framboidal' is used to describe pyrites that have raspberry-like aggregates of tiny spherical particles. Pyrite is also found in coals and is the main opaque mineral (Deer et al., 1992).

5 Geological setting

The studied areas, Lerhamn and Fågelsång, are located in Scania, southern Sweden. This province forms part of the Fennoscandian shield which in turn represents the northwestern part of the Baltica palaeocontinent (Bingen et al., 2008). In late Precambrian times the eastern margin of Baltica faced towards the northeast of Laurentia. Around 570–550 Ma (Ediacaran) Baltica was a separate continent after the separation from Laurentia more than hundred million years earlier, until it softly collided with Avalonia at about 443 Ma (end of Ordovician; Fig. 5). Fairly soon after the amalgamation with Avalonia, Baltica collided in a more dynamic way with Laurentia and Laurussia was formed as a result of the Caledonian Orogeny (Cocks & Torsvik, 2005; Gee & Stephenson, 2006).

Scania can be divided into a north-eastern part dominated by Proterozoic rocks that form the crystalline basement and a south-western part with sedimentary rocks resting on the crystalline basement. The border between these two parts forms a wide tectonic, structural lineament, the NW–SE trending Tornquist Zone (TZ) with large-scale horst and graben structures (Fig. 6; Andersson & Ladenberger, 2010; Calner et al., 2013). The TZ is a deformation zone extending from the North Sea through Jutland, Denmark, and Scania and as far as to the Black Sea (Erlström et al., 1997; Andersson & Ladenberger, 2010). In addition to prominent structural features, the TZ is characterized by numerous early Permian dolerite dykes and a

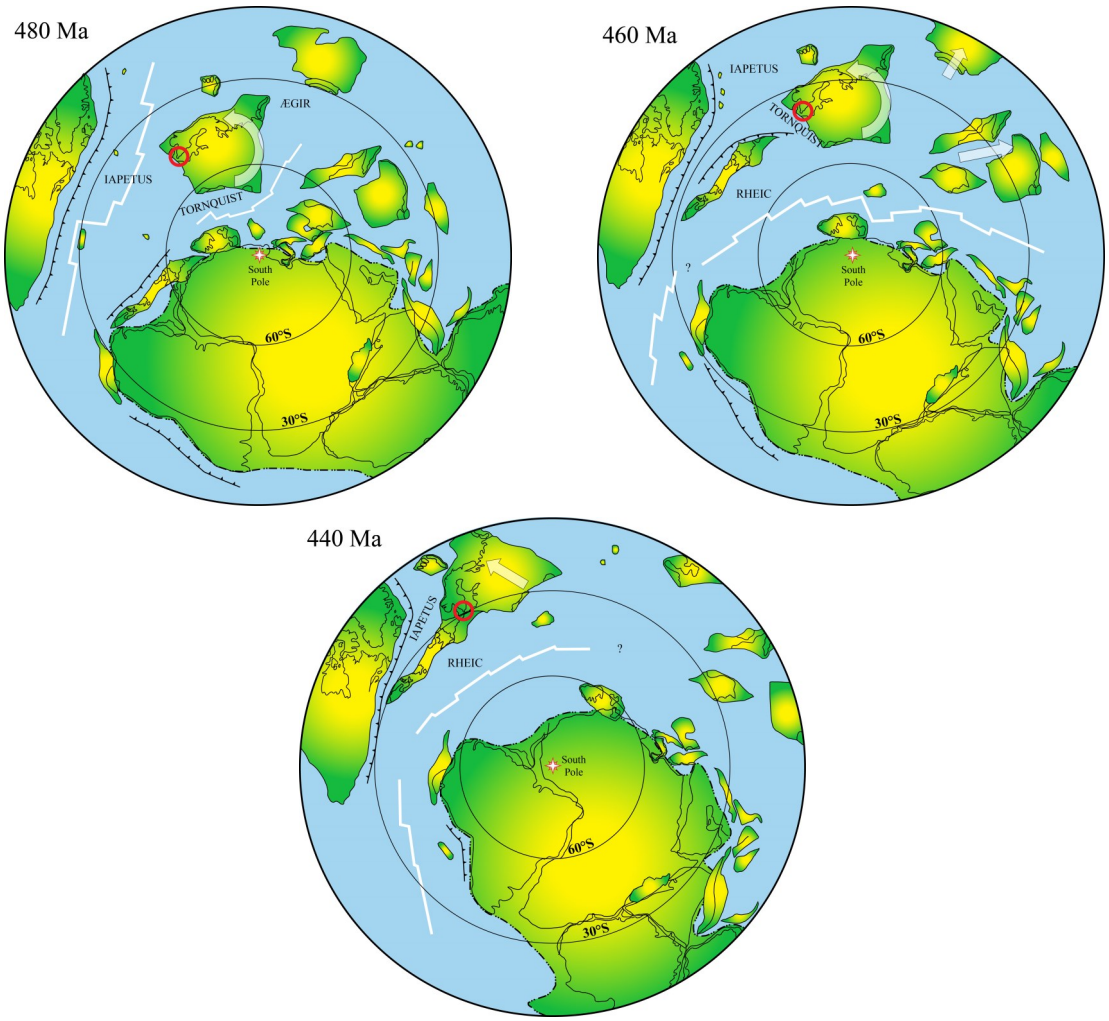

Fig. 5. Ordovician–early Silurian geography. The collision between Baltica and Avalonia took place at 460–440 Ma. Location of Scania is marked with a red circle. Modified from Cocks & Torsvik (2002).

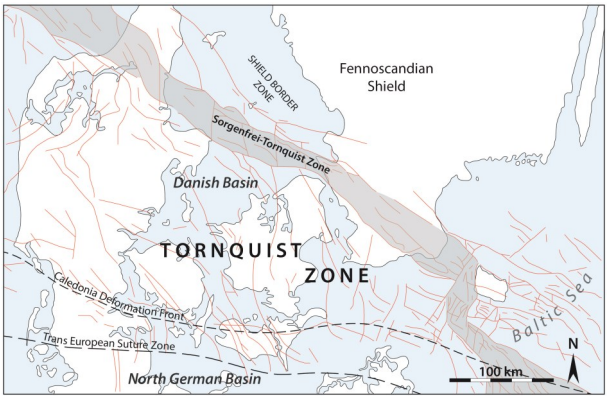

Fig. 6. Schematic map of the NW–SE trending tectonic lineament of the Tornquist Zone. Modified from Calner et al. (2013).

number of basaltic volcanic necks from the Mesozoic (Andersson & Ladenberger, 2010).

Lower Palaeozoic strata of Scania are mainly preserved in the Colonus Shale Trough (CST). The CST is a NW–SE trending structure within the Sorgenfrei-Tornquist Zone (Fig. 6), representing the western part of the TZ. The CST is an elongated and fault bounded structure stretching diagonally (NW–SE) through Scania (Fig. 7). Movements along the smaller scale faults within the CST has resulted in several uplifted fault-blocks exposing Cambrian through Ordovician parts of the succession. The lower Palaeozoic succession (1600 m) is mainly composed of shale and mudstone with subordinate limestone and sandstone units (Maletz & Ahlberg, 2011a; Calner et al., 2013).

Several deep wells in the CST have penetrated the ca. 60–140 m thick Ordovician succession of Scania. This succession consists predominantly of deeper-water shales and mudstones that accumulated along the southern margin of the Baltica plate (Calner et al., 2013). It is subdivided into the Bjørkåsholmen Formation, Tøyen Shale, Komstad Limestone, Almelund Shale, Sularp Shale, Skagen Limestone, Mossen Formation, Fjäcka Shale and the Lindegård Mudstone. The Bjørkåsholmen-, Komstad- and Skagen formations are the only regionally important formations in the Ordovician of Scania and they are important marker beds on a regional scale (Calner et al., 2013). The Ordovician succession is a typical representative of the Scanian litho- or confacies belt of Jaanusson (1976; Fig. 8 herein).

5.1 The Lerhamn drill core

A drill core was retrieved in 2008 by Borrbolaget, Västra Frölunda, in the small village of Lerhamn (N56°15'18.60", E12°31'33.46"; Fig. 9). It provides

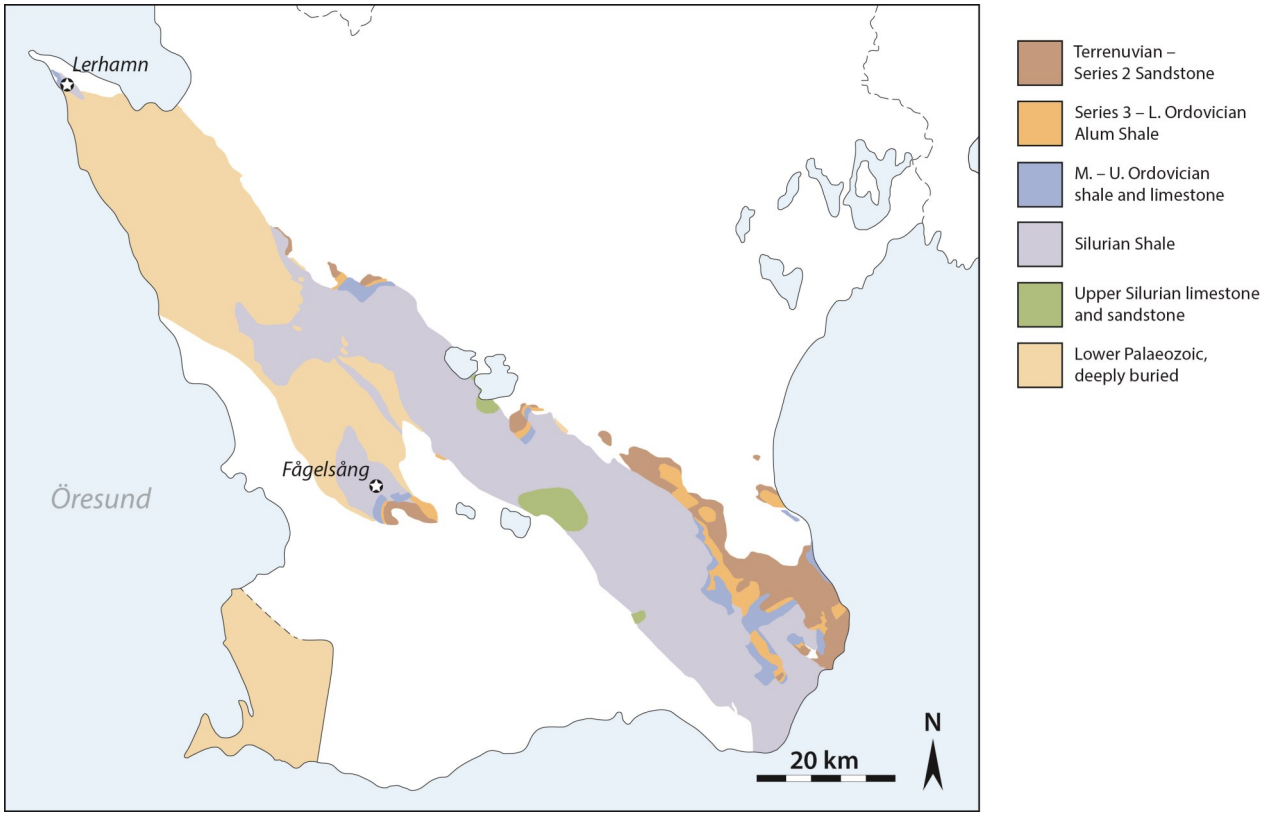

Fig. 7. Generalised map over the Colonus Shale Trough stretching in a NW–SE direction through Scania, along the Sorgenfrei-Tornquist Zone. Uplifted fault-blocks expose Cambrian through Ordovician strata composed of mainly shale and mudstone with subordinate limestone and sandstone. Modified from Calner et al. (2013).

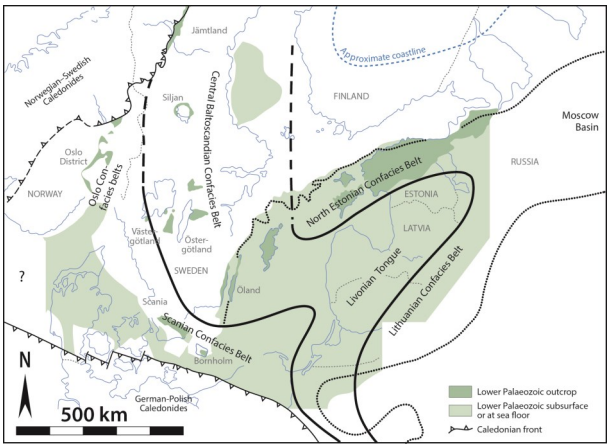

Fig. 8. Confacies belts introduced by Jaanusson (1976). Scania forms part of the Oslo–Scanian confacies belts, which include Scania, the western part of southern Sweden and Norway. Modified from Calner et al., 2013.

new important information about the graptolite biostratigraphy of the Tøyen Shale Formation. The Lerhamn drill core measures 71.18 m (9.07–80.25 m) and contains numerous well-preserved graptolites, which form the basis for a revised Lower and Middle Ordovician graptolite biozonation in Scania. Graptolites occur frequently and are preserved through coalification, often as a silvery shining film of organic matter representing the rhabdosome, or by pyritization in partial or full relief (Maletz & Ahlberg, 2011b). Associated fossils in the Lerhamn drill core are small brachiopods, some of these phosphatized, and fragmentary phyllocarids.

Lerhamn is located in the northwestern part of Scania, ca. 10 km north of Höganäs and south of the Kullaberg peninsula. Successions of Triassic and Jurassic age surround Ordovician and Silurian rocks that form an elongated inlier south of Kullaberg. The Palaeozoic succession of this inlier is known from a few outcrops in the area and confirmed from drill

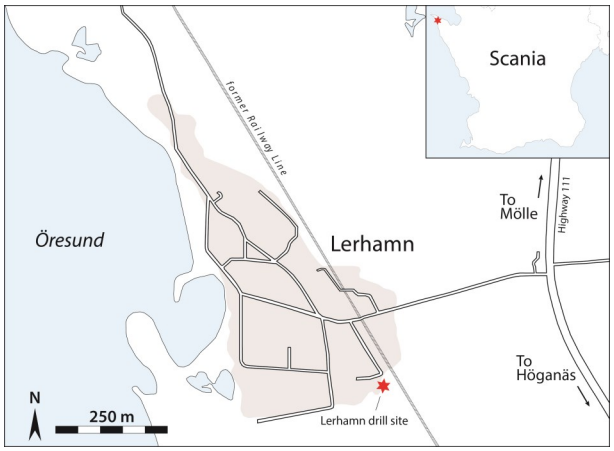

Fig. 9. Map over the village of Lerhamn showing the drill site (marked with a red asterisk). Modified from Maletz & Ahlberg (2011b).

cores (Lovisefred and Krapperup) to be several hundred meters thick (Maletz & Ahlberg, 2011b).

The Lerhamn drill core consists entirely of the Tøyen Shale Formation, which is dominated by Lower–Middle Ordovician grey to black shales and intercalated intervals of green shales (Fig. 10). Well-preserved pyrite of varying size, small irregular grains to larger well shaped crystals (Fig. 11A), can be observed throughout the core. Carbonates are largely restricted to vertical and subvertical fractures in the shale (Fig. 11B). A more detailed description of the lithology of the Tøyen Shale Formation is given below. For a more extensive description the reader is referred to Appendix A. The stratigraphic subdivision of the core is based on the extensive work of Maletz & Ahlberg (2011b), who provided a detailed graptolite zonation of the entire core.

5.1.1 Quaternary deposits (0–9.07 m)

The drill core starts at a depth of 8.97 m below Quaternary deposits (Fig. 10a). The uppermost part 10 cm of the drill core (8.97–9.07 m) consists of gravel with subrounded to subangular grains, 8–50 mm in size. However, this layer of gravel could simply originate from the upper layers and have simply fallen into the drill hole and should therefore not be taken into account.

5.1.2 Darriwilian (9.07–29.5 m)

The uppermost part of the Tøyen Shale Formation belongs to the Darriwilian Stage (Fig. 10a, b). This part of the succession is dominated by alternating grey–DI-2 shales at a depth of roughly 9.07–27 m and 27.5–29.5 m. A short interval with DI-3 shale is present at 27–27.5 m. At 12.09–12.13 m, there is 3 cm thick layer with black shale. Silt occurs almost throughout the entire succession in low–high amounts. Silt is absent at 11.75–12.13 m and 18.7–19.7 m. Carbonates are fairly common and found within fractures. Pyrite is common, whereas oxidized pyrite is only visible in the upper part of the succession (Fig. 11C). In the lower part of the Darriwilian, unaltered pyrite is abundant, and some grains are up to 15 mm. Fracture zones can be seen at 20.63–20.70 m, 20.88–21.00 m, 21.10–21.50 m (filled with carbonates and quartz; Fig. 11D) and 21.80–22.10 m. A more coherent fracture zone is present at 27.65–30.70 m (continuing down into the Dapingian).

5.1.3 Dapingian (29.5–35.25 m)

The Dapingian Stage comprises 5.75 m (Fig. 10b) and is dominated by DI-4 shales at 29.8–32.65 m and 33.3–34.5 m, separated by a layer of black shale. Overlaying the upper part of the DI-4 shale is a thin layer of DI-2 shale, which re-occurs at the bottom of the stage. Two separate layers of grey shale can be found together with DI-2 shale at the bottom of the stage. Silt occurs sporadically and is found at

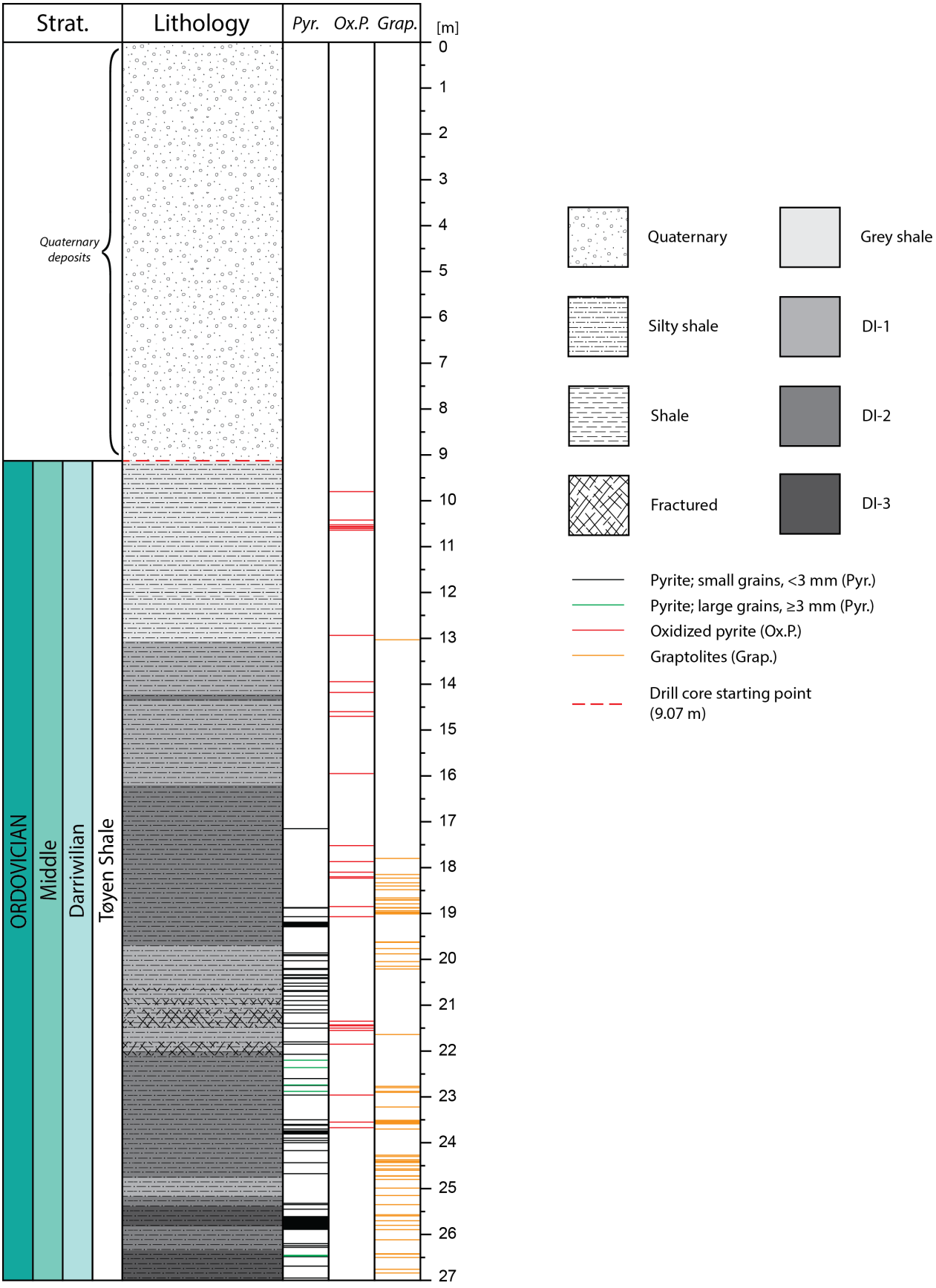

Fig. 10a. Stratigraphic column of the Lerhamn drill core (0–27 m). DI = darkness index, increases with increasing number.

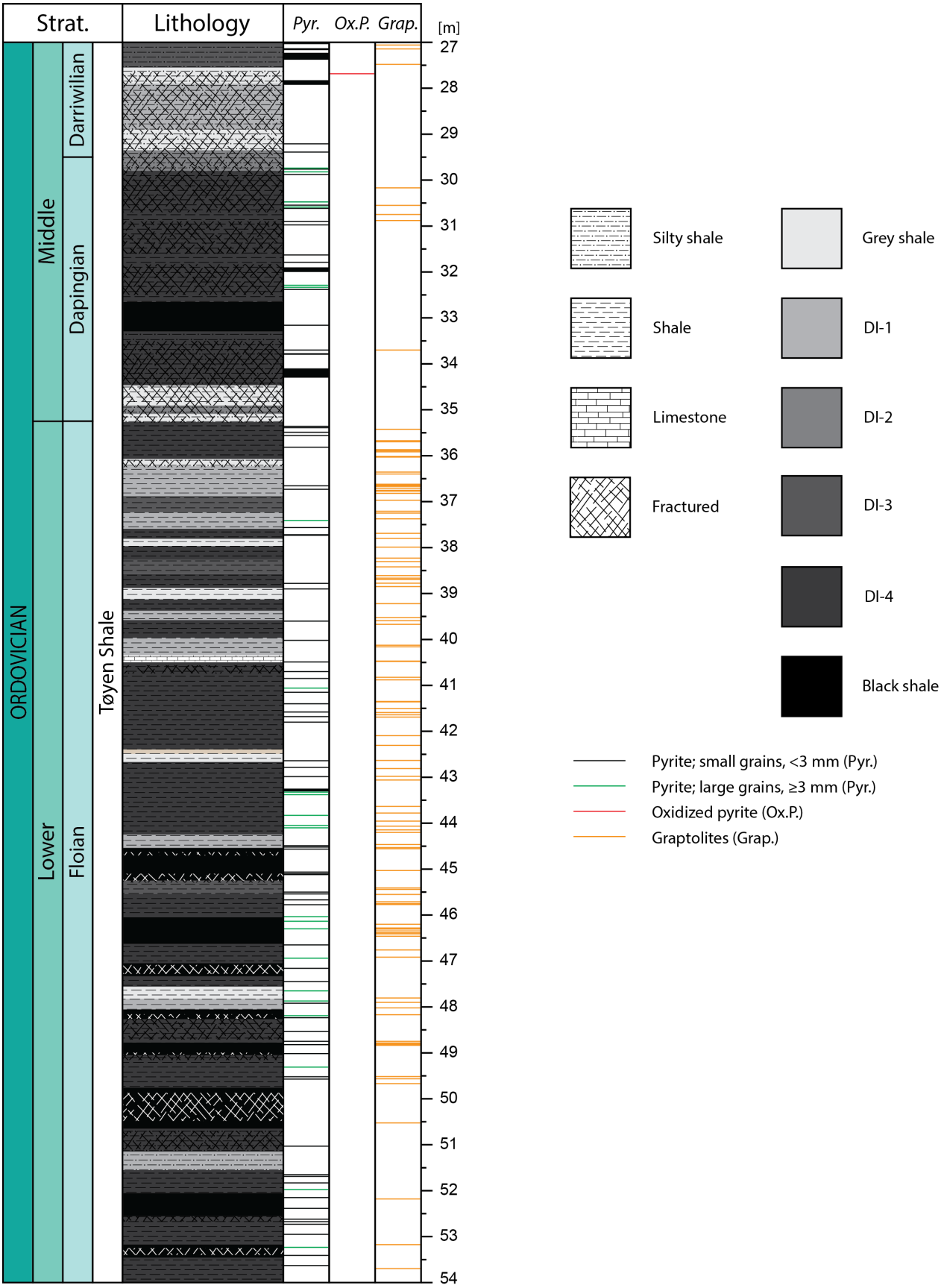

Fig. 10b. Stratigraphic column of the Lerhamn drill core (27–54 m). DI = darkness index, increases with increasing number.

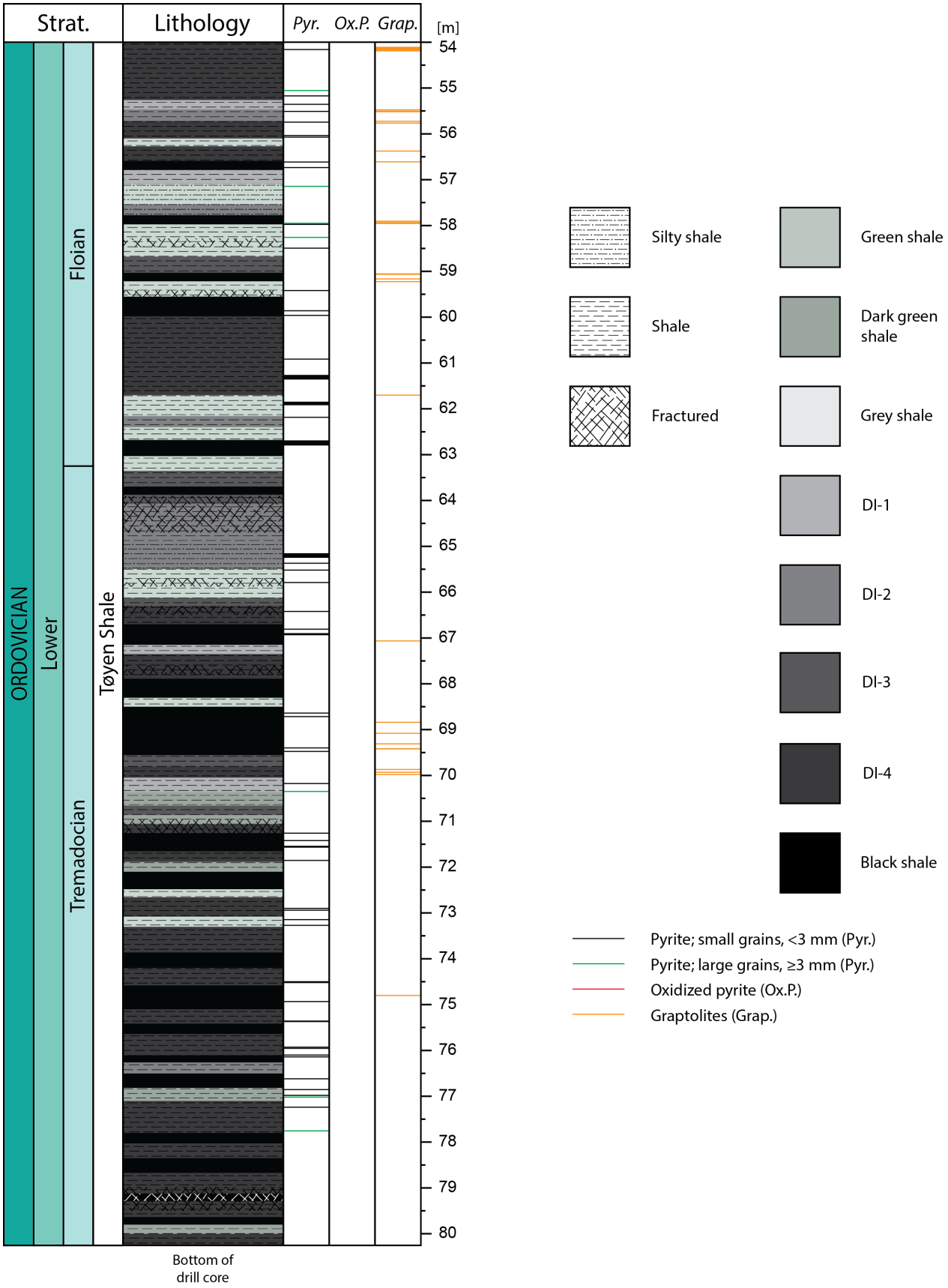

Fig. 10c. Stratigraphic column of the Lerhamn drill core (54–80.25 m). DI = darkness index, increases with increasing number.

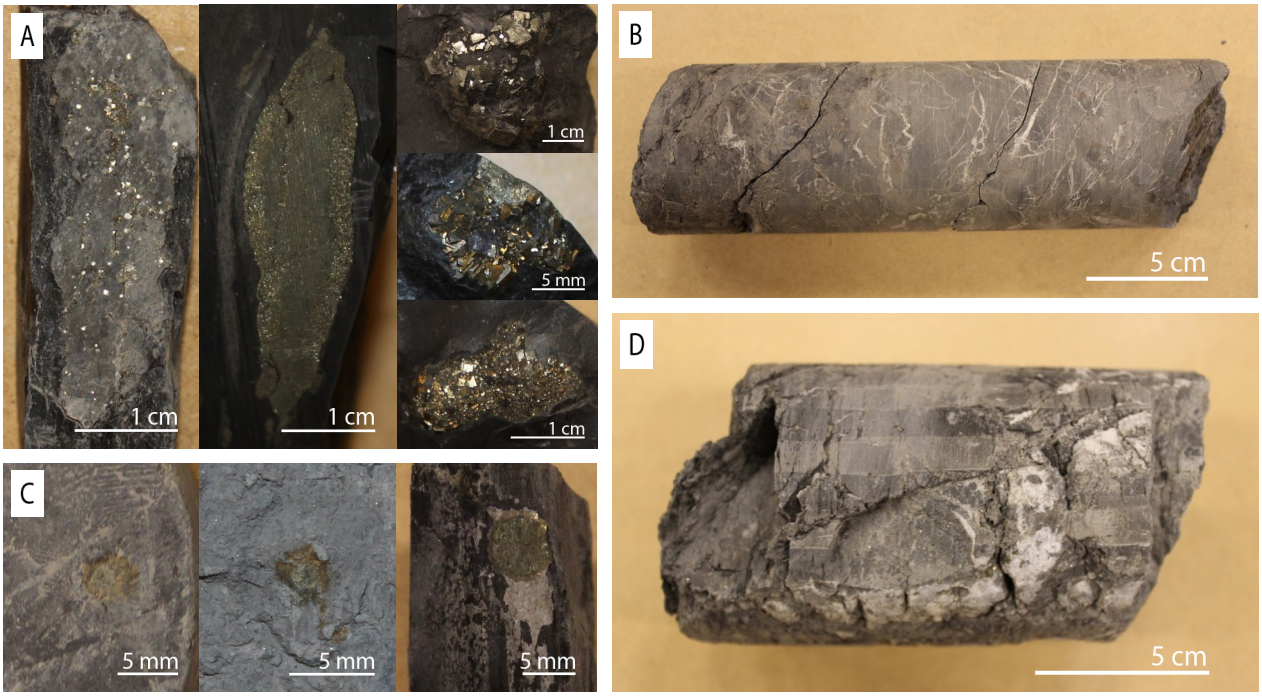

Fig. 11. A. Unaltered pyrite in the shale at a drilling depth of 20.59 m, 40.49 m, 48.19 m, 53.24 m and 55.10 m in the Lerhamn drill core. Large images are pyrite seen as cut-through. Small images are pyrite seen as drill core has broken off, showing specimens with well shaped crystals. **B**. Calcareous veins in the Lerhamn drill core. This piece of the core is approximately 24 cm long and forms part of a longer core at a drilling depth of 63.90–64.70 m. **C**. Oxidized pyrite in the shale at a drilling depth of 10.53 m, 19.82 m and 21.45 m in the Lerhamn drill core. **D**. Fracture zone in the Lerhamn drill core (21.10–21.50 m). This piece of the core is approximately 14 cm. The white minerals are carbonate (with some quartz) that has precipitated in cracks.

29.5–29.8 m, 33.3–34.5 m and 34.92–35.25 m in low–very low amounts. Carbonate is present in low concentrations and increases to moderate with depth. White veins of carbonates dominate the upper part of the succession, while in the lower part of the succession carbonate is mainly found within fractures in the shale. There is less pyrite compared to the Darriwilian part. Pyrite occurs at regular intervals and includes grains up to 25 mm in size. The entire Dapingian succession is more or less affected by fractures. Fracture zones are seen at 27.65–30.70 m (continuation from the Darriwilian), 30.90–31.60 m, 31.83–32.50 m and 33.50–35.28 m.

5.1.4 Floian (35.25–63.25 m)

The Floian is the thickest stage in the drill core and measures approximately 28 m (Figs. 10b and 10c). This stage is characterized by an increase in black shales, mostly occurring as thin alternating layers, and a decrease in grey–DI-2 shales. DI-4 shales predominate and make up the main part of the succession. The only limestone bed in the Lerhamn drill core, measuring 4.5 cm in thickness, has been recorded at 40.37–40.415 m. The lower part of the Floian is also characterized by green shales, which starts at around 56 m. Silt is only found within a few intervals, such as 36.09–36.25 m, 50.60–51.50 m and 57.10–57.79 m. The general carbonate concentration is moderate, except for certain intervals which lack carbonate or show high concentrations. Pyrite is common throughout the entire Floian, appearing at regular intervals. In general, the pyrite grains are larger than in the upper parts of the drill core, although the overall abundance of pyrite is lower. Fracture zones appear at different depths, the majority of them existing in the middle–lower part of the stage, e.g. at 48.16–48.71 m, 49.87–50.48 m, and 50.70–51.10 m. Compared to other stages in the core, clay and sometimes even silt are found within fractures in the Floian.

5.1.5 Tremadocian (63.25–80.25 m)

The lower part of the drill core belongs to the Tremadocian (Fig. 10c), which consists of alternating thin layers, dominated by DI-4 shales and black shales. Other shales found are green–dark green shales and DI-1–DI-3 shales. Silt is absent in this part of the drill core. The carbonate content is generally moderate, but some intervals have a low content or lack carbonates. Despite the overall decrease in pyrite, a few larger pyrite grains, as large as 15 mm, are found in this part of the drill core. Fractures are observed at 63.90–64.70 m, 66.30–66.50 m, 67.60-67.80 m, 70.95–71.30 m and 78.98–79.50 m.

5.2 The Fågelsång-3 drill core

One of the most well-known outcrop areas of Ordovician rocks in Baltoscandia is found at Fågelsång, which is located about 8 km east of Lund in south-west Scania (Bergström et al., 2000; Bergström & Ahlberg, 2004; Calner et al., 2013). The Fågelsång area is situated within the Colonus Shale Trough. Ordovician and Silurian shales dominate the area, except in its southern parts which is dominated by Cambrian sandstone and alum shale (Fig. 7).

The Ordovician succession at Fågelsång is unique in Baltoscandia with more than 50 recorded exposures of fossiliferous Ordovician and Cambrian strata and a virtually complete succession of graptolite zones. Nationally and internationally the graptolite succession in the Fågelsång area has served as standard for biostratigraphic correlations and the Global Stratotype Section and Point (GSSP) for the base of the Sandbian Stage and the Upper Ordovician Series was ratified by the International Commission on Stratigraphy in 2002 (Bergström & Ahlberg, 2004). In 2003 the `golden spike´ was hammered in the shale wall at the boundary level in section E14b of Moberg (1910), N55° 42'57.24", E13°19'02.98" (Calner et al., 2013). The fossils at locality E14 includes, apart from graptolites, also conodonts and chitinozoans (Bergström & Ahlberg, 2004).

In 2013 a drill core was retrieved near the settlement of Fågelsång, just south-east of the GSSP (section E14b of Moberg 1910), N55°42'56.16", E13° 19'6.29" (Calner et al., 2013), along the south bank of the Sularp Brook and to the north-west of the Rögle (Fågelsång) Brook (Fig. 12). The drill core (Fågelsång -3) measures 58.7 m and includes the Tøyen Shale, the Komstad Limestone, the Almelund Shale and the lowermost part of the Sularp Shale. Well-preserved graptolites can be found throughout the shales in the core.

The Fågelsång-3 drill core consists of Lower–Upper Ordovician strata dominated by grey to black shales, including a very short interval of dark green shale (Fig. 13). A prominent limestone succession, the Komstad Limestone, is also present in the core,

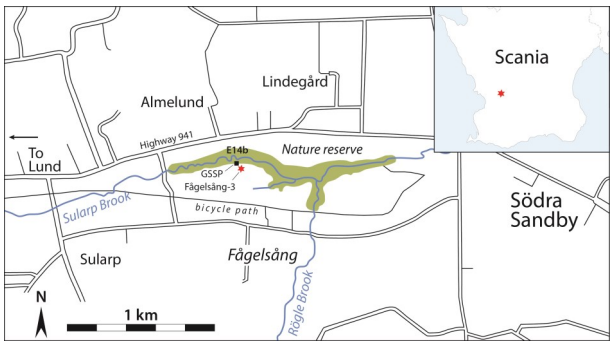

Fig. 12. Map over the Fågelsång area showing the location of the drill site (marked with a red asterisk). Modified from Bergström & Ahlberg (2004) and Calner et al. (2013).

consisting of limestone with subordinate marl and shale beds. Carbonates in the shaly parts of the drill core are largely restricted to vertical and subvertical fractures (cf. Fig. 11B). Pyrite is common throughout the entire core. A more detailed description of the lithology of the Fågelsång-3 drill core follows below. For a more extensive description the reader is referred to Appendix B. The stratigraphic subdivision of the core into formations and stages follows Bergström et al. (2002), Stouge & Nielsen (2003) and Bergström & Ahlberg (2004).

5.2.1 Sularp Shale Formation (6.17–6.42 m)

The lowermost part of the Sularp Shale Formation is represented in the Fågelsång core and consists of a 25 cm thick succession of black–DI-3 shale (Fig. 13a). The base of the formation is characterized by a pyritic phosphorite, also known as the Fågelsång phosphorite, spanning from 6.30–6.42 m (Fig. 14A). Silt is absent in this interval and no fractures occur. Minor carbonate veins are present.

5.2.2 Almelund Shale Formation (6.42–48.83 m)

The Almelund Shale Formation forms the major part of the core and is dominated by black shales with thin intervals of DI-3–DI-4 shales (Figs. 13a, b, c). The uppermost 7 m consist of DI-3 and DI-4 shales without silt. The shales grade into black shales around a core depth of 15 m. DI-4 shales are also present in the black shales in the lower part of the formation. Thin intervals of limestone are present at 14.72–14.88 m and 34.58–35.62 m. Bentonites occur as centimeter thick beds at 20.53–20.54 m, 31.77–31.82 m (Fig. 14B), 35.72–35.75 m, 36.35–36.37 m, 39.01–39.02 m, 39.56–39.59 m, 39.73–39.75 m and 48.79–48.84 m. Silt is common in the lower half of the Almelund Shale. A large variation in the occurrence of carbonates has been recorded throughout the formation, ranging from no carbonates to high concentrations. Pyrite is common in the Almelund Shale, appearing mainly at the depths of 6–9 m and 43–46 m, with grains up to 15 mm in size. Fractures occur at 15.85–16.01 m, 16.80–16.83 m (with clay mixture), 18.90–19.19 m (less fractured), 19.45–19.70 m and 19.89–20.25 (highly fractured, with clay mixture).

5.2.3 Komstad Limestone Formation (48.83–57.19 m)

The Komstad Limestone Formation is approximately 8 m thick and dominated by limestone (Fig. 13c). The limestone succession is roughly 7.6 m in total interrupted by a few intervals with black shales, DI-3 shales and bentonites. Ca 0.37 m of the formation consists of silty limestone, found at the base of the Komstad Limestone. Bentonites can be observed at 48.79–48.83 m, 49.15–49.25 m and 49.53–49.62 m. High amounts of silt appear at the very bottom of the

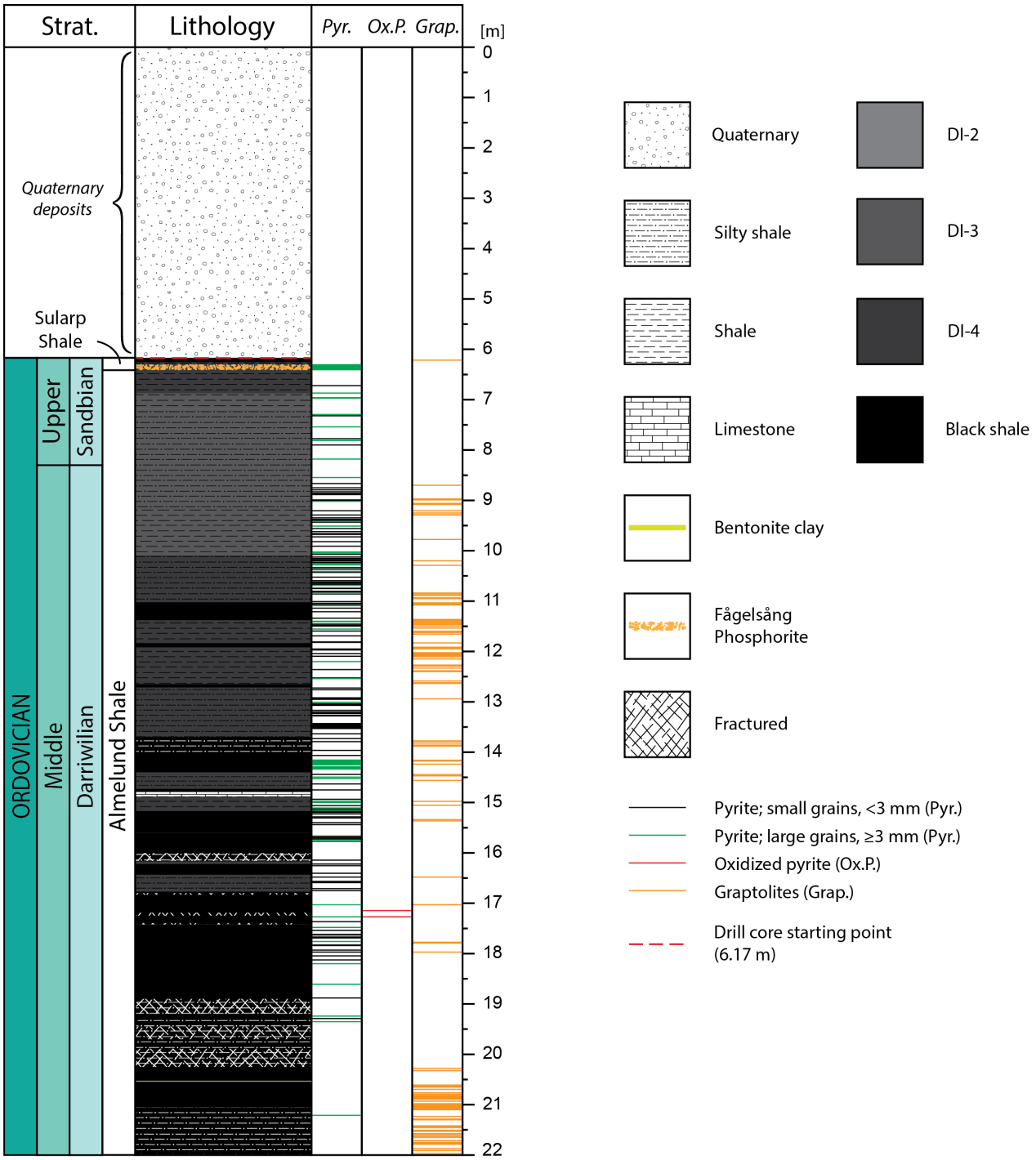

Fig. 13a. Stratigraphic column of the Fågelsång-3 drill core (0–22 m). DI = darkness index, increases with increasing number.

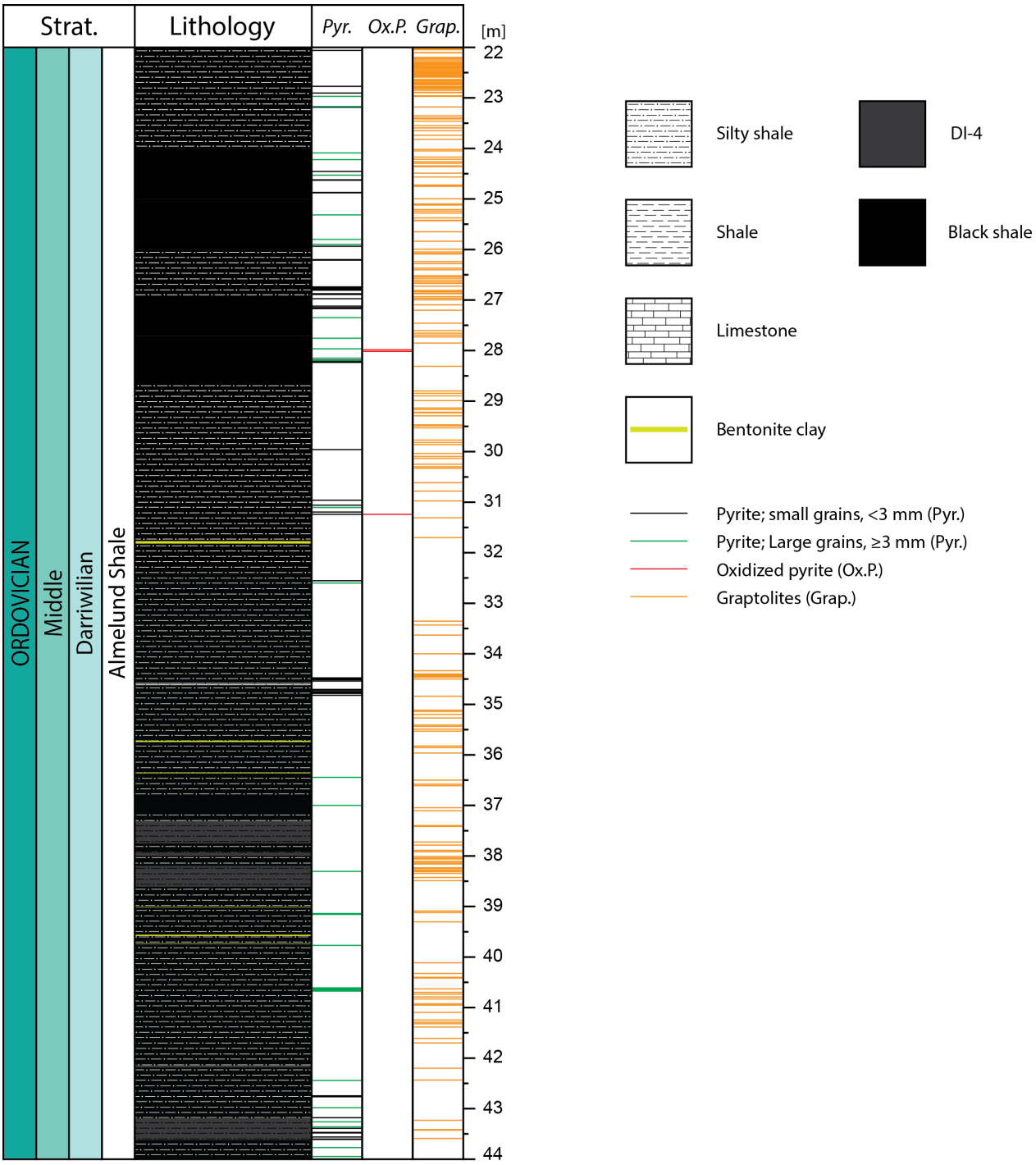

Fig. 13b. Stratigraphic column of the Fågelsång-3 drill core (22–44 m). DI = darkness index, increases with increasing number.

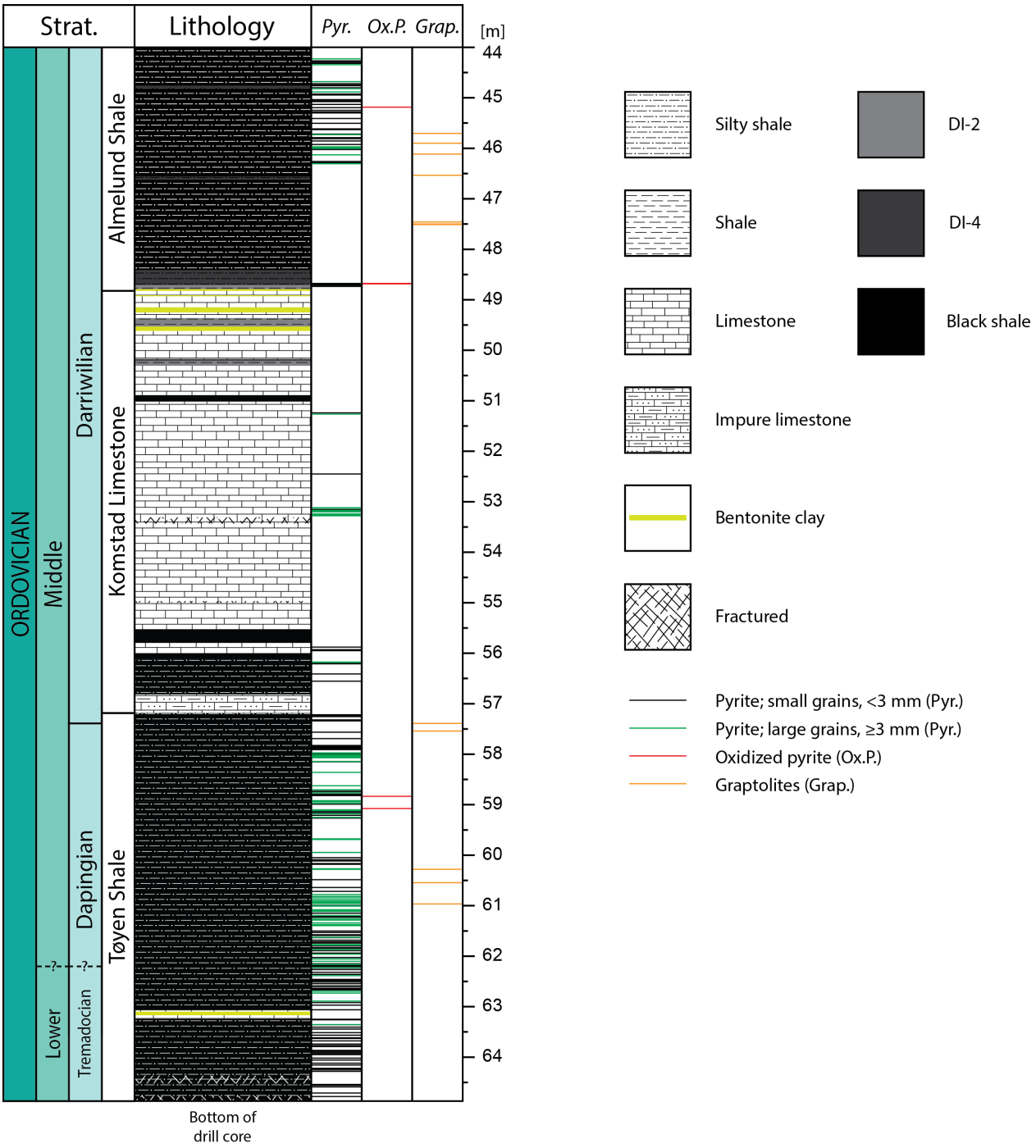

Fig. 13c. Stratigraphic column of the Fågelsång-3 drill core (44–64.87 m). DI = darkness index, increases with increasing number.

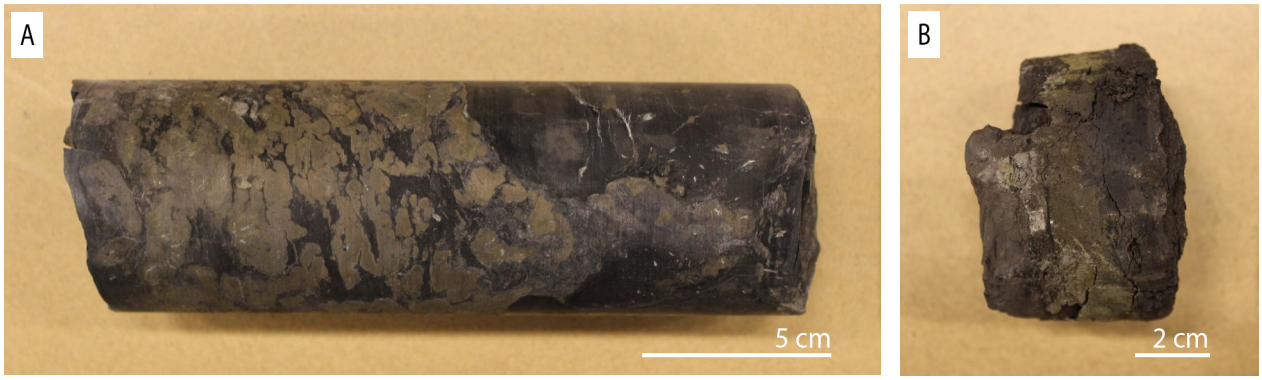

Fig. 14. A. Pyritic phosphorite from Fågelsång-3 drill core (drilling depth 6.30–6.42 m). **B**. Thin greenish to whitish bentonite bed in the Fågelsån-3 drill core (drilling depth 31.77–31.82 m).

formation. Pyrite occurs sparsely with the largest grain reaching 6 mm in size. Fractures occur at 53.31–53.43 m and 54.97–55.00 m.

5.2.4 Tøyen Shale Formation (57.19–64.87 m)

The Tøyen Shale Formation is represented in the lowermost part of the Fågelsång–3 drill core (Fig. 13c). This formation consists entirely of almost black shale, interrupted by a thin layer of limestone at 63.07–63.10 m and 63.17–63.24 m, and bentonite at 63.10–63.17 m. Silt occurs throughout the formation, but is absent in the limestone and bentonite layers. Carbonates occur, mostly in high concentration. Pyrite is abundant in the Tøyen Shale Formation and appears regularly throughout the succession, with grains up to 20 mm in size. Fractures occur at 64.37–64.52 m (containing clay-mixture with high concentrations of carbonate) and 64.77–64.87 m. Parts of the formation may also contain a clay-silt mixture with thin carbonate veins.

6 Methods

6.1 Sample preparation

The Lerhamn and Fågelsång-3 drill cores are stored at the Department of Geology, Lund University, Sweden. The drill cores were divided into different lithologies, with the exception of shale, which was further subdivided by color and shades of grey (Figs. 10 and 13). Hydrochloric acid (HCl) was used to confirm the presence of carbonates. Pyrite and graptolites were simultaneously marked on their respective depth. It should be noted that the number of pyrites and graptolites found are rough estimates. All specimens are found either on the surface of the cores or in gaps visible to the naked eye.

A stratigraphic column was created for the Lerhamn and Fågelsång-3 drill cores, based on the information obtained from the respective cores. Three additional columns were created, representing pyrites (one for oxidized and one for non-oxidized specimens) and graptolites encountered at different depths throughout the cores (Figs. 10 and 13).

Pyrite was later extracted from both cores for LA-ICP-MS (Laser ablation inductively coupled plasma mass spectrometry) analysis, using a hammer and a small flat-head screwdriver to gently loosen up the pyrite. The pyrite was saved in small test tubes with caps and carefully marked. A total of 388 samples (269 from Lerhamn and 119 from Fågelsång-3) were extracted from the cores. Before the samples could be sent for LA-ICP-MS analysis, preparation work was done which included crushing and polishing of the samples.

The samples were crushed using a pestle until appropriate pyrite grains sizes were achieved. To avoid contamination, the pestle was cleaned with a tissue after each sample crushing. One pyrite grain was handpicked from each sample under binocular microscope, and placed onto a planar disk with double-sided adhesive tape. For convenience, the pyrite grains were oriented after ascending depth. Three disks were used and given the initials L1; bigger pyrite grains extracted from Lerhamn, F1; bigger pyrite grains extracted from Fågelsång-3, and L2/F2; smaller pyrite grains extracted from the respective cores (L2 = Lerhamn and F2 = Fågelsång-3).

Each pyrite disk was covered with a 2.5 cm in diameter plastic ring and molded in epoxy resin, which was let to harden for approximately 1.5 week at room temperature. The hardened epoxy (Fig. 15) was then separated from the ring and polished using a Struers Rotopol-25®. A polishing cloth with diamond paste (Struers DP-paste M), grain size 6 µm, was first used to expose and smoothen up the surface of the pyrite grains. Afterwards, a polishing cloth with diamond paste grain size 3 µm was used until a shiny surface was achieved.

All three mounts were later taken to the LA-ICP-MS laboratory at Lund University for analysis. Because of possible alteration, due to the waiting time for the analysis, the mounts were re-polished as a precaution once more with a 3 µm grain size diamond

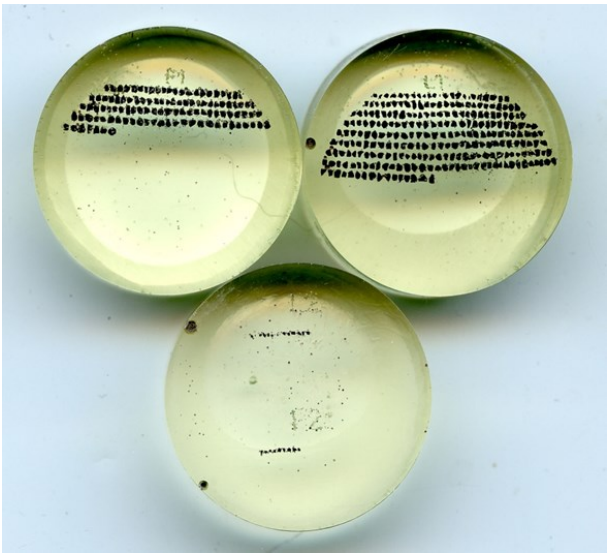

Fig. 15. Pyrite samples, F1 (top left.), L1 (top right) and L2/ F2 (bottom), in hardened epoxy.

paste. Due to high sensitivity for dust and other particles in the LA-ICP-MS the mounts were also air brushed and cleaned with ethanol to avoid any external contamination before they were analyzed.

6.2 Laser Ablation ICP-MS analysis

Analyses were done with Laser Ablation Inductively Coupled Spectrometry (LA-ICP-MS) using a 193 nm Cetac Analyte G2 excimer laser equipped with an two-volume HelEx2 sample holder and coupled to an Aurora Elite quadrupole.

Three sessions were done: one for testing, including tuning and set-up of the method, and two for analyses. In the analytical sessions, the laser was set up with 60 µm spot size, a fluence of 2.3-2.8 J/cm^2, 6 Hz repetition rate and 138 shots per analyses (Fig. 16). The signal was optimized and tuned with NIST-612 glass aiming at stable signal, low oxide production ($^{238}U^{16}O/^{238}U$ below 0.5%) and $^{232}Th/^{238}U$ around 1. Detailed analytical parameters are given in Appendix C. MASS-1 was used as primary reference material and ^{57}Fe as internal standard. We assume the Fe-concentration in the pyrite to be 46.6 wt. %. For each analytical session we started with 4 MASS-1 and continued with cycles of 12 unknowns and 2 MASS-1. We used BCR-2G as our secondary reference material, this material however has a different matrix and contain only documented concentrations a few of the measured elements. A total of 14 BCR-2G were analyzed during the second analytical session. For the elements reported for BCR-2G (V, Cr, Mn, Co, Cu, Ga, Mo, Sb and Pb) most plots within reasonable error of the accepted value, with the exception for Ga and Mn. The error anomalies for Ga and Mn could likely derive from polyatomic interferences where ^{69}Ga has mass interferences with e.g. $^{36}Ar + {}^{33}S$, $^{36}S + {}^{33}S$ and ^{55}Mn with e.g. $^{54}Fe + {}^{1}H$. In both analytical sessions we had problem with S and Hg memory effect caused by short wash-out time, and therefore, measured concentrations of these elements are likely affected by the memory effects.

7 Results

Data obtained from the LA-ICP-MS analysis for As and heavy metals are presented in Appendix D (for Lerhamn drill core) and Appendix E (for Fågelsång-3 drill core). Analyzed elements are shown in parts per million (ppm). Elements below the detection limit are labelled Bdl in the data set. Samples where elements were excluded from the analysis are labelled Nd (not determined). Further, it should be noted that all concentrations are based on specific isotopes (see masses measured in Appendix C) and re-calculated after relative natural abundance for all isotopes for that particular element.

7.1 The Lerhamn drill core

Analytical results from the Lerhamn drill core confirm high content of As with a significant increase peaking at ca. 40 m depth. This is indicated by an anomaly ranging from ca. 30–50 m depth in the diagram in Figure 17. Similar anomalies can be observed for V,

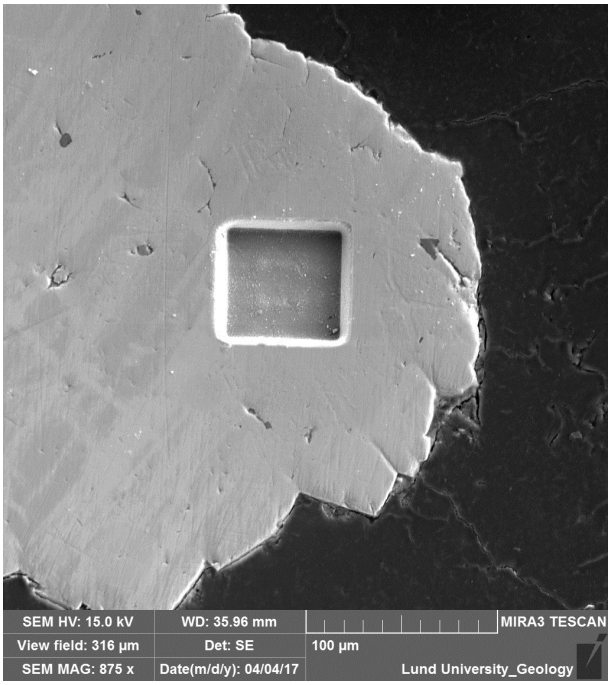

Fig. 16. Pyrite grain from Fågelsång-3 drill core (F2) at 44.96 m depth. The square-shaped crater measures 60x60 µm in size and is a result from laser shots. Image is taken with a Mira 3 Tescan SEM at Lund University. Photo: Leif Johansson.

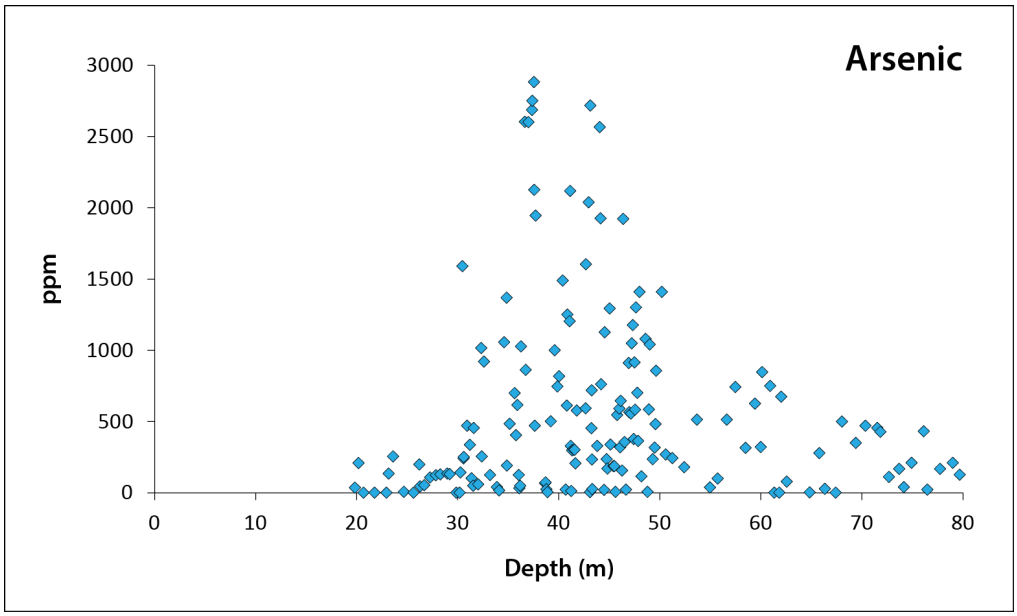

Fig. 17. Diagram showing arsenic concentrations in pyrite from the Lerhamn drill core. Measured values: highest = 17660 ppm, lowest = 0.04 ppm and average = 735.70 ppm. Excluded points: 17660 ppm (40.49 m), 6129 ppm (37.27 m) and 5504 ppm (37.26 m).

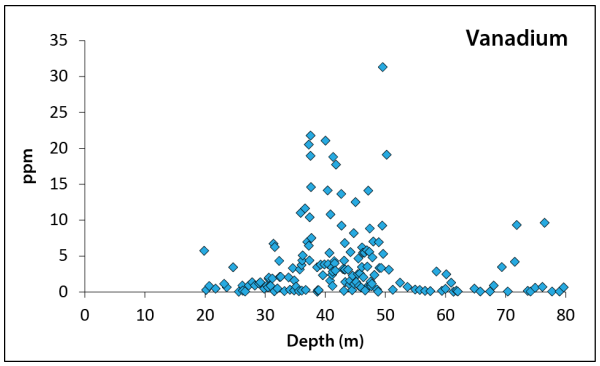

Fig. 18. Diagram showing V concentrations in pyrite from the Lerhamn drill core. Measured values: highest = 31.3 ppm, lowest = 0.0032 ppm and average = 3.92 ppm.

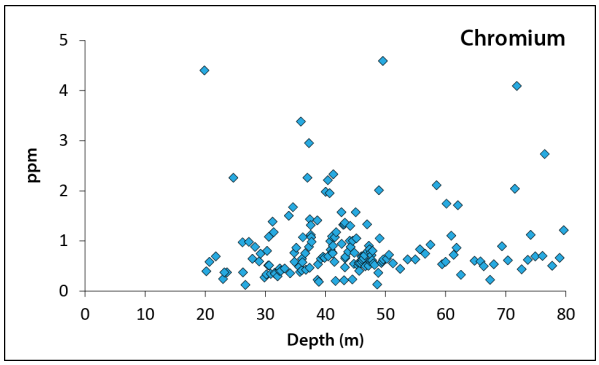

Fig. 19. Diagram showing Cr concentrations in pyrite from the Lerhamn drill core. Measured values: highest = 4.59 ppm, lowest = 0.12 ppm and average = 0.91 ppm.

Cr, Co, Mo, Cd, Sb, W, Hg and Pb, where Co Mo, Sb, Hg and Pb show concentrations up to 180 ppm and higher (Figs. 18–26). Highest values for As measure 17660 ppm, 6129 ppm and 5504 ppm, all excluded from the diagram in Figure 17, whereas the lowest value measures 0.04 ppm (Appendix D, Table D1). The average concentration is approximately 736 ppm. The significant difference in As and heavy metals between samples reflects difference in concentration from one pyrite grain to another.

7.2 The Fågelsång-3 drill core

Analytical results from the Fågelsång-3 drill core do not show any single significant As-anomaly, however, high content are present at varying depths (Fig. 27).

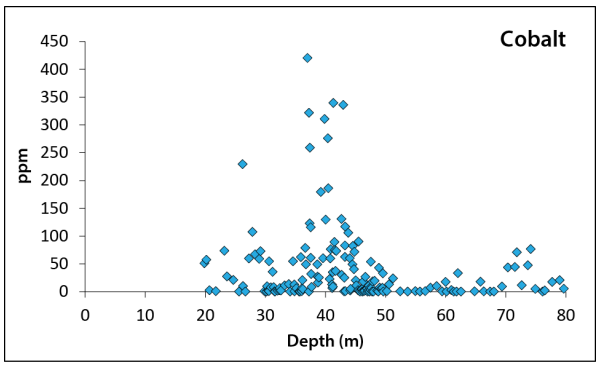

Fig. 20. Diagram showing Co concentrations in pyrite from the Lerhamn drill core. Measured values: highest = 420.1 ppm, lowest = 0.007 ppm and average = 41.32 ppm.

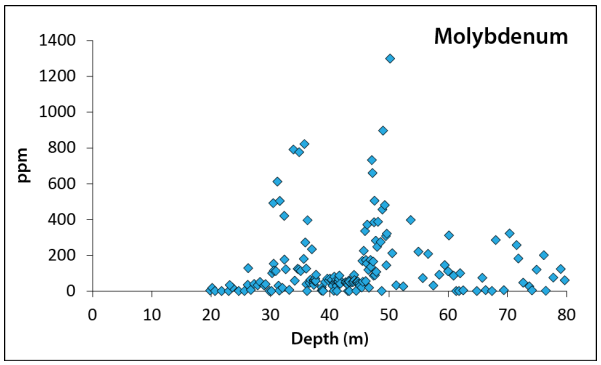

Fig. 21. Diagram showing Mo concentrations in pyrite from the Lerhamn drill core. Measured values: highest = 1299 ppm, lowest = 0.038 ppm and average = 140.57 ppm.

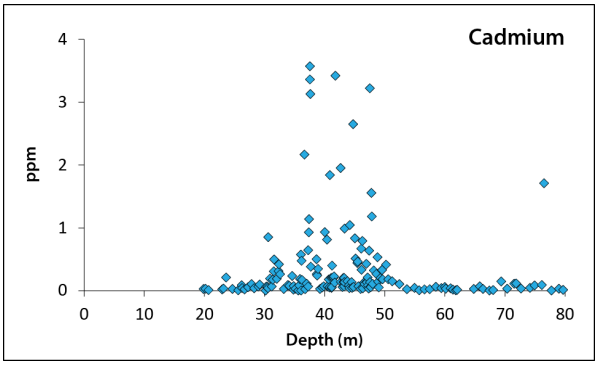

Fig. 22. Diagram showing Cd concentrations in pyrite from the Lerhamn drill core. Measured values: highest = 3.57 ppm, lowest = 0.001 ppm and average = 0.37 ppm.

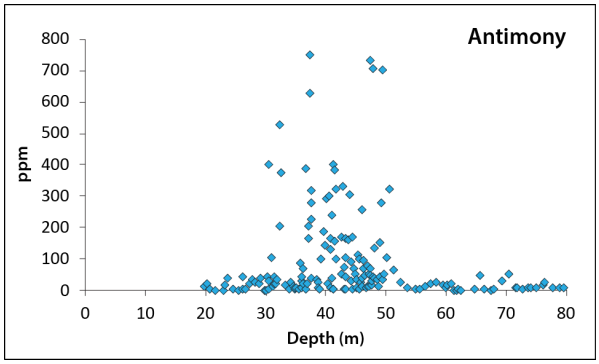

Fig. 23. Diagram showing Sb concentrations in pyrite from the Lerhamn drill core. Measured values: highest = 751 ppm, lowest = 0.0432 ppm and average = 92.04 ppm.

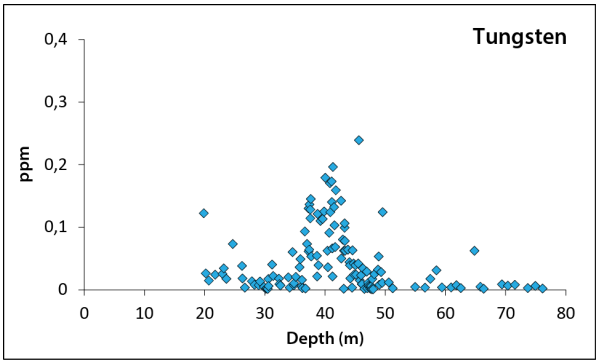

Fig. 24. Diagram showing W concentrations in pyrite from the Lerhamn drill core. Measured values: highest = 0.239 ppm, lowest = 0.0008 ppm and average = 0.045 ppm.

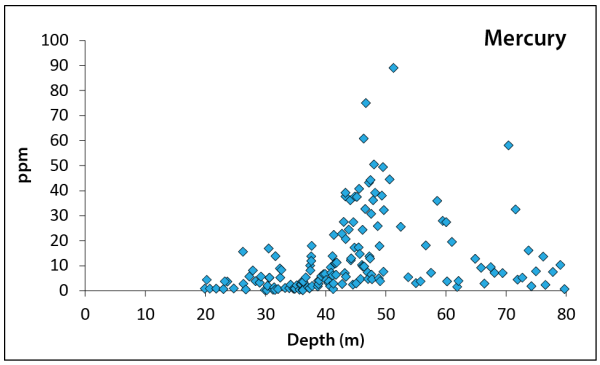

Fig. 25. Diagram showing Hg concentration in pyrite from the Lerhamn drill core. Measured values: highest = 319 ppm, lowest = 0.15 ppm and average = 15.75 ppm. Excluded points: 319 ppm (47.79 m) and 162.8 ppm (50.23 m).

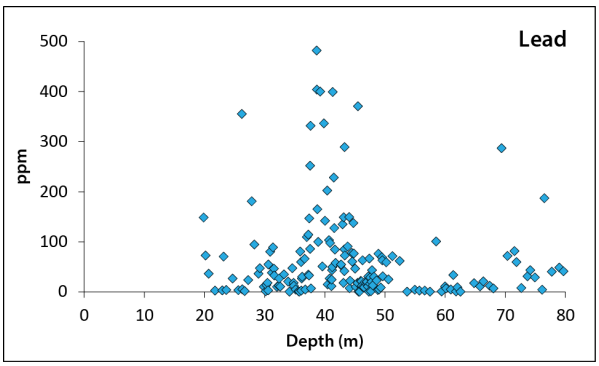

Fig. 26. Diagram showing Pb concentrations in pyrite from the Lerhamn drill core. Measured values: highest = 482 ppm, lowest = 0.0105 ppm and average = 64.42 ppm.

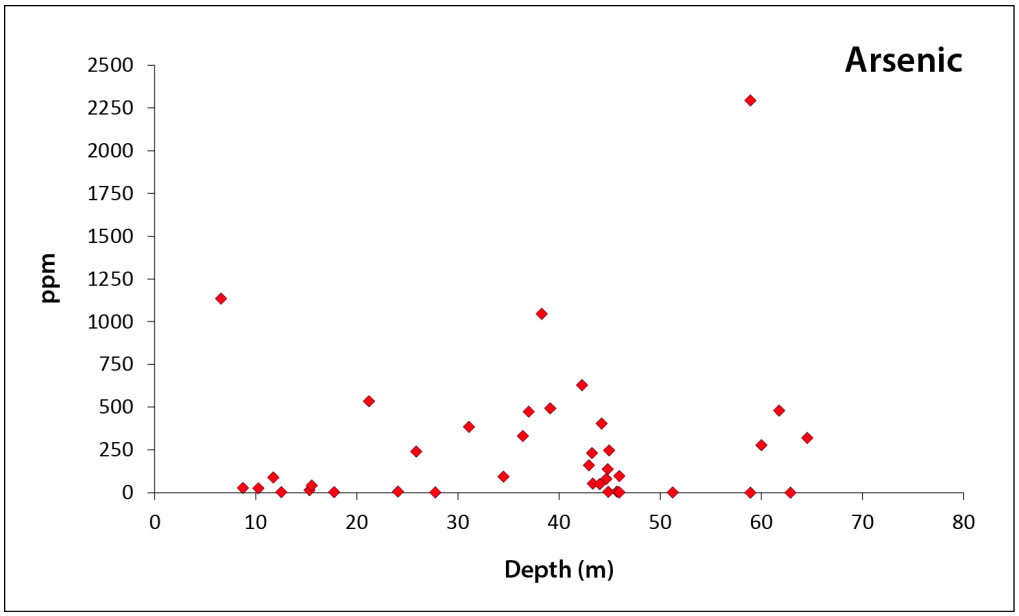

Fig. 27. Diagram showing arsenic concentrations in pyrite from the Fågelsång-3 drill core. Measured values: highest = 2295 ppm, lowest = 0.0076 ppm and average = 267.69 ppm.

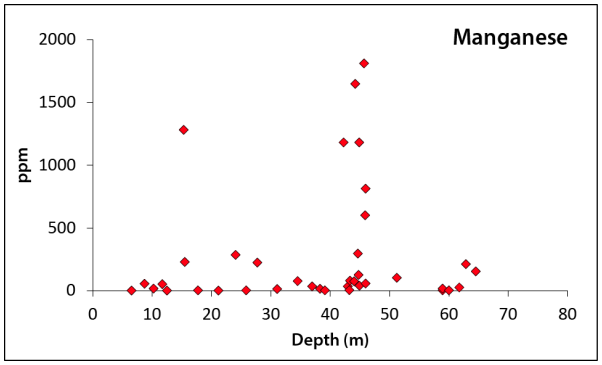

Fig. 28. Diagram showing Mn concentrations in pyrite from the Fågelsång-3 drill core. Measured values: highest = 1810 ppm, lowest = 0.06 ppm and average = 282.4 ppm.

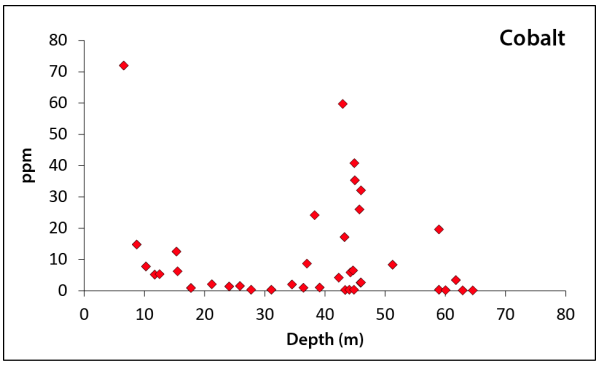

Fig. 29. Diagram showing Co concentrations in pyrite from the Fågelsång-3 drill core. Measured values: highest = 72 ppm, lowest = 0.066 ppm and average = 11.08 ppm.

Manganese, Co, Ag, Sb and Pb in the Fågelsång-3 drill core do, on the other hand, show an increase peaking at ca. 40 m respectively 45 m depth, similar to the Lerhamn drill core (Figs. 28–32). Looking at the As concentration, highest value measures 2295 ppm and lowest 0.076 ppm (Appendix E, Table E1). The average concentration is approximately 268 ppm.

7.3 Stratigraphical correlation

The Fågelsång-3 drill core succession consists predominantly of DI-2 to black shales, as a result of a high content of organic matter, probably due to deposition in a slightly O_2-deficient sea. It mainly comprises a stratigraphic interval dominated by Darriwilian strata. The Lerhamn drill core consists

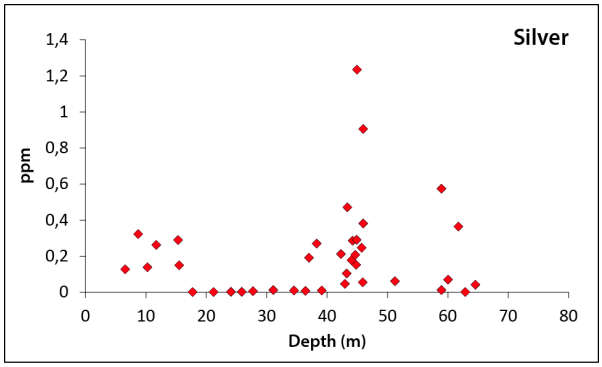

Fig. 30. Diagram showing Ag concentrations in pyrite from the Fågelsång-3 drill core. Measured values: highest = 1.234 ppm, lowest = 0.0004 ppm and average = 0.207 ppm.

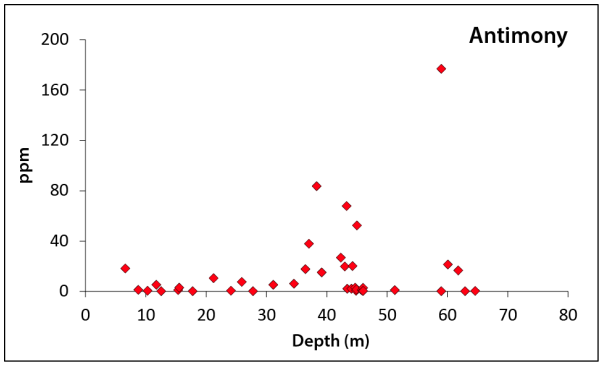

Fig. 31. Diagram showing Sb concentrations in pyrite from the Fågelsång-3 drill core. Measured values: highest = 176.8 ppm, lowest = 0.006 ppm and average = 16.07 ppm.

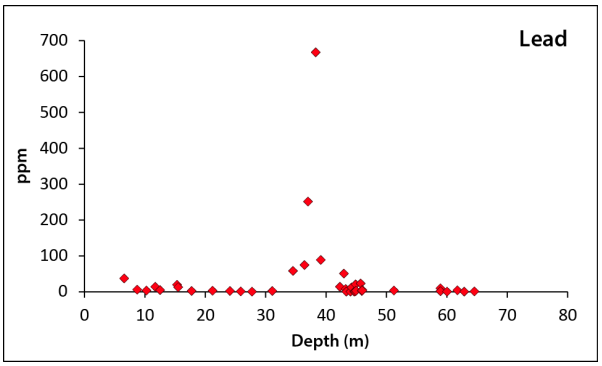

Fig. 32. Diagram showing Pb concentrations in pyrite from the Fågelsång-3 drill core. Measured values: highest = 667 ppm, lowest = 0.018 ppm and average = 36.03 ppm.

primarily of DI-1 and DI-2 shales belonging to the Tremadocian through lower Darriwilian stages. Furthermore, it should be noted that Komstad Limestone Formation is not present in the Lerhamn drill core. However, the graptolite stratigraphy (Maletz & Ahlberg, 2011b; Maletz & Ahlberg, 2017) shows that Komstad Limestone equivalents are represented by graptolitic shales in the Lerhamn drill core. Shales assigned to the *Arienigraptus zhejiangensis* and *Levisograptus sinicus* subzones are thus found in the upper part of the Lerhamn drill core and in the lower part of the Komstad Limestone in the Fågelsång-3 drill core. The Floian Stage seems to be missing in the Fågelsång-3 core, and most of the Dapingian is missing in both of the studied drill cores. An overview of the drill cores is shown in Figure 33.

7.4 Geochemical correlation

According to the geochemical data, analyzed pyrites show high As concentrations in both Lerhamn and Fågelsång-3 drill core with an average of 735.70 ppm and 267.69 ppm, respectively. We have thus an almost three times higher As concentration in the Lerhamn drill core compared to the Fågelsång-3 drill core. This significant contrast in concentration between the drill cores can be explained by the anomaly observed in Lerhamn at a depth of ca. 30–50 m (Fig. 17), which exhibits elevated concentrations, some of which are extreme, with up to 17660 ppm. Average As concentration for the anomaly measures 970.54 ppm (includes samples between 30.19–50.6 m depth), while the average As concentration above and below the anomaly is 220.87 ppm. The general As background concentration can therefore be approximated to around 221 ppm in Lerhamn and thus similar to the average in the Fågelsång-3 drill core. Figure 34 shows an overview of the As concentration of both drill cores merged together as illustrated in Figure 33.

Another stratigraphic part of interest is the overlapping interval between the two drill cores. This is important since this will give us a hint whether the high As concentration occurs locally, or could possibly be a global phenomenon occurring in shales from the same Ordovician stages. As mentioned earlier, the upper part (ca. 20.5 m) of the Lerhamn drill core is represented by a short overlapping interval in the lower part (ca. 6.5 m) of the Fågelsång-3 drill core (Fig. 33). The interval where the two drill cores overlap is therefore interesting for a comparison of the As concentration. Unfortunately, only two samples were extracted from this interval in the Fågelsång-3 drill core, and only one was analyzed, while a total of 17 samples were extracted and analyzed from the Lerhamn drill core. The highest As concentration measures 254.7 ppm, with an average of 91.69 ppm, for the Lerhamn drill core. This compared to the only one sample from the Fågelsång-3 drill core measuring 51.27 ppm. Since too few samples were extracted for analysis, a geochemical comparison for the interval between the two drill cores could not be done.

8 Discussion

8.1 Interpretation of data

Berner et al. (2013) conducted a study where they identified whether there is a connection between depositional conditions and pyrite trace-element composition. According to these authors, the site and mechanism for pyrite formation could be linked to trace-element contents in the pyrite. With the focus on diagenetic and syngenetic pyrites, the results showed that a high content of heavy metals was in general found in diagenetic pyrite formed within anoxic sediments. A low content of heavy metals is characteristic for syngenetic pyrite formed in euxinic environments, which are typically enriched in As, Mo and Bi. It should, however, be noted that this differs from site to site, and an overgeneralization of the result from this study should not be used as a direct transfer to results from other depositional sites (Berner et al., 2013). Looking at the data from the present study analyses,

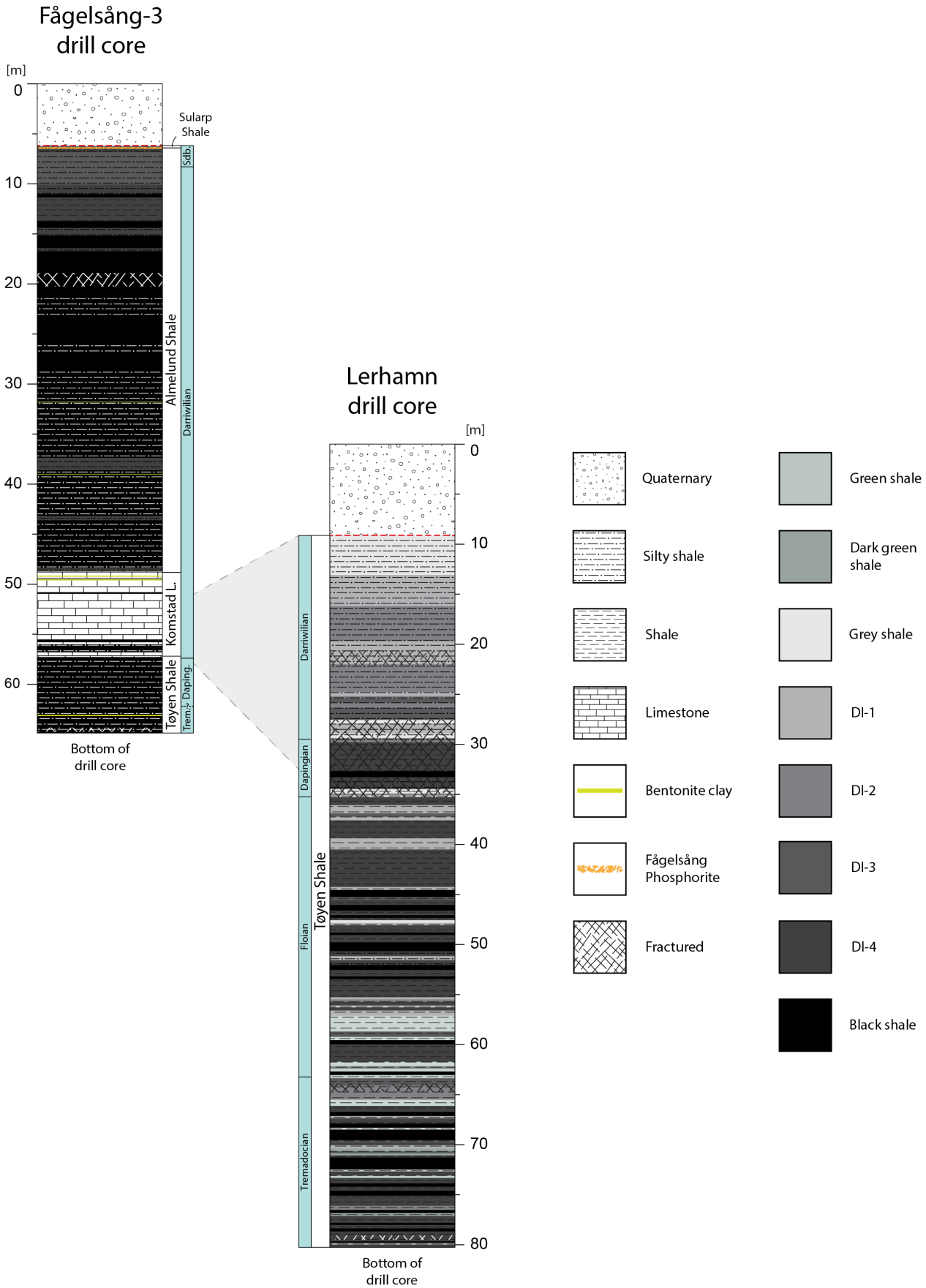

Fig. 33. Overview of the Fågelsång-3 and Lerhamn drill cores. Shaded area shows the stratigraphic overlap between the drill cores.

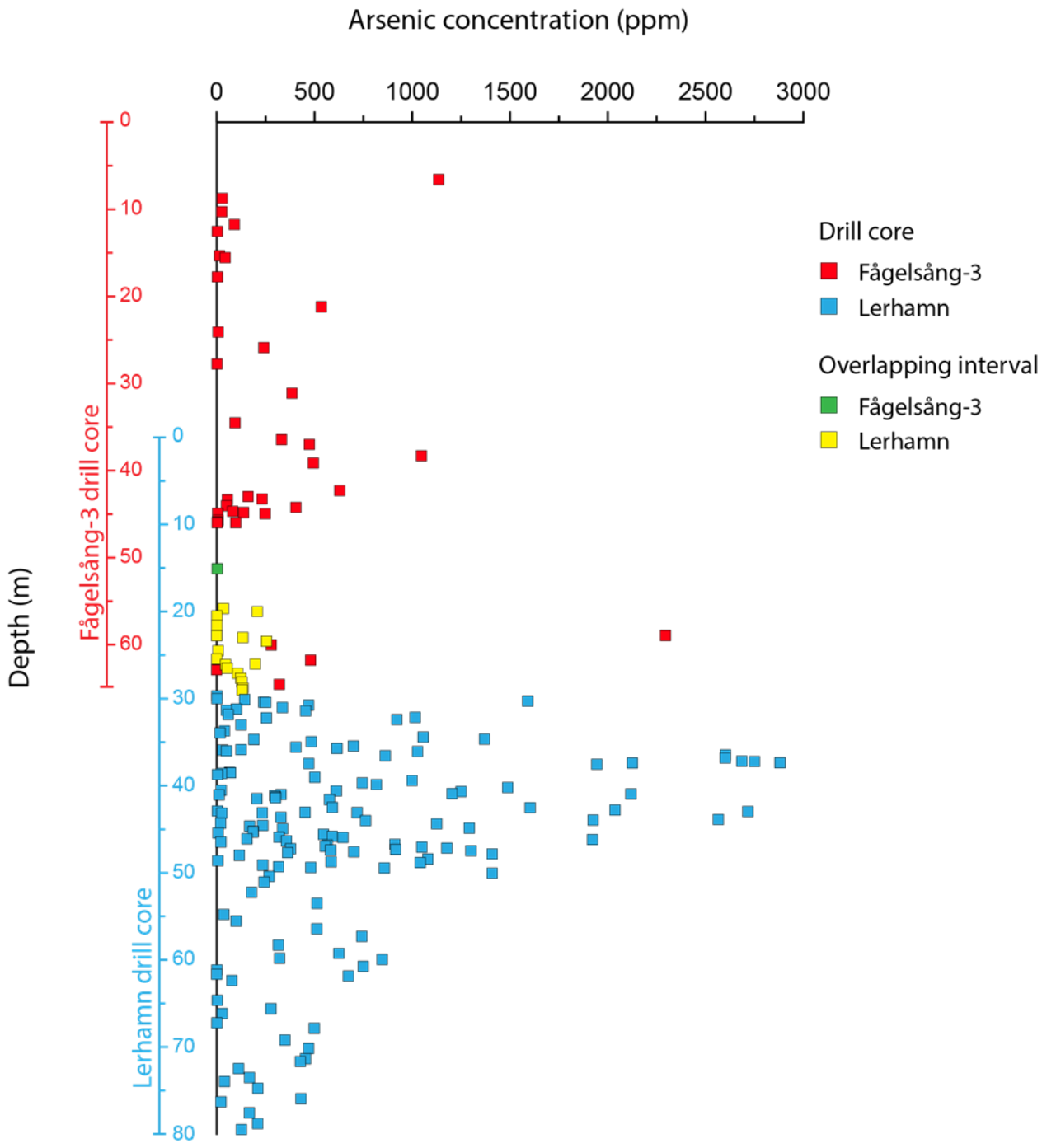

Fig. 34. Diagram showing an overview of the arsenic concentration of the Fågelsång-3 (red) and Lerhamn (blue) drill cores as portrayed in Figure 33. The interval where the drill cores overlap is shown in green and yellow color. Relative depth is displayed on the y-axis for respective core.

we do find high concentrations of heavy metals in both drill cores. These include Mn, Co, Cu, As, Se, Mo, Sb, Hg and Pb for the Lerhamn drill core. The same applies to the Fågelsång-3 drill core with the exception of Se and Hg (Table 2). As mentioned above, pyrite is generally diagenetically formed in muds and it often occurs in sediments that were formed under reducing conditions (Deer et al., 1992). The majority of the pyrite in the Lerhamn and Fågelsång-3 cores is found in DI-2 shales or black shales representing O_2-deficient (reducing) water, where black shale is indicative of highly dysoxic to anoxic water (Holland, 2017). Most of the pyrite found in our drill cores are thus interpreted as diagenetic pyrite formed in dysoxic to anoxic sediments.

Arsenic can derive from natural sources such as erosion and leaching from geological formations (Chung et al., 2014). Formation of iron sulfide minerals, like pyrite, is the main source of adsorption of As in anoxic environments (Bostick & Fendorf, 2003). Sedimentary pyrite is a known As-bearing sulfide and may contain concentrations of up to several weight percentages (Welch et al., 2000; Berner et al., 2013). Arsenic-bearing minerals are rarely found as inclusions, however, documentation from crystallochemical studies has showed that As has a preference for Fe and S substitution, two elements found in pyrite. The main mechanism that accounts for the uptake of As by pyrite is believed to derive from the sorption and co-precipitation of As with Fe-S mineral phases from As-rich water. Dysoxic to anoxic bottom water or pore water are two sources where As can be enriched (Berner et al., 2013).

Migration of As is highly affected by the strong sorption of clays, hydroxides and organic matter, limiting its mobility (Salminen et al., 2005). Both clays and organic matter are present in the Lerhamn and Fågelsång-3 drill cores. However, it is the organic matter in particular that is of great concern as high As concentrations may accumulate (Salminen et al., 2005). Arsenic is highly chalcophilic and, hence, has a high affinity for S. Sedimentary rocks, especially black shales, rich in organic matter are known to contain the highest S concentrations (Salminen et al., 2005; Albarede, 2011a). The accumulation of As in these sediments is therefore self-explanatory. Since the analyses in this study have been done on pyrite and not on shale, we do not know if the shale in the drill cores also contains high As concentrations. However, the XRF pilot study of the shale, which preceded the present study, showed similar As anomalies as the present LA-ICP-MS study of pyrite. This can be due to micro crystalline pyrite in the shale, or As absorbed by clay minerals or other minerals in the shale.

Increasing concentrations of dissolved sulfide in organic matter is promoted by bacterial reduction of seawater sulfate, but may also occur from volcanic activity (hot springs) (Mango & Ryan, 2015). However, our drill cores show no evidence of the latter. Sulfate contains both ^{32}S and ^{34}S, where the lighter isotope fractionates into dissolved sulfide in oxidizing to slightly reducing conditions. It then remains either as available sulfide or bonds with hydrogen to form H_2S, or with Fe to form pyrite. The heavier isotope, on the other hand, remains in the sulfate. In strongly reducing conditions, all available sulfate is reduced to dissolved sulfide, where the lighter isotope forms H_2S and the heavier isotope forms pyrite. As pyrite formation continues, the S supply will start to decrease, when soluble As becomes present it will substitute for S and adsorb into pyrite, increasing the As concentration (Mango & Ryan, 2015). In the study, Mango & Ryan (2015) shows a correlation between $\delta^{34}S$ and As, where increased $\delta^{34}S$ corresponded in general to high concentrations of As in pyrite (Fig. 35). High $\delta^{34}S$ reflects anoxic conditions when the As was incorporated in the pyrite. The analyses from the present study did not include any analyses of ^{32}S and ^{34}S, partly due to polyatomic interference, but mainly because we were only interested in the overall S concentration. Let's assume that the majority of the S in the pyrite is $\delta^{34}S$. At one point in time we must have had one or more events that resulted in severe dysoxia or anoxia, increasing the availability of $\delta^{34}S$ in the sediments in the Lerhamn drill core during the middle Floian to end of the Dapingian. More As could then accumulate, thus, giving rise to the anomaly with high concentrations of As seen at ca. 30–50 m depth (Fig. 17). The Ordovician Period is known to have experienced i.a. widespread volcanic activity, releasing high levels of CO_2 into the atmosphere, and intense tectonic activities with rapid plate movements, generating high rates of continental seafloor spreading (Munnecke et al., 2010; Cooper & Sadler, 2012; Holland, 2017). A global rise in atmospheric CO_2 in combination with the distribu-

Table 2: Average concentration of trace-elements in pyrite from Lerhamn and Fågelsång-3 drill cores. Note, W and Bi were not analyzed in the Fågelsång-3 drill core.

	Average ppm	
Elements	**Lerhamn**	**Fågelsång-3**
V	3.92	1.88
Cr	0.91	1.84
Mn	1325.31	282.4
Co	41.32	11.08
Cu	270.39	60.58
Ga	0.28	1.44
As	735.70	267.69
Se	29.75	8.12
Mo	140.57	106.17
Ag	7.17	0.21
Cd	0.37	0.075
Sb	92.04	16.07
W	0.045	–
Hg	15.75	0.38
Pb	64.42	36.03
Bi	0.036	–

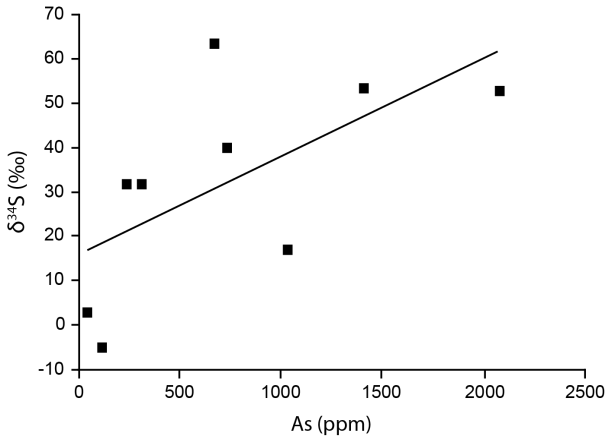

Fig. 35. Diagram illustrating correlation between $\delta^{34}S$ and As. Increased $\delta^{34}S$ are correlated with high arsenic concentration. Black dots represent studied samples from Mango & Ryan (2015). Modified from Mango & Ryan (2015).

tion of continental landmasses resulted in high global warming, an eustatic sea level rise and reduced oceanic circulation, leading to dysoxia and anoxia in marine basins (Munnecke et al., 2010; Mango & Ryan, 2015; Holland, 2017). One or more of the processes mentioned above may have caused conditions on a local scale that resulted in O_2-depleted conditions in the Lerhamn area, thus leading to an increase in As.

Other theories include a potential thrive in marine life in the Lerhamn area because of a transgression due to the eustastic sea-level rise during Floian times. A study by Li et al. (2017) showed a rapid increase in the diversity of graptolites in the Nanba section, in China, during the Floian–Dapingian. According to these authors, this coincided with a transgression, resulting in ecospace expansion during a sea-level rise (Li et al., 2017). Thriving of marine organisms lead to an increase in deposited organic material, which in turn promotes the anaerobic bacterial breakdown resulting in increased anoxic conditions and accumulation of S. Still another theory includes influx of S or As from nearby As-rich or S-rich areas that have been subjected to weathering. The influx of these elements may have occurred during a sea-level rise.

The results show a similar anomaly in the Lerhamn drill core for several heavy metals: V, Cr, Co, Mo, Cd, Sb, W, Hg and Pb, which coincide with the anomaly for As. Elements such as Cd, Sb, Hg and Pb are all chalcophilic and prefer bonding to S, whereas V is siderophile and Co, Mo and W are both chalcophile and siderophile (Salminen et al., 2005; Albarede, 2011a; Albarede, 2011b). Siderophile elements tend to bond with metallic Fe (Albarede, 2011b). Lastly, we have Cr, known for its ready substitution with Fe (Salminen et al., 2005). The exact cause for the anomaly for the heavy metals is hard to pin-point.

In the Fågelsång-3 drill core, we did not find any notable anomaly for As, however a minor anomaly peaking at around 40 m and 45 m, respectively, could be observed for the heavy metals Mn, Co, Ag, Sb and Pb. Their properties have been treated above, with the exception for Mn which readily substitutes for Fe, while Ag falls in the list among the chalcophile elements. The cause for the anomaly is assumed to be the same as with the Lerhamn drill core, based entirely on their properties.

8.2 Arsenic risk assessment

The relatively high concentrations of As in pyrite in the Lerhamn shale is of no concern in its present location. However, if these shales were excavated, crushed and deposited on the surface, exposed to the atmosphere, it would result in oxidation of the pyrite. This would then potentially increase the As and heavy metals in surface- and groundwaters, and could without precautions constitute a risk for the health of organisms.

A well-known example of how changes in the water chemistry can lead to catastrophic consequences is known from the Bengali region in India and Bangladesh. Farmers in the area used surface water for irrigation of crops yielding one harvest per year. By drilling wells, with help from international aid agencies, more water was available for irrigation, thus increasing the crop yield by 3–4 times (Selinus, 2010).

When these sediments formed, minerals including iron hydroxides were deposited. Bound to these iron hydroxides were, among other, As. Due to impermeable superficial layers, reducing conditions developed, resulting in As reduction from arsenate to arsenite. In addition, iron hydroxides dissolved. Changes in biochemical processes in combination with heavy water uptake led to As liberation into the water. As a result, over 200 000 people have been poisoned by As in Bangladesh, due to the high As concentration in the water. According to some sources it is believed that as many as 100 million people have been poisoned and have an increased risk of cancer (Selinus, 2010).

It is important to note that these sediments only contain moderate concentrations (<2–20 mg/kg) of As, which is fully comparable to normal concentrations as would be found in Swedish soil. The high accumulation of As in well water has simply risen from changes in the oxidation conditions (reduction of As) and the dissolution of the iron hydroxides. Another explanation given is that As has not leached from the soil, attributable to young sediments (Selinus, 2010).

There is a potential risk for local As-contamination of the environment if shale/pyrite with high As concentrations like those found between ca. 30–50 m in the Lerhamn drill core is exposed to surface conditions. The pyrite would readily oxidize, and As and heavy metals be released. The shale of Lerhamn type may occur in many locations in Scania and it is therefore advised to follow up on the mineralogy and geochemistry at building sites where the pyrite bearing Ordovician shale occurs. In case of high As and heavy metal content, the excavated rocks should be safely deposited to minimize oxidation of pyrite. Another

potential risk is if wells are drilled for production of water for consumption or irrigation. Pumping from the wells may change the oxidation/reduction conditions and eventually lead to an increased concentration of As and heavy metals. The result could be a modern Bangladesh scenario at a local scale.

8.3 Suggestions for future work

Due to limitations with regard to time and budget, this thesis only covers a small part of a broad study area. Further studies are required to fully understand the implications of As and heavy metals in the Ordovician environment at and around Lerhamn and Fågelsång. The following suggestions may be of interest for such further studies:

- Determine the As-concentration in the shale using LA-ICP-MS for more accurate results.
- Determine whether we have pyrite-zonation with regard to As. More than one generation of pyrite?
- Test whether the $\delta^{34}S$ and As correlation theory applies for the Lerhamn and Fågelsång-3 drill core.
- Do we find similar As-anomaly in other Ordovician shales elsewhere?
- Can the source(s) for the heavy metals be traced?

9 Conclusions

The Lerhamn and Fågelsång-3 drill cores are dominated by grey to black Ordovician shales. The Lerhamn drill core consists entirely of the Lower–Middle Ordovician Tøyen Shale Formation. The Fågelsång-3 drill core comprises, in descending order, the Upper Ordovician Sularp Shale, the Middle Ordovician Almelund Shale and Komstad Limestone formations, and the Lower–Middle Ordovician Tøyen Shale. Carbonates in the shale units are largely restricted to vertical and subvertical fractures. Pyrite of varying size, small irregular grains to larger well shaped crystals, are common throughout the entire succession in both drill cores.

The concentration of As in the Fågelsång-3 drill core ranges from 0.076 to 2295 ppm, with an average of 268 ppm. In the Lerhamn drill core, the concentration of As is generally higher, ranging from 0.04 to 17660 ppm. In average the As concentration in the Lerhamn core is 736 ppm. An As-anomaly is observed at ca. 30–50 m depth in the Lerhamn drill core, whereas no single significant As-anomaly was noted in the Fågelsång-3 drill core. The high concentration of As in both drill cores is a result of dysoxic to anoxic (bottom or pore) water. Interplay between high global warming, eustatic sea level rise and reduced oceanic circulation led to poorly oxygenized conditions in the marine basin during the Ordovician Period. This may have caused conditions on a local scale that resulted in O_2-depleted conditions during deposition of the Lerhamn succession. Other theories include thriving of marine organisms, leading to an increase in deposition of organic material, thus promoting anaerobic bacterial breakdown, resulting in generation of S. Another theory includes influx of S or As from nearby As-rich or S-rich areas.

In the Lerhamn drill core, there is a high concentration of the heavy metals Co, Mo, Sb, Hg and Pb, and an anomaly was observed for V, Cr, Co, Mo, Cd, Sb, W, Hg and Pb. In the Fågelsång-3 drill core, an anomaly peaking at 40 m and 45 m, respectively, was observed for Mn, Co, Ag, Sb and Pb, with high concentrations notable for Mn. The exact cause and source for the anomaly of the heavy metals is hard to pinpoint. However, the cause is assumed to be based entirely on their properties, being chalcophile or siderophile, thus having an affinity to bond to S or Fe, or substitute with Fe.

Shales enriched in trace-elements, such as those in the Lerhamn core, may occur at many locations in Scania. They pose a potential risk for local As-contamination of the environment if shale/pyrite with high As-concentrations like those at ca. 30–50 m are exposed to surface conditions. The pyrite would then oxidize and release As and heavy metals into the environment. Another potential risk involves the production of water for consumption or irrigation. This may change the oxidation/reduction conditions and eventually lead to an increased concentration of As and heavy metals. The result could be a potential contamination at a local scale.

10 Acknowledgements

First and foremost, I would like to express my sincere gratitude to Professor Leif Johansson and Professor Per Ahlberg, my supervisors, for the opportunity to work on this intriguing project, for their patient support and guidance, for all the comprehensive advices and constructive criticism, and for reviewing and helping to improve this thesis extensively. I would also like to thank Dr. Tomas Naeraa for his guidance and help running the LA-ICP-MS analyses, and for his useful insights and comments on the thesis. I would like to thank my fellow master students for the companionship and laughs that we shared, boosting the work morale till late hours. My grateful thanks are also extended to Joaen Stamsnijder for always taking the time to listen and exchange ideas, for all the useful tips, for the loyal companionship, and for tirelessly motivating and encouraging me throughout this thesis. Lastly, but most importantly, I would like to thank my beloved family from the bottom of my heart for always caring about my well-being, and for the unconditional love, support and encouragement throughout my studies – *të dua shumë dhe ju falenderoj përgjithmonë*.

11 References

Abernathy, C.O., Beringer, M., Calderon, R.L., McMahon, T. & Winchester, E., 2003: An update on some arsenic programs at the US EPA. *In* W.R. Chappell, C.O. Abernathy, R.L. Calderon & D.J. Thomas (eds): *Arsenic Exposure and Health Effects V*, 505–519. Elsevier, Amsterdam.

Albarede, F., 2011a: Chalcophile Elements. *In* M. Gargaud, R. Amils, J. Cernicharo Quintanilla, H.J. Cleaves, W.M. Irvine, D. Pinti & M. Viso (eds): *Encyclopedia of Astrobiology*. Springer, Berlin Heidelberg. Retrieved 2017-10-22, from http://www.oxfordreference.com.ludwig.lub.lu.se/view/10.1093/acref/9780199211944.001.0001/acref9780199211944-e-5893.

Albarede, F., 2011b: Siderophile Elements. *In* M. Gargaud, R. Amils, J. Cernicharo Quintanilla, H.J. Cleaves, W.M. Irvine, D. Pinti & M. Viso (eds): *Encyclopedia of Astrobiology*. Springer, Berlin Heidelberg. Retrieved 2017-12-14, from https://link.springer.com/referenceworkentry/10.1007%2F978-3-642-11274-4_1445 .

Andersson, M. & Ladenberger, A., 2010: Geokemiska kartan. Markgeokemi. Skåne och tätorterna Malmö, Lund och Helsingborg. *Sveriges geologiska undersökning K305*, 1–147.

Barnes, C.R., 2004: "Ordovician Oceans and Climate". *In* B.D. Webby, F. Paris, M.I. Droser & I.G. Percival (eds): *The Great Ordovician Biodiversification Event*, 72–76. Columbia University Press, New York.

Bergström, S.M. & Ahlberg, P., 2004: Guide to some classical Ordovician and Cambrian localities in the Fågelsång area, Scania, southern Sweden. *In* A. Munnecke, T. Servais & C. Schulbert (eds.): International Symposium on Early Palaeozoic Palaeogeography and Palaeoclimate, September 1–3, 2004, *Erlangen, Germany. Erlanger geologische Abhandlungen – Sonderband 5*, 81–90.

Bergström, S.M., Finney, S.C., Xu, C., Pålsson, C., Zhi-hao,W. & Grahn, Y., 2000: A proposed global boundary stratotype for the base of the Upper Series of the Ordovician System: The Fågelsång section, Scania, southern Sweden. *Episodes 23*, 102–108.

Bergström, S.M., Larsson, K., Pålsson, C. & Ahlberg, P., 2002: The Almelund Shale, a replacement name for the Upper *Didymograptus* Shale and the Lower *Dicellograptus* Shale in the lithostratigraphical classification of the Ordovician succession in Scania, southern Sweden. *Bulletin of the Society of Denmark 49*, 41–47.

Berner, R.A., 1984: Sedimentary pyrite formation: An update. *Geochimica et Cosmochimica Acta 48*, 605–615.

Berner, Z.A., Puchelt, H., Nöltner, T. & Kramar, U., 2013: Pyrite geochemistry in the Toarcian Posidonia Shale of south-west Germany: Evidence for contrasting trace-element patterns of diagenetic and syngenetic pyrites. *Sedimentology 60*, 548–573.

Berner, R.A. & Raiswell, R., 1983: Burial of organic carbon and pyrite sulfur in sediments over Phanerozoic time: a new theory. *Geochimica et Cosmochimica Acta 47*, 855–862.

Bingen, B., Andersson, J., Söderlund, U. & Möller, C., 2008: The Mesoproterozoic in the Nordic countries. *Episodes 31*, 29–34.

Bostick, B.C. & Fendorf, S., 2003: Arsenic sorption on triolite (FeS) and pyrite (FeS_2). *Geochimica et Cosmochimica Acta 67*, 909–921.

Boyle, R. & Jonasson, I., 1973: The geochemistry of arsenic and its use as an indicator element in geochemical prospecting. *Journal of Geochemical Exploration 2*, 251–296.

Burford, N., Carpenter, Y-Y., Conrad, E. & Saunders, C.D.L, 2011: The Chemistry of Arsenic, Antimony and Bismuth. *In* H. Sun (ed.): *Biological Chemistry of Arsenic Antimony and Bismuth*, 1–17. John Wiley & Sons, Ltd.

Calner, M., Ahlberg, P., Lehnert, O. & Erlström, M. (eds.), 2013: The Lower Palaeozoic of southern Sweden and the Oslo Region, Norway. Field Guide for the 3rd Annual Meeting of the IGCP project 591. *Sveriges geologiska undersökning Rapporter och meddelanden 133*, 1–96.

Chung, J.Y., Yu, S.D. & Hong, Y.S., 2014: Environmental Source of Arsenic Exposure. *Journal of Preventive Medical & Public Health 47*, 253–257.

Cocks, L.R.M. & Torsvik, T.H., 2002: Earth geography from 500 to 400 million years ago: a faunal and palaeomagnetic review. *Journal of the Geological Society, London, 159*, 631–644.

Cocks, L.R.M. & Torsvik, T.H., 2005: Baltica from the late Precambrian to mid-Palaeozoic times: The gain and loss of a terrane's identity. *Earth-Science Reviews 72*, 39–66.

Columbia Electronic Encyclopedia (C.E.E.), 6th ed. Q1 2017, p1-1, 1p. Columbia University Press, New York.

Cooper, R.A. & Sadler, P.M., 2012: The Ordovician Period. *In* F.M. Gradstein, J.G. Ogg, M. Schmitz & G. Ogg (eds): *The Geological Time Scale* 2012, 489–523. Elsevier B.V.

Cullen, W.R. & Reimer, K.J., 1989: Arsenic speciation in the environment. *Chemical Reviews 89*, 713–764.

Cullen, W.R. & Reimer, K.J., 2016: *Arsenic is Everywhere: Cause for Concern?*. Royal Society of Chemistry, Cambridge. 293 pp.

Deer, W. A., Howie, R. A. & Zussman, J., 1992: *An introduction to the rock-forming minerals*, 2nd ed. Longman, Harlow. 696 pp.

Del Razo, L.M., García-Montalvo, E.A., Valenzuela, O.L., 2003: Arsenic exposure alters purine metabolism in rats, mice and humans. *In* W.R. Chappell, C.O. Abernathy, R.L. Calderon & D.J. Thomas (eds): *Arsenic Exposure and Health Ef-*

fects V, 135–145. Elsevier, Amsterdam.

EFSA (European Food Safety Authority), 2014: Dietary exposure to inorganic arsenic in European population. EFSA Journal 2014;12(3):3597, 68 pp.

Erlström, M., Thomas, S. A., Deeks, N. & Sivhed, U., 1997: Structure and tectonic evolution of the Tornquist Zone and adjacent sedimentary basins in Scania and the southern Baltic Sea area. *Tectonophysics 271*, 191–215.

Fendorf, S., Nico, P.S., Kocar, B.D., Masue, Y. & Tufano, K.J., 2010: Arsenic Chemistry in Soils and Sediments. Retrieved 2017-04-11, from http://escholarship.org/uc/item/9jt907xz.

Foster, A.L., 2003: Spectroscopic investigation of arsenic species in solid phases. *In* A.H. Welch & K.G. Stollenwerk (eds): *Arsenic in Ground Water*, 27–65. Kluwer Academic Publishers, Boston.

Gee, D. G. & Stephenson, R. A., 2006: *European lithosphere dynamics*. Geological Society, London, Memoirs 32. 662 pp.

Haq, B.U. & Schutter, S.R., 2008: A Chronology of Paleozoic Sea-Level Changes. *Science 322*, 64–68.

Henke, R. K., 2009: Introduction. *In* K. Henke (ed.): *Arsenic Environmental Chemistry, Health Threats and Waste Treatment*, 1–7. John Wiley & Sons, Ltd.

Henke, R. K. & Hutchison, A., 2009: Arsenic Chemistry. *In* K. Henke (ed.): *Arsenic Environmental Chemistry, Health Threats and Waste Treatment*, 9–68. John Wiley & Sons, Ltd.

Holland, S.M., 2017: Ordovician Period. Encyclopædia Britannica inc. Retrieved 2017-10-22, from https://www.britannica.com/science/Ordovician-Period/Regional-extinctions-within-the-Ordovician.

Hu, Y., Jin, X., Wang, G. and Snow, E.T., 2003: Alteration of GSH level, gene expression and cell transformation in NIH3T3 cells by chronic exposure to low dose of arsenic. *In* W.R. Chappell, C.O. Abernathy, R.L. Calderon & D.J. Thomas (eds): *Arsenic Exposure and Health Effects V*, 167–177. Elsevier, Amsterdam.

Hughes, M.F., 2002: Arsenic toxicity and potential mechanisms of action. *Toxicology Letters 133*, 1–16.

Hughes, M.F., Thomas, D.J. & Kenyon, E., 2009: Toxicology and Epidemiology of Arsenic and its Compounds. *In* K. Henke (ed.): *Arsenic Environmental Chemistry, Health Threats and Waste Treatment*, 237–275. John Wiley & Sons, Ltd.

Jaanusson, V., 1976: Faunal dynamics in the Middle Ordovician (Viruan) of Balto-Scandia. *In* M.G. Bassett (ed.): *The Ordovician System: Proceedings of a Palaeontological Association Symposium, Birmingham, September 1974*, 301–326. University of Wales Press and National Museum of Wales, Cardiff.

Jenkins, D., 1980: *Biological monitoring of toxic trace metals*. Volume 2. Toxic trace metals in plants and animals of the world. Part I (Vol. 2). Washington, D.C.: U.S. Environmental Protection Agency.

Koljonen, T., 1992: *The geochemical atlas of Finland, part 2: Till.* Espoo: Geological Survey Finland. 218 pp.

Li, L.X., Feng, H.Z., Wang, W.H. & Chen, W.J., 2017: Graptolite diversification during the Floian and Dapingian (Early–Middle Ordovician): A case study from the Ningkuo Formation of Hunan Province, China. *Palaeoworld 26*, 431–443.

Liu, J., Chen, H., Kadiiska, M., Xie, Y. & Waalkes, M.P., 2003: Application of filter arrays to the study of arsenic toxicity and carcinogenesis. *In* W.R. Chappell, C.O. Abernathy, R.L. Calderon & D.J. Thomas (eds): *Arsenic Exposure and Health Effects V*, 295–303. Elsevier, Amsterdam.

Liu, Z., Mukhopadhyay, R., Shi, J., Ye, J. & Rosen, B.P., 2003: Structural proteomics of arsenic transport and detoxification. *In* W.R. Chappell, C.O. Abernathy, R.L. Calderon & D.J. Thomas (eds): *Arsenic Exposure and Health Effects V*, 241–253. Elsevier, Amsterdam.

Livsmedelsverket, 2017: "Arsenik". Retrieved 2017-10-12, from https://www.livsmedelsverket.se/livsmedel-och-innehall/oonskade-amnen/metaller1/arsenik.

Maletz, J. & Ahlberg, P., 2011a: Darriwilian (Ordovician) graptolite faunas and provincialism in the Tøyen Shale of the Krapperup drill core (Scania, southern Sweden). *In* J.C. Gutiérrez-Marco, I. Rábano & D. Garcí-Bellido (eds): *Ordovician of the world*. Cuadernos del Museo Geominero, 14. Instituto Geológico y Minero de España, Madrid, 3–9.

Maletz, J. & Ahlberg, P. 2011b: The Lerhamn drill core and its bearing for the graptolite biostratigraphy of the Ordovician Tøyen Shale in Scania, southern Sweden. *Lethaia 44*, 350–368.

Maletz, J. & Ahlberg, P., 2017 (in preparation): Preliminary graptolite biostratigraphy of the Fågelsång-3 drillcore.

Mango, H. & Ryan, P., 2015: Source of arsenic-bearing pyrite in southwestern Vermont, USA: Sulfur isotope evidence. *Science of the Total Environment 505*, 1331–1339.

Mason, B. & Berry, L.G., 1968: *Elements of mineralogy*. W.H. Freeman and Company, San Francisco. 500 pp.

Matschullat, J., 2000: Arsenic in the geosphere - A review. *The Science of the Total Environment 249*, 97–312.

Moberg, J.C., 1910: Guide for the principal Silurian districts of Scania (with notes on some localities of Mesozoic beds). *Geologiska Föreningens i Stockholm Förhandlingar 32*, 45–194.

Mukherjee, S., 2011: *Applied Mineralogy – Applications in Industry and Environment*. Springer, Dordrecht. 575 pp.

Munnecke, A., Calner, M. & Harper, D.A.T., 2010: How does sea level correlate with sea-water chemistry? A progress report from the Ordovician and Silurian. *Palaeogeography, Palaeoclimatology, Palaeoecology 296*, 213–216.

Nielsen, A.T, 2004: Ordovician Sea Level Changes: A Baltoscandian Perspective. *In* B.D. Webby, F. Paris, M.I. Droser & I.G. Percival (eds): *The Great Ordovician Biodiversification Event*, 84–93. Columbia University Press, New York.

Persson, A., 2017: Arsenik. Karolinska Institutionen, the institute for Environmental Medicine. Retrieved 2017-10-11, from http://ki.se/imm/arsenik.

Pichon, A., 2013: Arsenic complexes: Mellow yellow. *Nature Chemistry 5*, 78.

Price, R.E. & Pichler, T., 2005: Distribution, speciation and bioavailability of arsenic in a shallow-water submarine hydrothermal system, Tutum Bay, Ambitle Island, PNG. *Chemical Geology 224*, 122–135.

Redman, A., Macalady, D.L. & Ahmann, D., 2002: Natural Organic Matter Affects Arsenic Speciation and Sorption onto Hematite. *Environment Science and Technology 36*, 2889–2896.

Rickard, D., 2015: Pyrite – *A Natural History of Fool's Gold*. Oxford University Press, New York. 297 pp.

Rossman, T.G., Uddin, A.N., Burns, F.J. & Bosland, M.C., 2003: Does arsenic require a carcinogenic partner?. *In* W.R. Chappell, C.O. Abernathy, R.L. Calderon & D.J. Thomas (eds): *Arsenic Exposure and Health Effects V*, 197–209. Elsevier, Amsterdam.

Salminen, R. (Chief-editor), Batista, M.J., Bidovec, M., Demetriades, A., De Vivo, B., De Vos, W., Duris, M., Gilucis, A., Gregorauskiene, V., Halamic, J., Heitzmann, P., Lima, A., Jordan, G., Klaver, G., Klein, P., Lis, J., Locutura, J., Marsina, K., Mazreku, A., O'Connor, P.J., Olsson, S.Å., Ottesen, R.T., Petersell, V., Plant, J.A., Reeder, S., Salpeteur, I., Sandström, H., Siewers, U., Steenfelt, A. & Tarvainen, T., 2005: *Geochemical Atlas of Europe. Part 1 – Background Information, Methodology and Maps*. Espoo, Geological Survey of Finland. 526 pp.

Selinus, O., 2010: Arsenik – ett giftigt element. *In* O. Selinus (ed.): *Medicinsk geologi*, 331–355. Studentlitteratur AB, Lund.

Selinus, O., Cave, M., Kousa, A., Steinnes, E., Varet, J. & Ferreira da Silva, E., 2010: Medical Geology in Europe. *In* O. Selinus, R.B. Finkelman & Centeno, J.A. (eds.): *Medical Geology – A regional synthesis*, 259–303. Springer, Dordrecht.

Servais, T. & Harper, D.A.T, 2018: The Great Ordovician Biodiversification Event (GOBE): definition, concept and duration. *Lethaia*. DOI: 10.1111/let.12259

Smedley, P.L. & Kinniburgh, D.G., 2002: A review of source, behaviour and distribution of arsenic in natural waters. *Applied Geochemistry 17*, 517–568.

Snow, E.T., Hu, Y., Klein, B.C., McCluskey, K.L., Schuliga, M. & Sykora, P., 2003: Regulation of redox and DNA repair genes by arsenic: low dose protection against oxidative stress?. *In* W.R. Chappell, C.O. Abernathy, R.L. Calderon & D.J. Thomas (eds): *Arsenic Exposure and Health Effects V*, 305–319. Elsevier, Amsterdam.

Stollenwerk, K.G., 2003: Geochemical processes controlling transport of arsenic in groundwater: a review of adsorption. *In* A.H. Welch & K.G. Stollenwerk (eds): *Arsenic in Ground Water*, 67–100. Kluwer Academic Publishers, Boston.

Stouge, S. and Nielsen, A.T., 2003. An intergrated biostratigraphical analysis of the Volkhov-Kunda (Lower-Ordovician) succession at Fågelsång, Scania, Sweden. *Bulletin of the Geological Society of Denmark 50*, 75–94.

Stow, D.A.V., 2005: *Sedimentary Rocks in the Field: A Color Guide*. Elsevier, Burlington. 320 pp.

Tchounwou, P.B., Udensi, U.K., Isokpehi, R.D., Yedjou, C.G. & Kumar, S., 2015: Arsenic and Cancer. *In* S.J.S. Flora (ed.): *Handbook of Arsenic Toxicology*, 533–555. Academic Press. 752 pp.

Trouba, K., Nyska, A., Styblo, M., Dunson, D., Lomnitski, L., Grossman, S., Moser, G., Suttie, A., Patterson, R., Walton, F. & Germolec, D., 2003: Effect of antioxidants on the papilloma response and liver glutathione modulation mediated by arsenic in Tg.AC transgenic mice. *In* W.R. Chappell, C.O. Abernathy, R.L. Calderon & D.J. Thomas (eds): *Arsenic Exposure and Health Effects V*, 283–293. Elsevier, Amsterdam.

Tucker, M.E., 2011: *Sedimentary Rocks in the Field: A Practical Guide*. 4th ed. John Wiley & Sons, Chichester. 275 pp.

Vaughan, D.J. & Craig, J.R., 1978: *Mineral chemistry of metal sulfides*. Cambridge University press. 493 pp.

Wei, M., Wanibuchi, H., Morimura, K. & Fukushima, S., 2003: Carcinogenicity of dimethylarsinic acid and relevant mechanisms. *In* W.R. Chappell, C.O. Abernathy, R.L. Calderon & D.J. Thomas (eds): *Arsenic Exposure and Health Effects V*, 211–222. Elsevier, Amsterdam.

Welch, A.H., Westjohn, D.B., Helsel, D.R. & Wanty, R.B., 2000: Arsenic in Ground Water of the United States: *Occurrence and Geochemistry. Ground Water 38*, 589–604.

Wenzel, W.W., 2013: Arsenic. *In* B.J. Alloway (ed.): *Heavy Metals in Soils: Trace Metals and Metalloids in Soils and their Bioavailability*, 241–282. Springer, Dordrecht.

Yang, J., Kim, Y., Kim, J. & Park, Y., 2000: Environmental impacts and management strategies of trace metals in soil and groundwater in the Republica of Korea. *In* J. Huang & I. Iskander (eds): *Soil and groundwater pollution and remediation: Asia, Africa, and Oceania*, 270–289. Boca Raton: CRC Press/Lewis Publishers.

Appendix A

Description of the Lerhamn drill core. DI-1–DI-4 refers to the darkness of grey shales, ranging from 1 to 4, where 4 is almost black. Carbonates are dominated by thin limestone beds. Other types of carbonates include calcite veins in fractures.

Depth (m)	Description
Lerhamn – box 1	
8.97–9.07	***Gravel:*** subrounded, subangular. Well graded, 8–50 mm in size.
9.07–10.26	***Mix of gravel and grey shale*** *(9.07–9.13 m),* ***grey shale*** *(9.13–9.62 m and 9.69–10.26 m)* and ***DI-4 shale*** *(9.62–9.69 m)****:*** silty (low). High carbonate content (seen as veins). Oxidized iron (pyrite or other Fe-mineral) at 9.8 m.
10.20–11.35	***Grey shale:*** silty (high, with a decrease to moderate down-section). Moderate carbonate content (interspersed in fractures in the shale at 10.8 m and 11.13 m). Oxidized pyrite at 10.42 m, 10.53 m, 10.56 m, 10.58 m, 10.61 m and 10.64 m.
11.27–12.09	***Grey shale*** *(11.27–11.75 m),* ***DI-1 shale*** *(11.75–11.79 m)* and ***grey shale*** *(11.79–12.09 m)****:*** silty (low, decreases with depth to almost nothing). Very low to high carbonate content (interspersed in fractures at 11.27–11.75 m).
12.09–13.06	***DI-4/black shale*** *(12.09–12.13 m)* and ***grey shale*** *(12.13–13.06 m)****:*** no silt or carbonate content at 12.09–12.13 m. Low amount of silt and moderate to high carbonate content at 12.13–13.06 m. Oxidized pyrite at 12.94 m.
Lerhamn – box 2	
13.06–13.97	***DI-1 shale:*** silty (low to moderate amount). Moderate carbonate content (partly containing high amount). Oxidized pyrite at 13.95 m. Graptolite at 13.03 m.
13.79–14.69	***DI-1 shale*** *(13.79–14.22 m and 14.36–14.69 m)* and ***DI-3 shale*** *(14.22–14.36 m)****:*** silty (low). Moderate carbonate content at 13.79–14.10 m and low carbonate content at 14.10–14.69 m. Oxidized pyrite at 14.18 m.
14.21–15.22	***DI-1 shale:*** silty (high). High carbonate content. Possibly clay with high concentration of carbonate can be observed as well. Oxidized pyrite at 14.60 m and 14.70 m.
15.22–16.20	***DI-1 shale:*** silty (moderate). High carbonate content as calcite-filled, subvertical fractures in the upper part and interspersed in fractures down-section. Oxidized pyrite at 15.95 m.
Lerhamn – box 3	
16.00–17.00	***DI-2 shale:*** silty (low). Moderate carbonate content, mostly as calcite-filled, subvertical fractures or interspersed in fractures. Phosphatic brachiopod at 16.18 m.
17.00–17.80	***DI-2 shale:*** silty (low). Moderate carbonate content, but not to the same extent as above (an increase of calcite-filled, subvertical fractures). Oxidized pyrite at 17.52 m. Pyrite at 17.15 m. Graptolite at 17.52 m. The shale is moderately glossy at 17.73–17.80 m.
17.80–18.70	***DI-2 shale:*** silty (low). Moderate carbonate content. Oxidized pyrite at 17.87 m, 18.10 m, 18.20 m and 18.23 m. Graptolites at 17.80 m, 18.15 m, 18.23 m, 18.33 m, 18.40 m, 18.48 m, 18.66 m and 18.70 m. The shale is moderately glossy at 17.76–17.80 m and moderately glossy biotite appearance at 17.99–18.08 m.
18.70–19.70	***DI-2 shale:*** silty (very low to low amount). Moderate carbonate content; very low at the upper part and a substantial increase down-section (mostly calcite-filled, subvertical fractures at 19.05–19.70 m). Oxidized pyrite at 18.85 m and 19.07 m. Pyrite at 18.87 m (3 mm, shiny), 18.88 m, 19.07 m and 19.18–19.30 m. Graptolites at 18.71 m, 18.79 m, 18.87 m, 18.88 m, 18.94 m, 18.97 m, 18.99 m, 19.01 m and 19.63 m. Brachiopod at 19.60 m.

Depth (m)	Description
Lerhamn – box 4	
19.60–20.48	***DI-1 shale:*** silty (moderate). Moderate carbonate content, calcite-filled, subvertical fractures (increases down-section) and interspersed in fractures. Intervals with oxidized pyrite. Pyrite at 19.86 m, 19.90 m, 19.92 m, 20.03 m, 20.20 m, 20.22 m, 20.34 m and 20.40 m. Graptolites at 19.62 m, 19.77 m, 19.88 m, 20.05 m, 20.15 m and 20.21 m.
20.30–21.30	***DI-1 shale:*** silty (moderate, increasing down-section). Carbonate content; calcite-filled, subvertical fractures (thicker at 20.30–20.80 m) and interspersed in fractures at 20.80–21.30 m. Pyrite at 20.35 m, 20.42 m, 20.52 m, 20.59 m, 20.68 m, 20.70 m, 20.80 m, 20.90 m, 21.00 m, 21.10 m and 21.17 m. Fractured at 20.63–20.70 m, 20.88–21.00 m (less fractured) and 21.15 m (more fractured).
21.10–22.00	***DI-1 shale:*** silty (high, specifically around the fractured zone). High carbonate content (white, thick carbonate vein at 21.10–21.37 m). Oxidized pyrite at 21.35 m, 21.43 m, 21.45 m, 21.50 m, 21.55 m and 21.85 m. Pyrite at 21.40 m (very little), 21.50 m, 21.80 m, 21.85 m and some in the fracture zone. Graptolite at 21.64 m. Fracture zone at 21.10–21.50 m, filled with carbonate and minor quartz. Also present at 21.80–22.10 m.
22.00–23.00	***DI-2 shale:*** silty (low). Moderate carbonate content (calcite-filled, subvertical fractures and interspersed in fractures). Pyrite at 22.07 m, 22.20 m (well-preserved pyrite), 22.36 m (pyrite crystal), 22.60 m, 22.74 m (matte pyrite) and 22.88 m (well-preserved pyrite). Slightly glossy throughout the core.
Lerhamn – box 5	
22.70–23.70	***DI-2 shale:*** silty (low, increasing to moderate down-section). Moderate carbonate content (calcite-filled, subvertical fractures and interspersed in fractures). Oxidized pyrite 22.96 m and 23.55 m. Pyrite at 22.75 m, 22.96 m and 23.50 m. Graptolites at 22.77 m, 22.80 m, 22.88 m, 22.90 m, 23.22 m, 23.50–23.60 m and 23.70 m. Fracture zone similar to the one seen in box 4 (21.10–22.00 m).
23.50–24.50	***DI-2 shale:*** silty (high, decreasing down-section). Moderate carbonate content, majority as calcite-filled, subvertical fractures and minor interspersed in fractures (dominating at 24.27–24.50 m). Oxidized pyrite at 23.67 m. Pyrite at 23.60 m, 23.62 m, 23.70 m, 23.74 m, 23.78–23.86 m, 23.90 m, 23.95 m, 24.00 m and 24.17 m. Graptolite at 24.27 m, 24.30 m, 24.37 m and 24.43 m. Quartz at 23.60 m, 23.63 m and 23.65 m (25 mm).
24.40–25.38	***DI-2 shale*** *(24.40–24.77 m and 24.93–25.02 m)* and ***DI-1 shale*** *(24.77–24.93 m and 25.02–25.17 m)**:*** silty (low). Moderate carbonate content, calcite-filled, subvertical fractures (dominates at 24.70–25.38 m) and interspersed in fractures. Pyrite at 24.44 m and 24.68 m (very small mineral grain). Graptolite at 24.40 m, 24.42 m, 24.50 m, 24.57 m, 24.60 m, 24.72 m, 24.73 m, 24.80 m, 24.99 m and 25.15 m.
25.30–26.30	***DI-3 shale*** *(25.30–25.78 m)* and ***DI-2 shale*** *(25.78–26.30 m)**:*** silty (low, with increase to moderate at 26.10–26.30 m). Almost free from carbonate (with a minor increase at 26.00–26.30 m, as calcite-filled, subvertical fractures). Pyrite at 25.32 m, 25.35 m, 25.45 m and 25.60–25.90 m (very small mineral grains spread across). Graptolite at 25.35 m, 25.57 m, 25.60 m, 25.70 m, 25.80 m and 25.90 m.
Lerhamn – box 6	
26.10–27.00	***DI-3 shale:*** silty (low, decreasing down-section to almost nothing). Moderate carbonate content (decreasing down-section). Pyrite at 26.20 m, 26.25 m, 26.27–26.30 m, 26.46 m (15 mm, matte), 26.47 m (4 mm, matte), 26.49 m, 26.69 m and 26.95 m. Graptolite at 26.12 m, 26.42 m, 26.43 m, 26.50 m, 26.76 m, 26.84 m and 27.00 m.
27.00–27.55	***DI-3 shale:*** silty (low). Very low carbonate content. Pyrite at 27.03 m, 27.14 m, 27.16 m and 27.23–27.38 m (spread across). Graptolite at 27.06 m, 27.15 m and 27.48 m.

Depth (m)	Description
27.55–27.65	***Grey shale:*** silty (high). High carbonate content (with a mix of silt). Oxidized pyrite at 27.69 m. The core is broken into pieces (previously a fracture zone?).
27.65–27.90	***Grey shale:*** silty (moderate). Low carbonate content (spread across). Pyrite at 27.83–27.93 m. The interval is a minor fracture zone.
27.90–28.90	***DI-1 shale:*** silty (low). Moderate carbonate content. A mix of oxidized pyrite and pyrite throughout the interval. The entire interval is a fracture zone, however, less affected compared to the interval at 27.65–27.90 m. Slightly glossy at 28.10–28.50 m and moderately glossy at 28.50 m.
28.80–29.80	***DI-2 shale*** *(28.80–28.98 m)*, ***grey shale*** *(28.98–29.33 m)* and ***DI-2 shale*** *(29.33–29.80 m)**:*** no silt at 28.80–28.98 m and 29.33–29.80 m and moderately silty at 28.98–29.33 m. Low carbonate content (mostly in fractures). Pyrite at 29.21 m, 29.39 m, 29.74 m (6 mm, matte) and 29.76 m (8 mm, matte). Fractured throughout the interval, however, less affected compared to the interval at 27.90–28.90 m. Slightly glossy–moderately glossy at 28.80–28.98 m and moderately glossy at 28.98–29.80 m.
Lerhamn – box 7	
29.70–30.70	***DI-4 shale:*** no silt (minor increase at 30.28–30.46 m). Low carbonate content (mostly in veins). Pyrite at 29.82 m (25 mm in size), 29.88 m, 30.48 m, 30.55 m and 30.59 m. Graptolite at 30.17 m and 30.55 m. Around 30.34–30.46 m there is a thin clay bed. Fractured throughout the interval, similar to box 6 at 27.90–28.90 m. Moderately glossy in the upper part and increases down-section.
30.60–31.60	***DI-4 shale:*** no silt. Low carbonate content (mostly in fractures). Pyrite at 30.62 m, 30.98 m and 30.90 m. Graptolite at 30.75 m and 30.88 m. Fractured at 30.90–31.60 m (not to the same extent as seen in 29.70–30.70 m) with thin clay beds at 30.92–31.02 m. Moderately glossy at 31.20 m and increases down-section to moderately glossy biotite appearance.
31.50–32.50	***DI-4 shale:*** no silt. Low carbonate content (more than the interval above), some intervals have a higher content, while other lack carbonate. Pyrite at 31.63 m, 31.79 m, 31.90–32.00 m (matte in color) and 32.33–32.34 m. Fractured at 31.50–31.60 m and 31.83–32.50 m. Slightly glossy at 31.50–31.85 m, mix of moderately glossy biotite appearance and partly moderately glossy at 31.85–32.20 m, moderately glossy biotite appearance at 32.20–32.30 m and putative biotite at 32.30–32.50 m.
32.30–33.30	***DI-4 shale*** *(32.30–32.65 m and 33.06–33.30 m)* and ***black shale*** *(32.65–33.06 m)**:*** no silt. Very low carbonate content (mainly in veins). Pyrite at 32.38 m (large nodule, 25 mm in size) and 33.16 m. Clay bed at 32.56–32.63 m. Biotite(?) at 32.30–32.56 m. Moderately glossy at 32.65–33.30 m.
Lerhamn – box 8	
33.30–33.50	***DI-4 shale:*** silty (moderate). Low carbonate content. Moderately glossy biotite appearance to moderately glossy.
33.50–34.20	***DI-4 shale/DI-3 shale/DI-2 shale (mix):*** very low amount of silt. Moderate carbonate content, mostly in the fractures (white veins can be observed). Pyrite at 33.70 m, 33.78 m and 33.79 m. Graptolite at 33.70 m. Very fractured interval, with numerous fractures. Presumed gypsum-clay(?) layer, light grey-white in color can be observed.
34.10–34.47	***DI-4 shale:*** no silt. Very low carbonate content (in fractures). Pyrite at 34.10–34.30 m (very small grains). Fractured throughout the interval (continuation from interval above). Partly moderately glossy biotite appearance, otherwise moderately glossy.
34.47–34.92	***Grey-white shale:*** no silt. Moderate carbonate content (found in fractures). Fractured throughout the interval (as the one above). Presumed gypsum-clay(?) layer, grey-white in color, with carbonate intercalations can be observed.

Depth (m)	Description
34.92–35.10	***DI-2 shale:*** very low amount of silt. Moderate carbonate content (in fractures). At the base of the interval, a 10 mm wide layer containing high concentration of carbonate can be observed. Fractured throughout the interval (like the one above).
35.10–35.28	***Grey-white shale:*** low amount of silt. Moderate carbonate content (in fractures, some containing a high concentration). Three very small pyrite grains can be observed. Fractured as the one above. Moderately glossy, in particular at the base of the interval.
35.28–36.00	***DI-4 shale:*** no silt. Moderate carbonate content (thin calcite-filled, subvertical fractures). Pyrite at 35.36 m, 35.39 m, 35.49 m, 35.56 m and 35.82 m. Graptolite at 35.43 m, 35.68 m, 35.70 m, 35.87 m, 35.89 m, 35.92 m and 36.02 m. Moderately glossy down-section (35.84–36.00 m).
36.00–36.09	***DI-4 shale:*** no silt. Very low carbonate content. Graptolite at 36.03 m (well-preserved specimens). Partly moderately glossy.
36.09–36.25	***Grey-white shale:*** silty (moderate). Moderate carbonate content (mainly in fractures). Fractured zone with lumps of clay.
36.25–36.90	***DI-1 shale:*** no silt. Moderate carbonate content. Pyrite at 36.66 m. Graptolite at 36.36 m, 36.38–36.42 m, 36.62 m, 36.64 m, 36.67 m and 36.82 m.
Lerhamn – box 9	
36.70–37.60	***DI-3 shale*** *(36.70–36.75 m and 37.16–37.29 m)*, ***DI-4 shale*** *(36.75–36.79 m, 36.94–37.02 m, 37.35–37.41 m and 37.52–37.60 m)* and ***DI-1 shale*** *(36.79–36.94 m, 37.02–37.16 m, 37.29–37.35 m and 37.41–37.52 m)****:*** no silt. Moderate carbonate content (interspersed in fractures at 36.94–37.16 m). Pyrite at 36.73 m, 37.41 m (nodule) and 37.57 m. Graptolite at 36.66 m, 36.71 m, 36.76 m, 36.77 m, 36.97 m, 37.21 m, 37.25 m and 37.38 m.
37.70–38.60	***DI-1 shale*** *(37.60–37.65 m and 38.02–38.11 m)*, ***DI-4 shale*** *(37.65–37.82 m, 37.98–38.02 m and 38.11–38.28 m)*, ***grey shale*** *(37.82–37.98 m)* and ***DI-3 shale*** *(38.73–38.60 m)****:*** no silt. Low carbonate content at 37.70–38.28 m and high carbonate content at 38.28–38.60 m. Pyrite at 37.72 m (small mineral grains) and 37.72–37.75 m (matte). Graptolite at 37.69 m, 37.78–37.82 m (well-preserved specimens, especially at 37.81 m), 37.99 m, 38.23 m, 38.31 m and 38.42 m.
38.60–38.90	***DI-4 shale:*** no silt. Low carbonate content. Pyrite at 38.78 m and 38.90 m. Graptolite at 38.61 m, 38.67 m, 38.70 m, 38.78 m and 38.85 m. Partly moderately glossy at the base of the interval.
38.90–39.15	***Grey shale:*** no silt. No carbonate. Pyrite at 38.90 m.
39.15–39.40	***DI-4 shale:*** no silt. Low carbonate content (interspersed in fractures). Graptolite at 39.22 m.
39.40–39.60	***DI-1 shale:*** no silt. No carbonate. Graptolite at 39.53 m.
39.50–40.50	***DI-1 shale*** *(39.50–39.55 m)*, ***DI-4 shale*** *(39.55–39.60 m)*, ***grey shale*** *(39.60–39.66 m and 39.99–40.12 m)*, ***DI-4/DI-3 shale*** *(39.66–39.99 m)*, ***DI-1 shale*** *(40.12–40.37 m)* and ***limestone*** *(40.37–40.50 m)****:*** no silt. Low carbonate content (excluding the limestone). Pyrite at 39.60 m (5 mm in size) and 40.02 m. Graptolite at 39.59 m, 39.67 m, 40.13 m and 40.16 m.
Lerhamn – box 10	
40.40–40.42	***Limestone:*** no silt. Grey-white in color. Well-preserved quartz can be observed. Continuation of limestone interval above.
40.42–41.05	***DI-4 shale:*** no silt. Very low carbonate content, except at 40.56–40.74 m (within the fractured interval) which has high carbonate content. Pyrite at 40.49 m (matte), 40.70 m and 40.85 m. Graptolite at 40.47 m, 40.48 m, 40.83 m and 40.88 m. Fractured at 40.56–40.74 m, not to the same extent as the interval above. Moderately glossy, in particular within the fractured interval.

Depth (m)	Description
41.05–41.09	***Black shale:*** no silt. No carbonate. Pyrite at 41.06 m (good specimens can be observed, 15 mm in size).
41.09–41.40	***DI-4 shale:*** no silt. Almost no carbonate content. Pyrite at 41.15 m. Graptolite at 41.35 m.
41.40–42.02	***DI-4 shale:*** no silt. Very low carbonate content. Pyrite at 41.40 m (matte), 41.58 m (matte), 41.68 m (large grain, matte) and 41.80 m (matte). Graptolite at 41.36 m, 41.51 m, 41.59 m, 41.64 m and 41.69 m. There is a thin interval with ***DI-1/grey shale*** at 41.70–41.74 m and ***grey shale*** at 41.85–41.87 m and 41.95–41.97 m.
42.02–42.10	***Grey shale:*** no silt. No carbonate. Graptolite at 42.10 m. Intervals with slightly glossy biotite appearance.
42.10–42.30	***DI-4 shale:*** no silt. Moderate carbonate content (majority in calcite-filled, subvertical fractures). Graptolite at 42.31 m. The upper part is moderately glossy with putative biotite at 42.19–42.30 m.
42.35–42.62	***Grey shale:*** no silt. High carbonate content, limited within 42.35–42.49 m (large veins with high concentration). Slightly (greyish) glossy at 42.35–42.49 m. Greyish-light/golden to brown in color at 42.35–42.49 m. A short interval with ***DI-1 shale*** at 42.49–42.58 m can be observed.
42.62–43.30	***DI-4 shale:*** no silt. Moderate carbonate content. Pyrite at 42.64 m (matte), 42.79 m (matte), 42.99 m and 43.24–43.30 m (good specimens). Graptolite at 42.64 m, 42.81 m, 42.98 m and 43.06 m.
43.30–44.20	***DI-4 shale:*** no silt. Low carbonate content (calcite-filled, subvertical fractures and interspersed in fractures). Pyrite at 43.33 m, 43.38 m (matte), 43.83 m (matte), 44.05 m (matte) and 44.10 m. Graptolite at 43.64 m, 43.78 m, 43.96 m, 44.07 m and 44.15 m. There is a short interval of ***grey shale*** at 43.70–43.74 m.
Lerhamn – box 11	
44.20–45.20	***Black shale*** *(44.20–44.26 m, 44.49–44.65 m and 44.74–45.20 m)*, ***DI-1 shale*** *(44.26–44.45 m)* and ***DI-3 shale*** *(44.45–44.49 m and 44.65–44.74 m)****:*** no silt. Moderate carbonate content (mainly at 44.45–44.49 m in a fractured zone(?) at 44.63–44.70 m). Pyrite at 44.49 m, 44.52 m, 44.57 m, 45.07 m, 45.10 m and 45.12 m. Graptolite at 44.20 m, 44.42 m, 44.47 m, 44.53 m, 44.57 m and 45.03 m. Putative fractured zone can be observed at 44.63–44.70 m, but most of the core has broken into pieces.
45.10–45.30	***DI-1 shale:*** very low amount of silt. High carbonate content, in particular within the fractures (seen as white veins). The entire interval is fractured.
45.30–46.00	***DI-3 shale*** *(45.30–45.49 m)* and ***DI-4 shale*** *(45.49–46.00 m)****:*** no silt. No carbonate. Pyrite at 45.50 m, 45.54 m, 45.67 m and 45.78 m. Graptolite at 45.41 m, 45.44 m, 45.55 m, 45.71 m, 45.75 m and 45.77 m.
46.00–46.58	***Black shale:*** no silt. Low carbonate content. Pyrite at 46.04 m, 46.14 m (well-preserved specimen!) and 46.30 m (large grain, matte). Graptolite at 46.20 m, 46.28 m, 46.31 m, 46.35 m, 46.39 m, 46.41 m and 46.46 m.
46.58–47.00	***DI-4 shale:*** no silt. Low carbonate content. Pyrite at 46.65 m and 46.94 m (large grain, matte). Graptolite at 46.76 m and 46.92 m. The shale is slightly glossy in the middle of the interval.
47.00–48.00	***DI-4 shale*** *(47.00–47.04 m and 47.28–47.51 m)*, ***grey shale*** *(47.04–47.09 m, 47.51–47.60 m and 47.65–47.77 m)*, ***black shale*** *(47.09–47.18 m and 47.60–47.65 m)* and ***DI-1 shale*** *(47.18–47.28 m and 47.77–48.00 m)****:*** no silt. Very low carbonate content (mainly around the fractured interval). Pyrite at 47.16 m, 47.45 m, 47.65 m and 47.87 m. Graptolite at 47.81 m. Fractured interval at 47.09–47.28 m. Moderately glossy at the base of the interval.

Depth (m)	Description
Lerhamn – box 12	
47.90–48.80	***Black shale*** *(47.90–48.22 m and 48.72–48.80 m)* and ***DI-4 shale*** *(48.22–48.72 m)**:*** no silt. Moderate carbonate content, mainly within the fractured interval (a very large, white and thick vein containing high carbonate content can be observed). Pyrite at 47.92 m, 48.19 m (well-preserved cubic clusters), 48.24 m, 48.54 m, 48.82 m and 48.83 m. Graptolite at 47.90 m, 48.02 m, 48.17 m, 48.80 m, 48.82 m and 48.84 m. Fractured interval at 48.16–48.71 m, including a large, white vein and quartz.
48.80–49.70	***Black shale*** *(48.80–49.00 m and 49.50–49.61 m)*, ***DI-1 shale*** *(49.00–49.16 m)*, ***DI-4 shale*** *(49.16–49.50 m)* and ***DI-3 shale*** *(49.61–49.70 m)**:*** no silt. Moderate carbonate content (dominated by calcite-filled, subvertical fractures from the middle to the base of the interval). Pyrite at 48.75 m (matte), 49.02 m (matte vein), 49.30–49.32 m (two minerals, 20 mm in size), 49.52 m (vein with well-preserved minerals) and 49.57 m. Graptolite at 48.75 m, 48.79 m, 48.82 m, 49.52 m and 49.57 m. Fractured at 49.00–49.16 m (similar to above fracture zone, however fractured more extensively). Moderately glossy at 49.40 m and grading to slightly glossy biotite appearance down-section.
49.70–50.60	***Black shale*** *(49.70–50.60 m)* and ***DI-4 shale*** *(50.50–50.60 m)**:*** no silt. Moderate carbonate content. Few very small pyrite grains spread across, otherwise lacking pyrite. Graptolite at 49.67 m and 50.53 m. Intervals with putative graphite or charcoal can be observed. Fractured at 49.87–50.48 m (observed), but could be fractured all the way to 50.60 m. The upper part of the shale is moderately glossy, while it shifts between strongly glossy biotite appearance and moderately glossy down-section.
50.60–51.50	***DI-4 shale*** *(50.60–51.10 m)* and ***DI-1 shale*** *(51.10–51.50 m)**:*** very low amount of silt. Moderate carbonate content (spread across, majority found in fractures). Pyrite at 51.03 m. Fractured at 50.70–51.10 m, but may continue throughout the interval (the shale has broken into pieces in the basal 40 cm), with a muddy/silty appearance at the base of the interval.
Lerhamn – box 13	
51.70–52.50	***DI-4 shale*** *(51.70–52.18 m and 52.36–52.50 m)* and ***black shale*** *(52.18–52.36 m)**:*** no silt. Moderate carbonate content. Pyrite at 51.65 m, 51.69 m, 51.83 m, 51.98 m (large matte-shiny grain), 52.15 m (matte vein) and 52.39 m (matte). Graptolite at 52.18 m.
52.50–53.40	***Grey shale*** *(52.50–52.56 m)*, ***black shale*** *(52.56–52.68 m and 53.12–53.40 m)* and ***DI-4 shale*** *(52.68–53.12 m)**:*** high amount of silt in the grey shale, while the rest lack silt. Moderate carbonate content (mainly in fractured intervals). Pyrite at 52.62 m, 52.68 m (matte), 52.73 m (small, matte) and 53.24 m (well-preserved specimen). Graptolite at 53.18 m and 53.70 m. Fractured at 52.56–52.67 m (smaller fracture) and 53.25–53.40 m (larger fracture).
53.40–54.40	***DI-4 shale:*** no silt. Moderate carbonate content. Pyrite at 53.41 m (small grain), 53.63 m and 54.16 m (large, matte vein).
54.20–55.20	***DI-4 shale:*** no silt. Moderate carbonate content. Pyrite at 55.06 m (very large, matte grain). Graptolite at 54.10–54.20 m. Occasional intercalations of black shale intervals.
Lerhamn – box 14	
55.10–56.10	***DI-4 shale*** *(55.10–55.26 m, 55.47–55.54 m, 55.72–55.80 m and 55.95–56.10 m)*, ***DI-1 shale*** *(55.26–55.45 m)* and ***DI-2 shale*** *(55.54–55.72 m and 55.80–55.95 m)**:*** no silt. Moderate carbonate content. Pyrite at 55.07 m (matte), 55.17 m (5 mm, slightly matte), 55.36 (7 mm, slightly matte vein), 55.51 m, 55.75 m (10 mm, slightly matte), 56.04 m (10 mm, slightly matte) and 56.07 m (5 mm, matte). Graptolite at 55.48 m, 55.51 m, 55.52 m, 55.73 m and 55.77 m.

Depth (m)	Description
56.10–57.10	***Green shale*** *(56.10–56.27 m),* ***DI-4 shale*** *(56.27–56.40 m),* ***DI-1 shale*** *(56.40–56.50 m),* ***DI-3 shale*** *(56.50–56.59 m),* ***black shale*** *(56.59–56.79 m)* and ***DI-1 shale*** *(56.79–57.10 m)**:*** no silt. High carbonate content (majority of the carbonate is concentrated around the green shale). Pyrite at 56.62 m and 56.74 m. Graptolite at 56.38 m and 56.61 m.
57.10–58.10	***DI-4 shale*** *(57.10–57.20 m),* ***green shale*** *(57.20–57.55 m, 57.79–57.86 m and 57.99–58.10 m),* ***DI-3 shale*** *(57.55–57.79 m)* and ***black shale*** *(57.86–57.99 m)**:*** low amount of silt in the ***DI-3*** and ***DI-4 shale***, the rest lack silt. High carbonate content. Pyrite at 57.15 m (10 mm, matte) and 57.98 m (5 mm, matte). Graptolite at 57.91 m, 57.94 m and 57.96 m. A few intervals with moderately glossy biotite appearance, with the exception for the green shale that lack.
58.10–59.10	***Green shale*** *(58.10–58.17 m, 58.28–58.47 m and 58.53–58.69 m),* ***black shale*** *(58.17–58.28 m),* ***DI-4 shale/black shale*** *(58.47–58.53 m),* ***DI-3 shale*** *(58.69–58.81 m),* ***grey shale/DI-1 shale*** *(58.81–58.93 m)* and ***DI-4 shale*** *(58.93–59.10 m)**:*** no silt. Moderate carbonate content. Pyrite at 58.26 m and 58.49–58.50 m (two 5 mm, matte grains). Fractured at 58.28–58.47 m. Strongly glossy biotite appearance/biotite in the darker shales.
Lerhamn – box 15	
59.10–60.00	***Black shale*** *(59.05–59.07 m, 59.15–59.23 m, 59.34–59.42 m and 59.66–59.85 m),* ***DI-1 shale*** *(59.07–59.15 m),* ***green shale*** *(59.23–59.34 m, 59.42–59.57 m and 59.94–60.00 m)* and ***DI-4 shale*** *(59.57–59.66 m and 59.85–59.94 m)**:*** no silt. Low carbonate content (except in the fractured interval which has high carbonate content). Pyrite at 59.42 m (matte), 59.86 m (matte-shiny) and 59.96 m (3 mm, shiny vein). Graptolite at 59.06 m, 59.07 m, 59.17 m and 59.23 m. Fractured at 59.42–59.57 m, a few larger white veins can be observed. Moderately glossy biotite appearance and strongly glossy biotite appearance in the darker shales.
60.00–60.90	***DI-4 shale*** *(60.00–60.53 m and 60.64–60.84 m)* and ***green shale*** *(60.53–60.64 m and 60.84–60.92 m)**:*** no silt. Low carbonate content. Pyrite at 60.92 m (10 mm, shiny).
60.90–61.90	***DI-4 shale*** *(60.90–61.26 m and 61.40–61.70 m)* and ***green shale*** *(61.26–61.40 m and 61.70–61.90 m)**:*** no silt. Low carbonate content. Pyrite at 61.26–61.36 m (with occasional specimens of oxidized pyrite) and 61.86 m. Graptolite at 61.70 m. Moderately glossy and moderately glossy biotite appearance in the darker shales.
61.90–62.80	***DI-4 shale*** *(61.90–62.00 m, 62.51–62.60 m and 62.67–62.80 m),* ***green shale*** *(62.00–62.15 m, 62.39–62.51 m and 62.60–62.67 m),* ***DI-2 shale*** *(62.15–62.33 m)* and ***black shale*** *(62.33–62.39 m)**:*** no silt. Low carbonate content. Pyrite at 61.85–61.92 m (mixed with the carbonate), 62.19 m (5 mm, very shiny) and 62.69–62.80 m (mixed with the carbonate). Graptolite at 61.96 m and 62.21 m. Brachiopod at 62.40 m.
Lerhamn – box 16	
62.70–63.70	***Black shale*** *(62.70–62.90 m and 62.93–63.02 m),* ***green shale*** *(62.90–62.93 m, 63.02–63.08 m and 63.20–63.35 m)* and ***DI-3 shale*** *(63.08–63.20 m and 63.35–63.70 m)**:*** no silt. Moderate carbonate content. One or two pyrite specimens. Possible graptolites (one or two specimens) recorded.
63.70–64.70	***Black shale*** *(63.70–63.85 m),* ***DI-3 shale*** *(63.85–64.07 m)* and ***DI-1/DI-2 shale*** *(64.07–64.70 m)**:*** no silt (possibly in the fractured interval). High carbonate content (mainly in fractures in the fractured interval). Fractured at 63.90–64.70 m, with white veins (small–moderate in size) and some smaller fractures. Putative silt and clay can be observed in the fractured interval.
64.70–65.70	***DI-1/DI-2 shale*** *(64.70–64.98 m),* ***DI-2 shale*** *(64.98–65.50 m),* ***black shale*** *(65.50–65.57 m)* and ***green shale*** *(65.57–65.70 m)**:*** no silt (possibly in the fractured interval). Moderate carbonate content (thick, white veins can be observed). Pyrite at 65.15–65.25 m, 65.37 m and 65.52 m. Fractured at 65.70–65.88 m, with intervals of putative clay as

Depth (m)	Description
	in the fractured interval above.
65.70–66.70	***Green shale*** *(65.70–65.73 m and 65.98–66.12 m)*, ***DI-2 shale*** *(65.73–65.98 m)*, ***DI-3 shale*** *(66.12–66.30 m)* and ***DI-4 shale*** *(66.30–66.70 m)**:*** no silt. Moderate carbonate content. Pyrite at 65.79 m (matte-shiny) and 66.42 m. Fractured at 66.30–66.50 m, however, it has broken into pieces. Moderately glossy biotite appearance at 65.70–65.85 m.
Lerhamn – box 17	
66.50–67.30	***Black shale*** *(66.70–67.15 m)* and ***DI-1 shale*** *(67.15–67.30 m)**:*** no silt. Low carbonate content. Pyrite at 66.90–66.94 m. Graptolite at 67.07 m.
67.30–68.30	***DI-1 shale*** *(67.30–67.35 m)*, ***DI-4 shale*** *(67.35–67.88 m)*, ***black shale*** *(67.88–68.09 m and 68.20–68.30 m)* and ***DI-2 shale*** *(68.09–68.20 m)**:*** no silt. Moderate carbonate content. One or two pyrite specimens. Fractured at 67.60–67.80 m.
68.30–69.30	***Black shale*** *(68.30–68.38 m and 68.50–69.30 m)* and ***green shale*** *(68.38–68.50 m)**:*** no silt. Low carbonate content. Pyrite at 68.64 m and 68.72 m. Graptolite at 68.84 m and 69.08 m.
69.30–70.30	***Black shale*** *(69.30–69.55 m and 69.94–70.05 m)*, ***DI-3 shale*** *(69.55–69.80 m)*, ***DI-4 shale*** *(69.80–69.94 m)* and ***DI-1 shale*** *(70.05–70.30 m)**:*** no silt. Low carbonate content. Pyrite at 69.40 m, 69.48 m (matte-shiny) and 70.18 m. Graptolite at 69.31 m, 69.42 m, 69.42 m, 69.87 m, 69.93 m and 69.98 m.
Lerhamn – box 18	
70.20–71.20	***Black shale*** *(70.20–70.42 m and 70.82–70.94 m)*, ***dark green shale*** *(70.42–70.65 m and 70.94–71.06 m)*, ***DI-3 shale*** *(70.42–70.65 m)* and ***DI-4 shale*** *(71.06–71.20 m)**:*** no silt. Moderate carbonate content (except in thick fractures in the fractured interval which has high carbonate content). Pyrite at 70.36 m (15 mm, shiny, well-preserved grain). Fractured zone at 70.95–71.20 m, with clay-like beds in the upper part of the interval.
71.20–72.20	***Black shale*** *(71.20–71.66 m and 71.87–71.99 m)*, ***DI-4 shale*** *(71.66–71.87 m)* and ***dark green shale*** *(71.99–72.20 m)**:*** no silt. High carbonate content. Pyrite at 71.26 m (thin vein), 71.42 m, 71.55 m (thin vein), 71.57 m (thin vein) and 71.86 m. Fractured at 71.20–71.30 m (less fractured compared to the fractured interval above).
72.10–73.20	***Black shale*** *(72.10–72.48 m and 72.95–73.01 m)*, ***green shale*** *(72.48–72.66 m and 73.08–73.20 m)* and ***DI-4 shale*** *(72.66–72.95 m and 73.01–73.08 m)**:*** no silt. Very low carbonate content (spread across, mainly in the darker shales). Pyrite at 72.90 m, 72.94 m and 73.15 m.
73.20–74.20	***DI-4 shale*** *(73.20–73.37 m and 73.53–73.86 m)* and ***black shale*** *(73.37–73.53 m and 73.86–74.20 m)**:*** no silt. No carbonate. Pyrite at 73.27 m (thin vein), while very small grains can be found throughout the interval.
Lerhamn – box 19	
74.20–75.10	***DI-4 shale*** *(74.20–74.58 m, 74.80–74.87 m and 74.92–75.04 m)*, ***black shale*** *(74.58–74.80 m and 75.04–75.10 m)* and ***green shale*** *(74.87–74.92 m)**:*** no silt. Moderate carbonate content. Pyrite at 74.50 m, 74.52 m and 74.94 m (matte vein). Graptolite at 74.80 m.
75.10–76.10	***DI-4 shale*** *(75.10–75.41 m and 75.64–75.10 m)* and ***black shale*** *(75.41–75.64 m)**:*** no silt. Low carbonate content (thin, white veins). Pyrite at 75.36 m, 75.37 m, 75.93 m and 75.96 m.
76.10–77.10	***Black shale*** *(76.10–76.26 m and 76.50–76.82 m)*, ***DI-2 shale*** *(76.26–76.42 m)*, ***DI-4 shale*** *(76.42–76.50 m)*, ***green shale*** *(76.82–76.92 m)* and ***dark green shale*** *(76.92–77.10 m)**:*** no silt. Low carbonate content. Pyrite at 76.10 m, 76.14 m (matte vein),

Depth (m)	Description
	76.51 m (bronze-shiny), 76.62 m (gold-bronze-shiny), 76.86 m (bronze-shiny) and 76.98 m (matte, bronze colored).
76.80–77.80	***DI-4 shale:*** no silt. Low carbonate content. Pyrite at 77.02 m (gold-like), 77.24 m (matte) and 77.76 m (5 mm, matte).
Lerhamn – box 20	
77.80–78.80	***Black shale*** *(77.80–78.03 m, 78.35–78.43 m and 78.50–78.68 m)*, ***dark green shale*** *(78.03–78.12 m and 78.43–78.50 m)* and ***DI-4 shale*** *(78.12–78.35 m and 78.68–78.80 m)**:*** no silt. Moderate carbonate content (minor white veins in the upper part and at the base of the interval). Putative fracture interval at 77.80–78.00 m and at 78.52–78.80 m.
78.80–79.80	***DI-4 shale*** *(78.80–79.12 m and 79.29–79.64 m)* and ***black shale*** *(79.12–79.29 m and 79.64–79.80 m)**:*** no silt. Low carbonate content. One or two pyrite specimens. Fractured at 78.98–79.50 m, containing high carbonate content and quartz.
79.80–80.25	***Dark green shale*** *(79.80–79.87 m and 79.93–80.00 m)* and ***DI-4 shale*** *(79.87–79.95 m and 80.00–80.25 m)**:*** no silt. No carbonate.

Appendix B

Description of the Fågelsång-3 drill core. DI-1–DI-4 refers to the darkness of grey shales, ranging from 1 to 4, where 4 is almost black. Carbonates are dominated by limestone. Other types of carbonates include calcite veins in fractures.

Depth (m)	Description
Fågelsång-3 – box 1	
6.17–7.19	***Black shale*** *(6.17–6.26 m)*, ***bentonite clay*** *(6.26–6.28 m)*, ***DI-4 shale*** *(6.28–6.88 m)* and ***DI-3 shale*** *(6.88–7.19 m)**:*** no silt. Moderate carbonate content at 6.17–6.52 m (as calcite-filled, subvertical fractures and interspersed in fractures). Pyritic phosphorite at 6.30–6.42 m and pyrite at 6.72 m, 6.87 m (3 mm), 6.97 m and 6.97 m (3 mm). Graptolite at 6.22 m. Clay at 6.48–6.52 m. Moderately glossy at 6.70–6.83 m.
7.17–8.33	***DI-3 shale:*** silty (low). Moderate carbonate content (as calcite-filled, subvertical fractures and interspersed in fractures). Pyrite at 7.30 m (9 mm, matte), 7.32 m, 7.54 m (3 mm), 7.78 m, 7.81 m (3 mm), 7.90 m and 8.18 m (13 mm, matte vein).
8.33–9.17	***DI-3 shale:*** silty (moderate at 8.33–8.90 m). Low carbonate content (mainly as calcite-filled, subvertical fractures). Pyrite at 8.55 m (10 mm, matte vein), 8.67 m, 8.75 m, 8.79 m, 8.83 m, 8.86 m, 8.89 m, 8.99 m, 9.01 m, 9.02 m (4 mm, matte), 9.05 m and 9.08 m. Graptolites at 8.70 m, 8.97 m, 8.99 m 9.06 m and 9.08 m. Clay at 8.38–8.41 m, 8.44–8.50 m and 8.56–8.63 m (with biotite).
9.17–10.09	***DI-3 shale:*** no silt. Moderate carbonate content at 9.17–9.47 m and lack of carbonate at 9.47–10.09 m. Pyrite at 9.21 m, 9.29 m, 9.35 m, 9.38 m, 9.40 m, 9.41 m, 9.42 m (3 mm, shiny), 9.44 m, 9.51 m (4 mm, shiny), 9.56 m, 9.62 m, 9.66 m, 9.68 m, 9.73 m, 9.82 m, 9.91 m, 10.03 m (5 mm, matte), 10.03 m (6 mm, matte), 10.06 m (4 mm, shiny) and 10.07–10.08 m. Graptolites at 9.21 m, 9.25 m, 9.29 m, 9.29 m and 9.78 m.
Fågelsång-3 – box 2	
10.09–11.02	***DI-4 shale:*** silty (high at 10.29–10.49 m, 10.72–10.81 m and 10.91 m). Pyrite at 10.13 m, 10.16 m, 10.18 m, 10.19 m, 10.20 m, 10.23 m, 10.25 m, 10.25 m, 10.26 m (5 mm, matte), 10.28 m (6 mm, matte), 10.34 m, 10.37 m, 10.40–10.42 m (at 10.41 m (9 mm) and 10.42 m (5 mm), matte-shiny), 10.43 m, 10.53 m, 10.60 m, 10.63 m, 10.64 m, 10.67 m, 10.69 m (9 mm, matte), 10.69 m (3 mm, matte), 10.75 m, 10.75 m, 10.81 m, 10.82 m, 10.85 m (5 mm, matte), 10.86 m and 11.01 m. Graptolites at 10.20 m, 10.29 m, 10.84 m, 10.86 m, 10.89 m, 10.94 m, 10.95 m and 11.06 m. Clay and silt mixture can be observed at 10.41–10.46 m. Intervals with slightly glossy and moderately glossy throughout the interval.
11.02–11.92	***Black shale*** *(11.02–11.38 m and 11.84–11.92 m)* and ***DI-4 shale*** *(11.38–11.84 m)**:*** no silt. Very low carbonate content at 11.71–11.82 m. Pyrite at 11.05 m, 11.07 m, 11.09 m (4 mm, shiny), 11.14 m, 11.21 m, 11.34 m, 11.40 m (5 mm, matte, weathered), 11.41 m (5 mm, matte, weathered), 11.46 m, 11.48 m, 11.50 m, 11.56 m (4 mm, shiny), 11.60 m and 11.69 m. Graptolites at 11.04 m, 11.08 m, 11.37 m, 11.38 m, 11.40 m, 11.42 m, 11.44 m, 11.44 m, 11.47 m, 11.50 m, 11.54 m, 11.60 m, 11.61 m, 11.6235 m, 11.66 m and 11.83 m. Clay at 11.20–11.29 m and 11.87–11.92 m.
11.75–12.72	***Black shale*** *(11.75–11.89 m and 12.65–12.72 m)* and ***DI-4 shale*** *(11.89–12.65 m)**:*** no silt. Moderate carbonate content at 12.18–12.27 m and low carbonate content at 12.51–12.72 m (interspersed in fractures). Pyrite at 11.81 m, 11.82 m, 11.95 m, 11.97 m, 12.05 m, 12.10 m, 12.20 m (12 mm, matte), 12.36 m, 12.51–12.54 m and 12.54 m (13 mm, nodule). Graptolites at 11.92 m, 11.93 m, 11.95 m, 12.03 m, 12.04 m, 12.05 m, 12.07 m, 12.09 m, 12.11 m, 12.15 m, 12.27 m, 12.29 m, 12.33 m, 12.39 m, 12.40 m, 12.59 m, 12.62 m and 12.64 m.

Depth (m)	Description
12.69–13.70	***DI-4 shale:*** silty (very low). Low carbonate content. Pyrite at 12.73 m, 12.76 m, 12.92 m, 12.94 m, 12.95 m, 13.01 m (matte, smaller vein), 13.04 m, 13.06 m, 130.7 m, 13.17 m, 13.21 m, 13.23 m, 13.27 m, 13.28 m, 13.42–13.54 m and 13.64 m. Graptolite at 12.94 m. Minor parts moderately glossy.
Fågelsång-3 – box 3	
13.70–14.79	***Black shale*** *(13.70–14.40 m and 14.73–14.79 m)* and ***DI-4 shale*** *(14.40–14.73 m)**:*** silty (low at 13.76–14.00 m and 14.47–14.79 m). Low carbonate content. Pyrite at 13.73 m, 13.79 m, 13.97 m, 14.07 m (very large grain with its cubic shape visible on the side), 14.15–14.26 m (mix of smaller and larger grains; matte, shiny, bronze-colored), 14.28–14.35 m (same as previous), 14.44 m, 14.50 m (two grains; 4 mm and 3 mm, matte), 14.53 m (two grains; 5 mm, 3 mm, matte, shiny) and 14.75 m. Graptolites 13.78 m, 13.79 m, 13.82 m, 13.86 m, 13.88 m, 14.16 m, 14.18 m, 14.24 m, 14.45 m, 14.47 m and 14.56 m.
14.58–15.60	***Black shale*** *(14.58–14.72 m and 15.17–15.60 m)*, ***limestone*** *(14.72–14.88 m)* and ***DI-4 shale*** *(14.88–15.17 m)**:*** no silt. No carbonate content. Pyrite at 14.63 m, 14.94 m, 14.98 m (3 mm, shiny), 15.00 m (5 mm, weathered), 15.06 m, 15.11 m (two grains; 4 mm and 3 mm, matte, shiny), 15.13 m, 15.14 m, 15.15 m (two grains; 4 mm and 3 mm, matte), 15.18 m, 15.20 m, 15.23 m, 15.29 m, 15.31 m, 15.40 m and 15.44 m. Graptolites at 14.98 m, 15.06 m, 15.34 m and 15.37 m. Possible precipitation in a weathered, 2 cm wide cavity at 15.54–15.60 m. Moderately glossy biotite appearance at 14.58–14.62 m and moderately glossy at 15.53–15.60 m.
15.60–16.52	***Black shale*** *(15.63–16.17 m and 16.22–16.52 m)* and ***DI-4 shale*** *(16.17–16.22 m)**:*** silty (moderate, only within the fractured zone at 15.85–16.01 m). Moderate carbonate content, only within the fractured zone and from 16.10–16.52 m. Pyrite at 15.67 m, 15.70 m, 15.70 m, 15.73 m, 15.76 m (4 mm, weathered), 15.77 m, 16.15 m, 16.22 m, 16.26 m, 16.41 m, 16.57 m and 16.59 m. Fractured at 15.85–16.01 m. Moderately glossy biotite appearance at 16.01–16.19 m.
16.40–17.42	***Black shale*** *(16.40–16.44 m and 16.77–17.42 m)* and ***DI-4 shale*** *(16.44–16.77 m)**:*** silty (moderate; where we find clay or within the fractured zone). No carbonate content. Oxidized pyrite at 17.15 m and 17.27 m. Pyrite at 16.48 m, 16.71 m, 16.75 m, 17.03 m (3 mm, bronze-colored), 17.27 m (4 mm, matte) and 17.37 m. Graptolites at 16.48 m and 17.03 m. Fractured at 16.80–16.83 m, 17.19–17.25 m (with clay mixture) and 17.40–17.42 m (with clay mixture). Slightly glossy and moderately glossy at 16.47–16.71 m.
Fågelsång-3 – box 4	
17.42–18.65	***Black shale:*** no silt. No carbonate content. Pyrite at 17.48 m (5 mm, matte, bronze-gold-colored), 17.54 m, 17.62 m, 17.63 m, 17.67 m, 17.69 m, 17.76 m (8 mm, matte), 17.83 m, 17.84 m, 17.93 m, 17.97 m, 18.05 m, 18.13 m, 18.20 m (5 mm, matte) and 18.61 m (7 mm, matte lens). Graptolites at 17.78 m, 17.79 m and 17.97 m.
18.65–20.25	***Black shale:*** silty (high amount at 18.96–19.19 m and 19.30–20.25 m). No carbonate content. Pyrite at 18.88 m, 19.24 m (3 mm, bronze-colored), 19.29 m and 19.35 m (very large nodule). Fractured; less fractured at 18.90–19.19 m, more fractured (with clay mixture last 4 cm) at 19.45–19.70 m and highly fractured with clay mixture at 19.89–20.25 m. Slightly glossy biotite appearance at 18.65–19.30 m.
20.23–21.06	***Black shale*** *(20.23–20.53 m and 20.54–21.06 m)* and ***bentonite clay*** *(20.53–20.54 m)**:*** silty (only where we have clay; moderate). Very low carbonate content. Overall lack of pyrite. Graptolites at 20.28 m, 20.33 m, 20.61 m, 20.64 m, 20.65 m, 20.70 m, 20.77 m, 20.80 m, 20.82 m, 20.83 m, 20.83 m, 20.84 m, 20.85 m, 20.86 m, 20.88 m, 20.89 m, 20.93 m, 21.00 m, 20.98 m, 21.00 m, 21.03 m, 21.04 m and 21.05 m. Clay at 20.45–20.49 m, 20.52–21.53 m and 20.98–20.93 m.
21.00–22.00	***Black shale*** *(21.00–21.51 m and 21.59–22.00 m)* and ***DI-4 shale*** *(21.51–22.59 m)**:*** silty (moderate). Moderate carbonate content. Pyrite at 21.20–21.23 m (14 mm and 11 mm,

Depth (m)	Description
	matte-shiny). Graptolites at 21.03 m, 21.04 m, 21.05 m, 21.06 m, 21.08 m, 21.09 m, 21.10 m, 21.24 m, 21.29 m, 21.30 m, 21.42 m, 21.44 m, 21.46 m, 21.51 m, 21.53 m, 21.58 m, 21.59 m, 21.62 m, 21.63 m, 21.65 m, 21.72 m, 21.75 m, 21.77 m, 21.79 m, 21.88 m, 21.91 m and 21.97 m. Clay at 21.80–21.85 m (and possibly at 21.39–21.42 m).
Fågelsång-3 – box 5	
22.00–23.00	***Black shale:*** silty (low). No carbonate content. Pyrite at 22.06 m, 22.77 m, 22.91 m and 22.97 m (4 mm, shiny pyrite nodule). Graptolites at 22.03 m, 22.05 m, 22.11 m, 22.18 m, 22.20 m, 22.22 m, 22.24 m, 22.27 m, 22.30 m, 22.32 m, 22.33 m, 22.35 m, 22.37 m, 22.38 m, 22.40 m, 22.41 m, 22.43 m, 22.45 m, 22.46 m, 22.48 m, 22.50 m, 22.52 m, 22.53 m, 22.55 m, 22.56 m, 22.58 m, 22.59 m, 22.64 m, 22.66 m, 22.67 m, 22.70 m, 22.71 m, 22.72 m, 22.74 m, 22.77 m, 22.79 m, 22.80 m, 22.81 m, 22.82 m, 22.85 m, 22.89 m, 22.90 m, 22.96 m and 22.97 m.
23.00–24.00	***Black shale:*** silty (very low, but there are intervals with a moderate amount especially in the presence of clay). Moderate carbonate content. Pyrite at 23.17 m (4 mm, nodule) and 23.19 m. Graptolites at 23.18 m, 23.36 m, 23.36 m, 23.40 m, 23.42 m, 23.46 m, 23.55 m, 23.60 m, 23.65 m, 23.74 m and 23.82 m. Clay at 23.32–23.35 m.
24.00–25.00	***Black shale:*** no silt. High carbonate content. Pyrite at 24.09 m (4 mm, shiny), 24.21 m (4 mm, shiny), 24.46 m, 24.53 m (15 mm, matte), 24.61–24.64 m and 24.86–24.89 m. Graptolites at 24.02 m, 24.05 m, 24.17 m, 24.22 m, 24.27 m, 24.30 m, 24.35 m, 24.36 m, 24.49 m, 24.57 m, 24.73 m, 24.74 m, 24.75 m and 25.00 m.
25.00–26.00	***Black shale:*** no silt. High carbonate content. Pyrite at 25.32 m (12 mm, shiny) and 25.80 m (nodule). Graptolites at 25.10 m, 25.12 m, 25.21 m, 25.24 m, 25.28 m, 25.38 m, 25.42 m, 25.43 m, 25.65 m and 25.84 m. Slightly glossy at 25.72–25.78 m.
Fågelsång-3 – box 6	
25.90–26.92	***Black shale:*** silt (low). No carbonate. Pyrite at 25.90 m (large shiny grain), 25.94 m, 26.20 m, 26.21 m, 26.74 m, 26.76 m, 26.78 m, 26.81 m, 26.88 m and 26.89 m. Graptolites at 26.00 m, 26.05 m, 26.08 m, 26.09 m, 26.24 m, 26.28 m, 26.37 m, 26.40 m, 26.52 m, 26.54 m, 26.57 m, 26.61 m, 26.64 m, 26.67 m, 26.73 m, 26.83 m, 26.86 m and 26.88 m. A few intervals with thin layers of clay-silt mixture.
26.78–27.71	***Black shale:*** no silt. Moderate carbonate content at 27.29–27.71 m. Pyrite at 26.81 m, 26.98 m, 27.12 m, 27.15 m, 27.17 m and 27.35 m (15 mm, matte-shiny vein). Graptolites at 26.81 m, 26.94 m, 26.97 m, 27.00 m, 27.10 m, 27.20 m, 27.46 m, 27.61 m and 27.66 m. Slightly glossy biotite appearance in the upper part of the interval and at 27.36–27.46 m.
27.63–28.67	***Black shale:*** no silt. Low carbonate content. Oxidized pyrite at 27.99 m and 28.02 m. Pyrite at 27.76 m (two grains; 13 mm and 8 mm, matte-shiny), 27.97 m (6 mm, matte), 28.15 m (5 mm, matte-shiny), 28.19 m, 28.20 m (3 mm, matte, reddish) and 28.20–28.25 m. Graptolites at 27.70 m, 27.73 m, 27.85 m and 28.31 m. Slightly glossy biotite appearance and moderately glossy biotite appearance at 28.45–28.67 m.
28.67–29.60	***Black shale:*** silty (low amount, however high amount in the presence of clay). No carbonate content. Graptolites at 28.80 m, 28.85 m, 28.90 m, 28.99 m, 29.14 m, 29.17 m, 29.22 m, 29.23 m, 29.29 m and 29.49 m. Clay at 28.27–29.40 m, and clay-silt mixture at 28.06–28.19 m.
Fågelsång-3 – box 7	
29.45–30.47	***Black shale:*** silty (low amount, however moderate to high amount in the presence of clay and clay-silt mixture). Very low carbonate content. Pyrite at 29.96 m. Graptolites at 29.47 m, 29.53 m, 29.77 m, 29.82 m, 29.86 m, 30.04 m, 30.10 m, 30.14 m, 30.25 m, 30.30 m and 30.33 m. Clay (mostly on the surface of the core) at 30.17–30.20 m and 30.36–30.47 m, including intervals with minor clay and clay-silt mixture.
30.39–31.33	***Black shale:*** silty (low amount, however high amount in the presence of clay). No

Depth (m)	Description
	carbonate content. Oxidized pyrite at 31.24 m. Pyrite at 30.96 m, 31.06 m, 31.11 m (20 mm, shiny), 31.20 m and 31.24 m. Graptolites at 30.62 m, 30.78 m, 30.98 m and 31.31 m. Clay at 30.39–30.48 m, 30.54–30.58 m, 30.64–30.76 m and 30.82–30.95 m.
31.33–32.33	***Black shale*** *(31.33–31.77 m and 31.82–32.33 m)* and ***bentonite clay*** *(31.77–31.82 m)**:*** silty (high). Low carbonate content. Graptolite at 31.70 m. Clay-silt mixture can be observed throughout the core. Moderately glossy biotite at 31.82–32.33 m.
32.30–33.29	***Black shale:*** silty (high). Very low carbonate content. Pyrite at 32.56 m and 32.60 m (4 mm, gold-like). Clay-silt mixture can be observed throughout the core. Slightly glossy biotite appearance at 32.30–33.29 m.
Fågelsång-3 – box 8	
33.29–34.51	***Black shale:*** silty (high). No carbonate content. Graptolites at 33.36 m, 33.43 m, 33.63 m, 33.96 m, 34.00 m, 34.34 m and 34.50 m. Clay at 33.29 m. A lot of clay-silt mixture at 33.50–34.51 m. Moderately glossy biotite appearance at 33.29–33.57 m, 34.28 m, and 34.38 m.
34.40–35.41	***Black shale*** *(34.40–34.58 m and 35.62–35.41 m)* and ***limestone*** *(34.58–35.62 m)**:*** silty (high). Low carbonate content (excluding the limestone). Pyrite at 34.48 m, 34.50 m, 34.50 m, 34.51 m, 34.52 m, 34.54 m, 34.71 m, 34.71 m, 34.74 m, 34.76 m, 34.77 m, 34.79 m and 34.82 m. Graptolites at 34.40 m, 34.42 m, 34.44 m, 34.46 m, 34.84 m, 35.12 m, 35.14 m, 35.20 m and 35.27 m. Clay at 34.94–35.07 m and 35.62 m. Clay-silt mixture fairly common throughout the interval. Slightly glossy and moderately glossy at 35.62–35.74 m.
35.41–36.36	***Black shale*** *(35.41–35.72 m and 35.75–36.36 m)* and ***bentonite clay*** *(35.72–35.75 m)**:*** silty (low). No carbonate content. Graptolites at 35.41m, 35.44 m, 35.49 m, 35.53 m, 35.83 m, 35.86 m and 35.97 m. Low content of clay-silt mixture.
36.28–37.31	***Black shale*** *(36.28–36.35 m and 36.37–37.31 m)* and ***bentonite clay*** *(36.35–36.37 m)**:*** silty (low). Low carbonate content. Pyrite at 36.45 m (6 mm, matte vein) and 37.00 m (12 mm, matte lens). Graptolites at 36.50 m, 36.58 m, 36.61 m, 37.05 m and 37.11 m. Low content of clay-silt mixture. Moderately glossy biotite appearance at 36.37–36.47 m, 36.63–36.79 m and 36.94–37.00 m.
Fågelsång-3 – box 9	
37.17–38.08	***DI-4 shale*** *(37.17–37.75 m and 37.92–38.00 m)* and ***black shale*** *(37.75–37.92 m and 38.00–38.08 m)**:*** silty (high). Very low carbonate content at 37.17–37.87 m and moderate carbonate content at 37.87–38.08 m. Graptolites at 37.40 m, 37.42 m, 37.73 m, 37.79 m, 37.89 m, 37.92 m, 38.01 m, 38.04 m and 38.06 m. Clay at 37.75–37.80 m. Moderately glossy biotite appearance at 37.81–37.92 m and 38.00–38.08 m.
38.07–39.09	***Black shale*** *(38.07–38.20 m, 38.61–38.92 m, 38.95–39.01 m and 39.02–39.09 m)*, ***DI-4 shale*** *(38.20–38.61 m)*, ***limestone*** *(38.92–38.95 m)* and ***bentonite clay*** *(39.01–39.02 m)**:*** silty (low). No carbonate content (excluding the limestone). Pyrite at 38.31 m (4 mm, mate). Graptolites at 38.11 m, 38.14 m, 38.16 m, 38.24 m, 38.26 m, 38.29 m, 38.31 m, 38.35 m, 38.43 m and 38.49 m. Clay at 38.78–38.80 m. Moderately glossy biotite appearance at 38.41–38.85 m.
39.09–40.07	***Black shale*** *(39.09–39.56 m, 39.59–39.71 m and 39.75–40.07 m)*, ***bentonite clay*** *(39.56–39.59 m and 39.73–39.75 m)* and ***limestone*** *(39.71–39.73 m)**:*** silty (moderate). No carbonate content (excluding the limestone). Pyrite at 39.14 m (7 mm), 39.16 m (5 mm, gold-shiny) and 39.77 m (5 mm, gold-shiny). Graptolites at 39.09 m, 39.12 m and 39.31 m. Moderately glossy biotite appearance at 39.18–39.55 m and 39.59–40.59 m.
40.07–41.03	***Black shale:*** silty (low). No carbonate content. Pyrite at 40.60–40.69 m (ex. 5 mm grains etc.). Graptolites at 40.12 m, 40.33 m, 40.40 m, 40.42 m, 40.63 m, 40.70 m, 40.74 m, 40.79 m, 40.83 m, 40.93 m and 40.95 m. Occasionally moderately glossy and moderately glossy biotite appearance.

Depth (m)	Description
Fågelsång-3 – box 10	
41.02–42.04	***Black shale:*** silty (moderate). No carbonate content. Graptolites at 41.10 m, 41.25 m, 41.29 m, 41.32 m, 41.39 m, 41.61 m and 41.70 m. Slightly glossy biotite appearance and moderately glossy biotite appearance within thin beds throughout the interval.
41.92–42.84	***Black shale*** *(41.92–42.14 m and 42.19–42.84 m)* and ***DI-4 shale*** *(42.14–42.19 m)**:*** silty (low). High carbonate content at 42.32–42.84 m. Pyrite at 42.44 m (3 mm, shiny), 42.74–42.75 m and 42.77 m. Graptolites at 42.20 m and 42.44 m. Clay layer at 41.92–41.94 m. Strongly glossy biotite appearance at 42.07–42.10 m and moderately glossy biotite appearance at 42.18–42.26 m.
42.84–43.80	***Black shale*** *(42.84–43.19 m and 43.62–43.80 m)* and ***DI-4 shale*** *(43.19–43.62 m)**:*** silty (moderate amount, however high amount in the presence of clay). No carbonate. Pyrite at 42.98 m (6 mm, matte vein), 43.18 m, 43.26 m (three grains; 4 mm, 4 mm and 5 mm, matte), 43.36 m (5 mm, matte, gold-shiny), 43.39 m, 43.47 m, 43.48 m, 43.56 m, 43.60 m, 43.61 m and 43.77 m (6 mm, matte). Graptolites at 43.23 m, 43.42 m, 43.43 m and 43.59 m. Minor fracture zone (clay and shale) at 43.13–43.25 m. Clay at 43.57–43.80 m. Slightly glossy at 43.31 m.
43.80–44.76	***Black shale:*** silty (low at 43.80–44.00 m, high at 44.00–44.17 m, moderate at 44.17–44.29 m and high 44.29–44.76 m). Moderate carbonate content, decreasing down-section. Pyrite at 43.95 m (3 mm, shiny), 44.23 m (4 mm, shiny), 44.27 m, 44.29 m, 44.32 m, 44.32 m, 44.35 m (5 mm, shiny), 44.68 m (10 mm, shiny), 44.75 m and 44.75 m. Clay layer at 44.40–44.46 m and clay at 44.52–44.73 m.
Fågelsång-3 – box 11	
44.69–45.71	***DI-4 shale*** *(44.69–44.81 m)* and ***black shale*** *(44.81–45.71 m)**:*** silty (moderate to high, alternating throughout the interval). Low carbonate content. Oxidized pyrite at 45.19 m. Pyrite at 44.72 m, 44.76 m, 44.80 m, 44.82 m (6 mm, shiny), 44.89 m (3 mm, matte, bronze-colored), 44.93 m, 44.95 m, 45.04 m, 45.06 m, 45.08 m, 45.13 m, 45.20 m, 45.25 m, 45.28 m, 45.30 m, 45.41 m, 45.51 m, 45.62 m and 45.63 m. Clay can be observed throughout the interval.
45.68–46.70	***Black shale*** *(45.68–46.56 m and 46.63–46.70 m)* and ***DI-4 shale*** *(46.56–46.63 m)**:*** silty (moderate to high, alternating throughout the interval). Low to high carbonate content. Pyrite at 45.72 m, 45.73 m (3 mm, shiny, weathered), 45.79 m, 45.81 m, 45.86 m, 45.93 m, 45.97 m (3 mm, shiny), 45.99 m, (two grains; 7 mm, 4 mm, gold-shiny), 46.00 m (3 mm, matte-shiny), 46.01 m, 46.03 m, 46.13 m (3 mm, shiny), 46.26 m, 46.29 m and 46.31 m (9 mm, matte, weathered, bronze-colored to brownish). Graptolites at 45.71 m, 45.90 m, 46.12 m and 46.54 m. Occasionally low content of clay.
46.65–47.69	***Black shale:*** silty (low at 46.65–47.27 m and high at 47.27–47.41 m). Very low carbonate content. Graptolites at 47.46 m, 47.50 m and 47.51 m. A mixture of clay and soil at 47.30–47.36 m.
47.67–48.71	***Black shale*** *(47.67–48.42 m)* and ***DI-4 shale*** *(48.42–48.71 m)**:*** no silt. High carbonate content at 48.64–48.71 m.
Fågelsång-3 – box 12	
48.62–49.64	***DI-2 shale*** *(48.62–48.79 m and 49.37–49.53 m)*, ***bentonite clay*** *(48.79–48.83 m, 49.15–49.25 m (mixed with grey shale) and 49.53–49.62 m)*, ***limestone*** *(48.83–48.91 m, 48.93–48.96 m, 48.96–49.15 m, 49.25–49.37 m and 49.62–49.64 m)* and ***mix of shale and bentonite clay*** *(48.91–48.93 m)**:*** no silt. No carbonate content (excluding the limestone). Oxidized pyrite at 48.67–48.70 m. Pyrite at 48.67–48.75 m (many grains; matte, shiny, weathered, bronze-colored). Green mineral observed at 48.70 m, putative glauconite.
49.37–50.41	***Bentonite clay*** *(49.37–49.44 m)*, ***limestone*** *(49.44–50.18 m and 50.31–50.41 m)*, ***DI-4 shale*** *(50.18–50.21 m)* and ***DI-2 shale*** *(50.21–50.31 m)**:*** no silt. No carbonate content (excluding the limestone).

Depth (m)	Description
50.38–51.41	***Limestone*** *(50.38–50.75 m, 50.79–50.89 m and 51.02–51.41 m),* ***DI-4 shale*** *(50.75–50.79 m),* ***black shale*** *(50.89–50.94 m and 50.96–51.02 m)* and ***dark green shale*** *(50.94–50.96 m):* no silt. No carbonate content (excluding the limestone). Pyrite at 51.24 m and 51.27 m (two grains; 4 mm, matte, weathered and 4 mm, matte-shiny).
50.41–52.45	***Limestone*** *(51.41–52.45 m):* no silt. Pyrite at 52.45 m.
Fågelsång-3 – box 13	
52.45–53.29	***Limestone:*** no silt. Pyrite at 53.12 m (3 mm, gold-shiny), 53.13 m (4 mm, gold-shiny), 53.15–53.16 m, 53.18 m (4 mm, matte, weathered), 53.18 m (4 mm, matte), 53.20 m (6 mm, gold-like), 53.23–53.26 m (large grains, gold-like), 53.26 m (4 mm, gold-like), 53.27–53.29 m (large grains, gold-like). Darker parts at 52.68–52.97 m.
53.18–54.19	***Limestone:*** no silt. Darker parts at 53.43–53.52 m, 53.74–53.80 m, 53.96–53.98 m and 53.99–54.02 m. Fractured at 53.31–53.43 m.
54.19–55.23	***Limestone:*** no silt. Darker parts at 54.19–54.36 m and 54.44–54.52 m. Fractured at 54.97–55.00 m.
55.21–56.12	***Limestone*** *(55.21–55.26 m, 55.29–55.53 m and 55.80–56.00 m),* ***dark green shale*** *(55.26–55.29 m)* and ***black shale*** *(55.53–55.80 m and 56.00–56.12 m):* no silt. Moderate to high carbonate content at 55.53–55.80 m and low to moderate at 56.00–56.12 m. Pyrite at 55.88 m, 55.93 m and 55.95 m. Limestone lenses can be observed at 55.57 m (25 mm in size) and 55.75 m (20 mm in size).
Fågelsång-3 – box 14	
56.12–57.15	***Black shale*** *(56.12–56.82 m)* and ***limestone*** *(56.65–56.67 m and 56.82–57.15 m):* silty (high amount at 56.12–56.82 m and low amount at 56.82–57.15 m). High carbonate content. Pyrite at 56.18 m (3 mm, matte), 56.18 m (4–5 mm grains, matte), 56.20 m, 56.21 m, 56.41 m and 56.56 m. Clay-silt mixture can be observed at 56.12–56.25 m (moderate), 56.25–56.44 m (high) and 56.44–56.82 m (low to moderate). The clay-silt mixture has high carbonate content.
57.12–58.01	***Limestone*** *(57.12–57.19 m)* and ***black shale*** *(57.19–58.01 m):* silty (high). High carbonate content. Pyrite at 57.22 m, 57.24 m, 57.26 m, 57.32 m, 57.33 m, 57.34 m, 57.57 m, 57.69 m, 57.82–57.88 m, 57.88 m, 57.89 m, 57.90 m, 57.91 m, 57.99 m and 58.00–58.01 m. Graptolites at 57.39 m and 57.54 m. Clay-silt mixture (moderate to low, with high carbonate content) can be observed.
57.95–58.94	***Black shale:*** silty (low to moderate). Low carbonate content. Oxidized pyrite at 58.84 m. Pyrite at 57.98 m (5 mm, gold-matte), 58.00 m (many grains, gold-shiny), 58.01 m (5 mm, gold-shiny), 58.03 m (several larger grains, gold-shiny), 58.04 m (5 mm, gold-shiny), 58.05 m (5 mm, gold-shiny), 58.05 m (4 mm, gold-shiny), 58.07 m (3 mm, gold-white), 58.15 m, 58.15 m, 58.36 m (4 mm, matte, weathered), 58.63 m (3 mm, gold-shiny), 58.71 m (larger grains, matte, weathered), 58,72 m, 58.74 m, 58.77 m (5 mm, matte, weathered), 58.79 m, 58.80 m and 58.82 m.
58.88–59.86	***Black shale:*** silty (low to moderate). Moderate carbonate content. Oxidized pyrite at 59.08 m. Pyrite at 58.92 m (4 mm, matte, weathered), 58.94 m (large grain, matte), 58.97 m (3 mm, gold-shiny), 58.99 m, 59.10 m (two larger grains, shiny), 59.12 m (4 mm, matte, shiny), 59.14 m, 59.16 m, 59.18 m (3 mm, gold-shiny), 59.21 m, 59.25 m (large grain, gold-shiny), 59.26 m, 59.27 m and 59.67–59.70 m (two very large grain, matte-shiny). Clay-silt mixture (low to moderate, with high carbonate content) can be observed.
Fågelsång-3 – box 15	
59.86–60.90	***Black shale:*** silty (low to moderate). Moderate carbonate content. Pyrite at 59.95 m (6 mm, matte vein), 60.05 m, 60.09 m, 60.12 m, 60.17 m, 60.18 m, 60.27 m (4 mm, matte vein), 60.28 m (large pyrite, matte), 60.49 m, 60.64 m, 60.72 m, 60.78 m (large pyrite, shiny, bronze-gold-colored), 60.81–60.83 m (two very large grains, matte-shiny) and

Depth (m)	Description
	60.90 m (13 mm, bronze-gold-colored). Graptolites at 60.28 m and 60.55 m. Clay-silt mixture (low, with high carbonate content) can be observed.
60.82–61.75	***Black shale:*** silty (moderate to high amount at 60.82–61.30 m and low to moderate amount at 61.30–61.75 m). Moderate carbonate content. Pyrite at 60.83 m (17 mm, matte, weathered, gold-like), 60.87 m (3 mm, matte, gold-shiny), 60.91 m (3 mm, matte, weathered, gold-like), 60.94 m (two grains: 4 mm, matte, gold-like), 60.96 m (9 mm, very matte, gold-like), 60.99 m, 61.00 m (7 mm, very matte, gold-like), 61.01 m (7 mm, very matte, gold-like), 61.07–61.13 m (large grains, matte, weathered, gold-like), 61.14–61.16 m, 61.20 m (6 mm, matte, gold-like), 61.21–61.24 m, 61.27 m (7 mm, very matte, gold-like), 61.29 m (15 mm, weathered, gold-like), 61.34 m (two large grains; 18 mm and 20 mm, weathered, gold-shiny), 61.38 m (5 mm, matte, weathered, gold-like), 61.39 m (11 mm, matte-shiny, gold-like), 61.40 m (5 mm, matte-shiny, gold-like), 61.50 m, 61.53 m, 61.58 m, 61.59 m, 61.63 m (12 mm nodule, gold-shiny with small cubes), 61.64 m, 61.69 m, 61.72 m and 61.74 m. Graptolite at 60.97 m.
61.74–62.71	***Black shale:*** silty (high). High carbonate content. Pyrite at 61.76–61.79 m (two grains; 19 mm and 9 mm (vein), gold-shiny, slightly weathered), 61.80 m, 61.83 m, 61.85 m, 61.87 m (18 mm, very matte, weathered), 61.89 m, 61.94 m, 61.95–61.97 m (two grains; 12 mm and 7 mm, very matte, weathered veins with small cubes inside), 62.03 m, 62.06 m (a few larger grains, very matte, weathered), 62.09–62.12 m (two grains; 20 mm and 8 mm, very matte, weathered), 62.15 m, 62.16–62.18 m (two grains; 18 mm and 8 mm (vein), very matte, weathered), 62.18–62.20 m, 62.21 m, 62.23 m (5 mm, matte, gold-shiny), 62.24 m, 62.27 m, 62.32 m, 62.36 m, 62.39 m (12 mm, matte, weathered), 62.46 m, 62.48 m, 62.49 m, 62.51 m, 62.55 m, 62.59 m, 62.60 m, 62.64 m, 62.66 m, 62.67 m and 62.70 m (6 mm nodule, shiny with cubes). Clay-silt mixture (moderate, with high carbonate content) can be observed.
62.69–63.70	***Black shale*** *(62.69–63.07 m and 63.24–63.70 m)*, ***limestone*** *(63.07–63.10 m and 63.17–63.24 m)* and ***bentonite clay*** *(63.10–63.17 m)****:*** silty (high amount at 62.76–62.89 m, 63.07–63.10 m and 63.34–63.37 m, otherwise a moderate amount). High carbonate content at 62.76–62.89 m, 63.07–63.11 m and 63.18–63.25 m, while the rest of the interval has low carbonate content. Pyrite at 62.73 m (7 mm, matte, weathered), 62.89 m (cluster of nodules, matte, weathered cubes), 62.92 m, 62.97 m, 63.06 m, 63.25 m, 63.26 m, 63.36 m (two grains; 11 mm and 13 mm, very matte, weathered), 63.41 m, 63.45 m, 63.52 m and 63.63 m. At 62.83–62.88 m there is a black shale with veins of limestone.
Fågelsång-3 – box 16	
63.51–64.52	***Black shale:*** silty (high). High carbonate content. Pyrite at 63.57 m, 63.62 m, 63.67–63.69 m, 63.74 m, 63.77 m, 63.79 m, 63.87 m, 63.89 m, 63.91 m, 63.92–63.93 m (shiny vein), 63.95 m, 64.02 m, 64.05–64.07 m (matte, weathered vein, split into smaller), 64.12 m, 64.16 m, 64.22 m, 64.23 m, 64.25 m, 64.28 m and 64.28 m. Fracture zone with putative clay (containing high carbonate content) at 64.37–64.52 m.
64.52–64.87	***Black shale:*** silty (high). High carbonate content. Pyrite at 64.54 m, 64.56 m, 64.59 m, 64.71 m and 64.78 m. Fractured at 64.77–64.87 m.

Appendix C

Table C1: Analytical parameters for LA-ICP-MS analysis of pyrites. A fluence rate of 2.30 J/cm^2 was used on the L1 samples. This was later increased to 2.80 J/cm^2 and applied to the rest of the samples (F1, F2 and L2 samples).

LA-ICP-MS	
Laser ablation system *(Cetac Analyte G2, excimer laser[1])*	
Sample holder	HelEx2 Active 2-volume
Laser wavelength	193 nm
Pulse width	<4 ns
Repetition rate	6 Hz
Spot size	60 μm
Fluence	2.30 J/cm^2, 2.80 J/cm^2
Burst count	138 shots
Carrier gas	He and N2 mixed downstream with Ar
Carrier gas flow	He 0.8 L/min, N2 0.03 L/min
Background collection	20 seconds
Ablation duration	23 seconds
Wash-out delay	30 seconds
ICP-MS instrument *(Aurora Elite, quadrupole ICP-MS[2])*	
Detection system	Single collector
Sample introduction	Via conventional tubing
RF power	1.4 kW
Sample gas flow	Ca. 0.93 L/min Ar
Dwell time	10 ms (millisecond) for each
Masses measured	^{33}S, ^{51}V, ^{52}Cr, ^{55}Mn, ^{59}Co, ^{65}Cu, ^{69}Ga, ^{75}As, ^{82}Se, ^{98}Mo, ^{107}Ag, ^{114}Cd, ^{121}Sb, ^{184}W, ^{193}Ir, ^{202}Hg, ^{208}Pb and ^{209}Bi.

(1) LA-system: made by Photon Machines
(2) ICP-MS instrument: made by Bruker

Appendix D

Table D1: Compilation of data from LA-ICP-MS analysis for Lerhamn drill core. Isotopes analyzed include ^{33}S, ^{51}V, ^{52}Cr, ^{55}Mn, ^{59}Co, ^{65}Cu, ^{69}Ga, ^{75}As, ^{82}Se, ^{98}Mo, ^{107}Ag, ^{114}Cd, ^{121}Sb, ^{184}W, ^{193}Ir, ^{202}Hg, ^{208}Pb and ^{209}Bi. Note, all concentrations are based on above mentioned isotopes and re-calculated after relative natural abundance for all isotopes for that particular element. *Bdl* = below detection limit, refers to isotopes that are not present in sufficient concentrations to be detected by the instrument. *Nd* = not determined, no analysis was done. *Rejected* = no data was retrieved. *DI* = darkness index, the darker the shale the higher the number.

			Measured elements (ppm)									
Spot I.D	**Sample**	**Depth (m)**	**As**	**S**	**V**	**Cr**	**Mn**	**Co**	**Cu**	**Ga**	**Se**	**Bedrock**
Output_1_1	L1	17.55	*Rejected*	*Rejected*	*Rejected*	*Rejected*	*Rejected*	*Rejected*	*Rejected*	*Rejected*	*Rejected*	No data retrieved
Output_1_2	L1	18.88	*Rejected*	*Rejected*	*Rejected*	*Rejected*	*Rejected*	*Rejected*	*Rejected*	*Rejected*	*Rejected*	No data retrieved
Output_1_3	L1	19.85	34.7	459000	5.73	4.4	990	51.2	42	1.521	4	DI-1
Output_1_4	L1	20.20	207.4	396900	0.257	0.39	0.185	57.5	241	0.008	3.1	DI-1
Output_1_5	L1	20.69	1.01	454000	0.8	0.58	8.5	2.35	157	0.213	5.7	DI-1
Output_1_6	L1	21.77	0.58	442000	0.445	0.69	46.2	0.98	*Bdl*	0.113	3.8	DI-1
Output_1_7	L1	22.96	0.04	407500	*Bdl*	0.24	0.126	*Bdl*	*Bdl*	0.001	0.1	DI-2
Output_1_8	L1	23.61	254.7	401500	0.618	0.37	0.168	27.23	*Bdl*	0.037	*Bdl*	DI-2
Output_1_9	L1	23.17	133.8	407200	1.109	0.37	0.093	73.39	*Bdl*	0.043	15.9	DI-2
Output_1_10	L1	24.68	7.01	446000	3.41	2.26	22.1	21.1	*Bdl*	0.852	7.3	DI-2
Output_1_11	L1	25.63	0.64	411300	0.007	*Bdl*	29.53	0.093	*Bdl*	0.009	1.21	DI-3
Output_1_12	L1	26.22	197.5	412500	0.872	0.97	0.692	229.3	58	0.035	44.6	DI-2
Output_1_13	L1	26.29	45.22	402100	0.158	0.37	0.4	9.89	*Bdl*	0.154	10.5	DI-2
Output_1_14	L1	26.70	53.3	445000	0.042	0.12	0.563	0.026	*Bdl*	*Bdl*	5.7	DI-3
Output_1_15	L1	27.28	107	409300	0.869	0.98	0.901	59.7	238	0.05	17.8	DI-3
Output_1_16	L1	27.85	122.3	401200	1.336	0.64	0.516	107.6	76	0.033	27.4	Grey shale
Output_1_17	L1	28.29	128.5	400300	0.86	0.88	0.653	67.3	23	*Bdl*	26	DI-1
Output_1_18	L1	28.97	134.1	401500	1.13	0.59	0.347	58.83	*Bdl*	0.022	8.6	Grey shale
Output_1_19	L1	29.21	131	401600	1.34	0.74	0.613	72.6	157	0.02	18.2	Grey shale
Output_1_20	L1	29.87	1.1	455000	0.442	0.27	45.1	0.904	28	0.086	11.7	DI-4
Output_1_21	L1	30.19	1.08	459000	*Bdl*	0.33	42.3	0.045	*Bdl*	*Bdl*	12.1	DI-4
Output_1_22	L1	30.30	142.4	397100	0.873	0.8	8.51	9.59	*Bdl*	0.002	1.3	DI-4
Output_1_23	L1	30.48	1590	404800	0.629	0.51	270.3	1.558	330	0.111	251.5	DI-4
Output_1_24	L1	30.59	240.4	392300	1.81	1.08	537	0.9	*Bdl*	0.157	27.3	DI-4

Spot I.D	Sample	Depth (m)	Measured elements (ppm)									Bedrock
			As	S	V	Cr	Mn	Co	Cu	Ga	Se	
Output_1_25	L1	30.62	250.3	409200	1.984	0.51	0.646	54.68	*Bdl*	0.016	5.3	DI-4
Output_1_26	L1	30.93	470.2	400900	0.837	0.34	21.96	7.59	*Bdl*	*Bdl*	6.4	DI-4
Output_1_27	L1	31.21	335.7	402800	1.86	1.38	142	35.7	*Bdl*	0.216	13.4	DI-4
Output_1_28	L1	31.39	100.7	431000	6.69	1.17	46.3	7.84	24	0.542	29.1	DI-4
Output_1_29	L1	31.53	49.2	436000	0.058	0.36	0.765	0.439	*Bdl*	*Bdl*	8	DI-4
Output_1_30	L1	31.60	454.7	399500	6.24	0.34	1303	0.052	1210	0.056	12.7	DI-4
Output_1_31	L1	32.04	59	439000	0.464	0.29	26.5	1.81	*Bdl*	*Bdl*	31.5	DI-4
Output_1_32	L1	32.34	1015	417000	4.316	0.4	1.212	2.395	*Bdl*	0.121	2.4	DI-4
Output_1_33	L1	32.40	253.9	411400	2.061	0.45	0.431	6.62	*Bdl*	0.066	*Bdl*	DI-4
Output_1_34	L1	32.60	921	390800	2.103	0.4	3.1	2.043	*Bdl*	0.01	8.6	DI-4
Output_1_35	L1	33.21	124.1	401100	0.109	0.45	4620	11.27	310	0.007	19	Black shale
Output_1_36	L1	33.90	39.2	394000	2	1.5	115.4	13.6	94	0.266	9.2	DI-4
Output_1_37	L1	34.12	16.75	395000	0.3	0.35	15.74	0.023	119	*Bdl*	18.9	DI-4
Output_1_38	L1	34.61	1056	394500	3.3	1.67	153.1	54.5	226	0.268	5.9	Grey shale
Output_1_39	L1	34.84	1369	392000	0.194	0.76	165	12.71	360	0.029	6.4	Grey shale
Output_1_40	L1	34.88	190.2	395100	1.578	0.58	322	0.6	9	0.013	13.5	Grey shale
Output_1_41	L1	35.14	484	390600	0.719	0.86	606	6	310	0.024	11.4	Grey shale
Output_1_42	L1	35.63	699	399000	0.091	0.48	663	0.18	360	*Bdl*	4.7	DI-4
Output_1_43	L1	35.77	404.2	395700	3.117	0.38	450	0.099	*Bdl*	*Bdl*	6.2	DI-4
Output_1_44	L1	35.92	615	403400	11	3.38	222.4	62.1	123	0.5	21.8	DI-4
Output_1_45	L1	36.05	124.5	409700	3.715	0.41	2174	0.734	660	*Bdl*	219.3	DI-4
Output_1_46	L1	36.10	30.83	394100	0.173	0.64	41.18	5.9	*Bdl*	0.014	*Bdl*	Grey shale
Output_1_47	L1	36.19	49.8	402000	4.37	0.57	2.61	20.5	*Bdl*	0.131	17.9	Grey shale
Output_1_48	L1	36.26	1027	404100	5.06	1.07	17.6	4.51	*Bdl*	0.182	10.3	DI-1
Output_1_49	L1	36.66	2602	395900	11.61	0.75	3.56	78.8	*Bdl*	0.076	32.7	DI-1
Output_1_50	L1	36.75	862	408700	0.241	0.42	35.99	49.1	95	0.024	0.5	Grey shale DI-I
Output_1_51	L1	37.01	2601	403700	6.95	2.26	623.2	420.1	66	0.592	5.2	DI-3
Output_1_52	L1	37.26	5504	395900	6.42	0.88	15.84	0.268	190	0.002	0.3	DI-1
Output_1_53	L1	37.27	6129	404600	20.52	2.95	29.01	321.6	*Bdl*	1.28	5.4	DI-1
Output_1_54	L1	37.37	2685	399300	4.36	0.46	1.436	122.7	99	0.006	26.4	DI-1
Output_1_55	L1	37.41	2750	405500	10.39	1.43	3.73	258.8	65	0.336	10.6	DI-1
Output_1_56	L1	37.56	2881	405000	21.76	1.31	13.74	115.8	32	0.72	30.8	DI-1

			Measured elements (ppm)									
Spot I.D	**Sample**	**Depth (m)**	**As**	**S**	**V**	**Cr**	**Mn**	**Co**	**Cu**	**Ga**	**Se**	**Bedrock**
Output_1_57	L1	37.58	2126	397500	18.93	1.12	7.9	60.8	*Bdl*	0.217	39.7	DI-1
Output_1_58	L1	37.64	470.7	402700	14.58	1.07	1.98	31.52	123	0.069	59.8	DI-4
Output_1_59	L1	37.73	1944	399500	7.5	0.98	19.74	8.43	102	0.052	2.1	DI-4
Output_1_60	L1	38.66	65.6	409400	3.42	1.41	2.19	49.1	*Bdl*	0.342	2.3	DI-4
Output_1_61	L1	38.70	71.2	399000	0.019	0.22	25.1	26.9	*Bdl*	0.004	*Bdl*	DI-4
Output_1_62	L1	38.78	24.1	388800	0.21	0.53	0.61	16.2	*Bdl*	0.035	3	DI-4
Output_1_63	L1	38.91	3.61	394000	0.21	0.18	0.71	25.3	*Bdl*	0.01	3.4	Grey shale
Output_1_64	L1	39.23	501.6	398400	3.797	0.64	1.075	179.2	*Bdl*	0.03	30.9	DI-4
Output_1_65	L1	39.60	999	394500	2.323	0.68	2.956	60.14	101	0.067	4	DI-4
Output_1_66	L1	39.88	744.9	399400	3.815	0.66	2.181	310.7	*Bdl*	0.01	27.9	DI-1
Output_1_67	L1	40.06	817	405300	21.05	1.98	44.3	129.7	182	0.395	17.6	DI-1
Output_1_68	L1	40.40	1488	405900	14.12	2.21	13.86	275.9	243	1.03	6.7	DI-1
Output_1_69	L1	40.49	17660	404300	3.85	0.69	17	185.8	*Bdl*	0.103	7.8	Limestone
Output_1_70	L1	40.71	22.63	427100	5.4	1.95	6.42	22.48	*Bdl*	0.755	16.1	DI-4
Output_1_71	L1	40.80	612	402300	1.531	0.99	21.48	59.6	173	0.094	4.7	DI-4
Output_1_72	L1	40.87	1250	402000	10.79	0.82	7.52	76.2	121	0.009	30.6	DI-4
Output_1_73	L1	41.09	1204	401200	3.372	1.09	4.83	12.64	160	0.02	8	DI-4
Output_1_74	L1	41.13	2118	399500	2.377	0.77	15.3	6.36	42	0.133	2.3	DI-4
Output_1_75	L1	41.20	328.8	400500	0.809	0.75	27.77	35	270	0.111	0.5	DI-4
Output_1_76	L1	41.25	12.1	449000	2.79	0.9	2.61	8.93	*Bdl*	0.259	0.3	DI-4
Output_1_77	L1	41.34	297	410800	18.8	2.33	38.7	339.5	232	0.786	13.6	DI-4
Output_1_78	L1	41.52	301.5	405900	4.277	0.58	3.209	89.3	74	0.033	20.8	DI-4
Output_1_79	L1	41.57	300.6	404800	3.96	1.07	1.37	74.8	*Bdl*	9.4	8.3	DI-4
Output_1_80	L1	41.67	205.3	410700	2.968	0.2	0.16	37.35	*Bdl*	*Bdl*	14.4	DI-4
Output_1_81	L1	41.79	577	412300	17.72	1.17	3.12	73.1	126	0.111	38.7	DI-4
Output_1_82	L1	42.68	591.7	405100	13.62	1.57	5.42	130.6	181	0.406	7.7	DI-4
Output_1_83	L1	42.71	1603	402800	9.21	0.94	9.79	29.9	310	0.245	4.3	DI-4
Output_1_84	L1	42.98	2037	412900	3.18	1.32	5.37	335.7	300	0.156	12.5	DI-4
Output_1_85	L1	43.10	3.47	484000	0.125	0.21	0.017	0.399	*Bdl*	0.006	2.5	DI-4
Output_1_86	L1	43.15	2716	410100	4.35	1.33	4.55	24.94	165	0.185	7.8	DI-4
Output_1_87	L1	43.24	451.9	406800	3.079	0.47	4.6	83	86	0.046	14	DI-4
Output_1_88	L1	43.27	718	413500	6.8	1.36	6.69	62.37	219	0.231	17.6	DI-4

			Measured elements (ppm)									
Spot I.D	**Sample**	**Depth (m)**	**As**	**S**	**V**	**Cr**	**Mn**	**Co**	**Cu**	**Ga**	**Se**	**Bedrock**
Output_1_89	L1	43.31	233	418200	3.112	0.65	1.51	117	*Bdl*	0.026	21.6	DI-4
Output_1_90	L1	43.33	25.9	453000	1.35	0.68	1.17	0.715	*Bdl*	0.159	2	DI-4
Output_1_91	L1	43.82	328.1	415400	3.09	0.78	3.67	106	70	0.06	16	DI-4
Output_1_92	L1	44.07	2565	417500	0.996	1	5.06	59.96	175	0.038	29.4	DI-4
Output_1_93	L1	44.14	1925	403100	1.542	1.3	34.9	2.234	123	0.063	*Bdl*	DI-4
Output_1_94	L1	44.20	761.5	400400	5.53	0.88	8.89	4.95	127	0.039	19.6	DI-4
Output_1_95	L1	44.50	19.83	438000	0.22	0.23	0.135	49	*Bdl*	0.05	50.6	DI-1
Output_1_96	L1	44.57	1125	408000	2.245	1	9.7	82.06	149	*Bdl*	30.7	Black shale
Output_1_97	L1	44.76	235.4	411400	8.18	0.54	2.374	40.34	42	*Bdl*	14.9	Black shale
Output_1_98	L1	44.83	168.7	402300	1.111	0.76	5.81	71.6	152	0.016	11	Black shale
Output_1_99	L1	45.06	1292	406400	12.51	1.57	11.21	20.2	212	0.184	2.4	Black shale
Output_1_100	L1	45.14	337.4	404100	1.354	1.05	8.22	11.26	124	0.066	4.9	Black shale
Output_1_101	L1	45.43	187	403400	2.461	0.5	11.48	2.613	9	0.005	33.7	DI-3
Output_1_102	L1	45.53	185.8	417100	4.639	0.56	2.594	90.12	*Bdl*	*Bdl*	25.9	DI-3
Output_1_103	L1	45.63	6.44	418600	0.806	0.4	*Bdl*	1.37	*Bdl*	0.166	4.9	DI-4
Output_1_104	L1	45.78	546	411200	2.542	0.56	177.3	0.007	116	*Bdl*	6.6	DI-4
Output_1_105	L1	46.00	591	418300	0.588	0.69	587	4.22	400	0.076	18.1	DI-4
Output_1_106	L1	46.10	319	404300	3.443	0.58	6.71	4.59	*Bdl*	0.029	1.8	Black shale
Output_1_107	L1	46.13	645	411400	6.18	0.63	214	0.158	211	0.068	24.8	Black shale
Output_1_108	L1	46.29	154.9	428100	5.44	0.7	1.79	18.28	*Bdl*	0.092	4.8	Black shale
Output_1_109	L1	46.38	1922	406400	2.039	0.65	1790	1.027	66	0.006	119.9	Black shale
Output_1_110	L1	46.53	356.4	404200	5.45	0.71	1807	1.83	264	0.004	80.9	Black shale
Output_1_111	L1	46.65	21.1	460000	0.184	0.49	28400	26.61	1860	0.007	3.17	DI-4
Output_1_112	L1	46.93	911	406100	5.79	1.33	77	5.29	83	0.166	14.4	DI-4
Output_1_113	L1	47.00	565	395600	3.52	0.79	121	0.056	179	0.01	11.4	DI-4
Output_1_114	L1	47.15	555	406100	14.09	0.5	2750	2.24	43.6	0.047	68.1	Black shale
Output_1_115	L1	47.25	1049	414900	0.92	0.9	1324	10.83	114.9	0.175	51.3	Black shale
Output_1_116	L1	47.36	1177	403800	5.55	0.83	9	0.088	2.4	0.061	0.7	DI-4
Output_1_117	L1	47.43	377.6	419400	8.83	0.59	771	6.23	486	0.057	174.9	DI-4
Output_1_118	L1	47.51	915	421000	0.955	0.61	2660	2.94	201	0.82	217	DI-4
Output_1_119	L1	47.57	582	412100	1.42	0.77	2713	53.7	140.3	0.112	14.2	Grey shale
Output_1_120	L1	47.66	1300	415200	0.763	0.71	605	6.35	124.9	0.015	31.9	Grey shale

			Measured elements (ppm)									
Spot I.D	**Sample**	**Depth (m)**	**As**	**S**	**V**	**Cr**	**Mn**	**Co**	**Cu**	**Ga**	**Se**	**Bedrock**
Output_1_121	L1	47.79	701	436800	1.119	0.61	54700	0.135	10870	2.27	41.1	Grey shale
Output_1_122	L1	47.87	362.5	416800	4.79	0.8	4	18.14	12.8	0.082	3	DI-1
Output_1_123	L1	48.02	1409	429000	7.01	0.55	16400	0.295	575	1.53	552	DI-1
Output_1_124	L1	48.19	115.6	412800	2.331	0.52	0.5	19.39	2.1	0.155	3.8	Black shale
Output_1_125	L1	48.61	1080	404200	0.327	0.13	34300	1.87	397	0.008	66.5	DI-4
Output_1_126	L1	48.80	5.39	393200	0.019	0.36	0.5	0.179	13.3	*Bdl*	0.3	Black shale
Output_1_127	L1	48.93	585	407900	6.91	2.01	2007	42.7	142.3	0.477	43.9	Black shale
Output_1_128	L1	49.02	1041	407600	3.313	1.05	138	7.24	31.8	0.097	10.3	Black shale
Output_1_129	L1	49.32	235.2	413400	3.316	0.56	0.5	5.75	1	0.092	1.9	DI-4
Output_1_130	L1	49.50	316.3	411100	9.21	0.59	2.9	6.8	2.2	0.086	5.9	DI-4
Output_1_131	L1	49.58	481	413500	31.3	4.59	117	33	140	0.81	23.5	DI-4
Output_1_132	L1	49.64	857	405300	5.29	0.63	3721	0.056	1708	0.02	126	DI-4
Output_1_133	L1	50.23	1409	415300	19.08	0.64	29300	1.09	1722	0.033	143.6	Black shale
Output_1_134	L1	50.60	267.7	399900	3.081	0.72	4.8	13.21	6.7	0.02	1.9	Black shale
Output_1_135	L1	51.25	242.7	417700	0.28	0.55	4058	23.65	58.9	0.045	72.8	DI-1
Output_1_136	L1	52.44	178.8	406400	1.265	0.44	1266	0.58	310	0.013	58	Black shale
Output_1_137	L1	53.70	513	404000	0.68	0.63	488	0.132	67.3	0.007	8.9	DI-4
Output_1_138	L1	54.98	36.3	404200	0.323	0.63	782	0.948	12.9	0.01	6.3	DI-4
Output_1_139	L1	55.74	99	403500	0.239	0.83	78	0.013	52.3	0.026	2.8	DI-4
Output_1_140	L1	56.63	512	423000	0.138	0.74	950	0.992	189	*Bdl*	55.4	DI-4
Output_1_141	L1	57.50	742	391200	0.101	0.92	8.1	7.09	9.9	*Bdl*	1.6	Green shale
Output_1_142	L1	58.50	315.4	398900	2.84	2.11	245	9.97	332	0.337	30.7	Green shale
Output_1_143	L1	59.44	625	404100	0.122	0.53	704	0.517	343	0.007	74.1	Green shale
Output_1_144	L1	60.01	321.5	404300	0.407	0.58	1518	17.47	15.8	0.023	36.9	DI-4
Output_1_35	L2	60.15	846	414500	2.42	1.74	1628	0.136	*Bdl*	0.295	252.6	DI-4
Output_1_145	L1	60.94	749.4	395700	1.28	1.1	32	3.02	240	0.055	14.4	DI-4
Output_1_36	L2	61.35	0.787	424200	0.0032	0.72	66.2	0.1832	24	0.162	36.49	DI-4
Output_1_146	L1	61.84	0.08	404500	0.151	0.86	44	0.015	5.1	0.176	3.2	Green shale
Output_1_37	L2	62.04	673	410100	0.0281	1.71	13.28	33.1	72	0.093	0.01	Green shale
Output_1_147	L1	62.57	77.4	401500	*Bdl*	0.32	958	0.022	2.5	0.021	2.4	Green shale
Output_1_148	L1	64.84	2.89	423300	0.453	0.6	3.7	0.434	11.7	0.069	27.5	DI-2
Output_1_149	L1	65.80	277.5	395800	0.034	0.59	6.1	17.83	35.5	0.01	1.5	Green shale

			Measured elements (ppm)									
Spot I.D	**Sample**	**Depth (m)**	**As**	**S**	**V**	**Cr**	**Mn**	**Co**	**Cu**	**Ga**	**Se**	**Bedrock**
Output_1_150	L1	66.35	27.8	480000	*Bdl*	0.49	0.1	0.459	2.8	0.013	3.3	DI-4
Output_1_151	L1	67.42	0.97	410800	0.048	0.22	67	0.164	42.3	0.052	21.5	DI-4
Output_1_152	L1	68.05	499	405700	0.878	0.53	74	0.117	69.3	0.131	3.7	Black shale
Output_1_153	L1	69.40	349	408000	3.45	0.89	2.3	9.14	14.3	0.185	*Bdl*	Black shale
Output_1_154	L1	70.37	470.1	413100	0.03	0.61	3.2	43.67	6.6	0.019	1.4	Dark green shale
Output_1_155	L1	71.55	454	416300	4.17	2.04	594	44.1	64.2	0.622	54.3	Black shale
Output_1_38	L2	71.86	428	410500	9.3	4.09	2409	70.8	77	4.21	251.2	DI-4
Output_1_156	L1	72.68	111.6	391100	*Bdl*	0.43	518	11.65	173	0.028	1.7	DI-4
Output_1_157	L1	73.71	167.9	402100	0.14	0.62	1.8	47.5	13.5	0.033	*Bdl*	DI-4
Output_1_39	L2	74.16	39.2	405100	0.0291	1.12	2750	76.5	8670	0.0268	5.63	Black shale
Output_1_158	L1	74.94	210.1	403400	0.554	0.69	135	5.03	314	0.07	4.1	Black shale
Output_1_159	L1	76.14	431.1	390700	0.69	0.7	61	0.199	143	0.059	0.8	Black shale
Output_1_40	L2	76.50	21.21	395900	9.6	2.73	2.88	2.27	23	1.33	7.06	DI-2
Output_1_160	L1	77.76	166.9	409200	0.033	0.5	16.0	17.41	158	0.013	1.9	DI-4
Output_1_161	L1	79.00	209.3	421100	0.039	0.66	10.7	20.71	42.9	0.006	8.1	DI-4
Output_1_41	L2	79.68	126.3	386400	0.618	1.21	213	5.2	304	0.27	17.8	Black shale

(Cont. Appendix D)

Spot I.D	Sample	Depth (m)	Measured elements (ppm)									Bedrock
			Mo	Ag	Cd	Sb	W	Ir	Hg	Pb	Bi	
Output_1_1	L1	17,55	*Rejected*	*Rejected*	*Rejected*	*Rejected*	*Rejected*	*Rejected*	*Rejected*	*Rejected*	*Rejected*	No data retrieved
Output_1_2	L1	18,88	*Rejected*	*Rejected*	*Rejected*	*Rejected*	*Rejected*	*Rejected*	*Rejected*	*Rejected*	*Rejected*	No data retrieved
Output_1_3	L1	19,85	2.68	0,781	0,025	11,99	0,122	*Bdl*	0,82	148,4	0,204	DI-1
Output_1_4	L1	20,20	17.19	11,61	0,028	21,49	0,026	*Bdl*	4,28	72,5	*Bdl*	DI-1
Output_1_5	L1	20,69	0.111	0,289	0,008	0,74	0,0145	*Bdl*	0,82	36,2	0,0015	DI-1
Output_1_6	L1	21,77	0.052	0,094	*Bdl*	0,39	0,024	0,0019	0,84	2,24	0,0014	DI-1
Output_1_7	L1	22,96	0.183	0,0017	0,017	0,0489	0,0254	0,0009	0,6	2,79	0,0012	DI-2
Output_1_8	L1	23,61	20.1	0,228	0,207	36,09	0,0172	*Bdl*	3,65	3,67	0,0046	DI-2
Output_1_9	L1	23,17	33.1	0,004	0,034	14,27	0,034	*Bdl*	3,68	70,4	0,009	DI-2
Output_1_10	L1	24,68	0.111	0,564	0,026	2,71	0,073	*Bdl*	0,91	26,4	0,3	DI-2
Output_1_11	L1	25,63	0.042	0,0208	0,006	0,133	*Bdl*	*Bdl*	*Bdl*	3,28	0,0004	DI-3
Output_1_12	L1	26,22	35.2	1,9	0,086	40,63	0,038	0,0014	15,52	355	0,0047	DI-2
Output_1_13	L1	26,29	128.5	0,0366	0,038	1,742	0,018	0,0031	2,71	5,08	0,0002	DI-2
Output_1_14	L1	26,70	6.77	0,0061	0,019	2,205	0,0033	*Bdl*	0,44	1,585	0,0014	DI-3
Output_1_15	L1	27,28	40.21	3,23	0,055	19,14	*Bdl*	*Bdl*	5,63	23,51	0,0054	DI-3
Output_1_16	L1	27,85	32.04	0,373	0,103	35,11	0,0134	*Bdl*	8,05	180,5	0,0195	Grey shale
Output_1_17	L1	28,29	51.2	0,209	0,035	22,79	0,0079	0,0006	3,81	94,3	0,0233	DI-1
Output_1_18	L1	28,97	30.58	0,031	0,065	21,44	0,007	*Bdl*	3,15	35,88	0,0043	Grey shale
Output_1_19	L1	29,21	37.79	0,946	0,096	36,93	0,0131	*Bdl*	5,62	46,93	*Bdl*	Grey shale
Output_1_20	L1	29,87	0.038	0,171	*Bdl*	0,125	0,0042	*Bdl*	0,31	9,63	0,0167	DI-4
Output_1_21	L1	30,19	0.13	0,149	0,001	0,189	0,0016	*Bdl*	0,2	1,201	*Bdl*	DI-4
Output_1_22	L1	30,30	99.3	0,011	0,064	44,36	0,0021	0,0001	1,93	13,18	*Bdl*	DI-4
Output_1_23	L1	30,48	491.2	9,88	0,061	30,28	0,001	*Bdl*	16,89	17,72	0,0003	DI-4
Output_1_24	L1	30,59	152	1,56	0,04	3,76	0,017	*Bdl*	5,14	2,59	0,0017	DI-4
Output_1_25	L1	30,62	114.2	*Bdl*	0,851	401,1	0,0057	0,0002	5,2	54,32	0,0004	DI-4
Output_1_26	L1	30,93	111.9	0,0452	0,192	102,4	*Bdl*	*Bdl*	*Bdl*	79,9	0,0041	DI-4
Output_1_27	L1	31,21	612	0,95	0,065	13,55	0,04	*Bdl*	0,39	38	0,0023	DI-4
Output_1_28	L1	31,39	29.89	0,454	0,174	41,1	0,0219	*Bdl*	1,3	88,8	0,0353	DI-4
Output_1_29	L1	31,53	2.7	0,078	0,306	20,28	*Bdl*	*Bdl*	0,29	46,1	0,0004	DI-4
Output_1_30	L1	31,60	504	42,12	0,495	22,5	*Bdl*	*Bdl*	13,78	32,5	0,0228	DI-4
Output_1_31	L1	32,04	16.93	0,099	0,188	32,2	*Bdl*	*Bdl*	0,61	9,7	0,044	DI-4

			Measured elements (ppm)									
Spot I.D	**Sample**	**Depth (m)**	**Mo**	**Ag**	**Cd**	**Sb**	**W**	**Ir**	**Hg**	**Pb**	**Bi**	**Bedrock**
Output_1_32	L1	32,34	420.4	0,0175	0,31	528,1	0,0175	*Bdl*	9,25	9,55	11,96	DI-4
Output_1_33	L1	32,40	175.3	0,388	0,419	203,1	0,009	*Bdl*	4,99	16,32	26,38	DI-4
Output_1_34	L1	32,60	122.4	0,016	0,262	377	0,0066	*Bdl*	8,14	8,27	10,19	DI-4
Output_1_35	L1	33,21	6.96	1,448	0,025	14,03	*Bdl*	*Bdl*	0,76	19,98	34,58	Black shale
Output_1_36	L1	33,90	791	0,954	0,089	3,15	0,0199	*Bdl*	0,78	11,71	20,39	DI-4
Output_1_37	L1	34,12	57.7	0,0341	0,074	24,11	0,0032	*Bdl*	2,5	0,45	0,0371	DI-4
Output_1_38	L1	34,61	124.7	3,22	0,233	12,13	0,06	0,0006	0,83	47,1	0,0014	Grey shale
Output_1_39	L1	34,84	121.1	1,506	0,015	4,87	0,0071	*Bdl*	0,74	17,5	0,0183	Grey shale
Output_1_40	L1	34,88	776	1,013	0,071	5,42	0,0101	*Bdl*	0,79	11,79	0,0007	Grey shale
Output_1_41	L1	35,14	112	5,09	0,028	6,65	0,0204	*Bdl*	2,12	4,64	0,0077	Grey shale
Output_1_42	L1	35,63	179.8	11,75	*Bdl*	3,45	*Bdl*	*Bdl*	0,41	1,04	0,0532	DI-4
Output_1_43	L1	35,77	821	0,085	0,081	85,5	0,036	0,0006	2,43	0,039	*Bdl*	DI-4
Output_1_44	L1	35,92	271.4	3,29	0,184	27,1	0,049	*Bdl*	2,5	80,5	0,0135	DI-4
Output_1_45	L1	36,05	125.8	26,76	0,571	42,34	*Bdl*	*Bdl*	3,67	59,4	0,0225	DI-4
Output_1_46	L1	36,10	38.33	0,781	*Bdl*	7,7	0,0054	0,0007	0,33	2,28	0,004	Grey shale
Output_1_47	L1	36,19	0.535	0,308	0,474	19,4	0,0156	0,0008	0,16	26,3	*Bdl*	Grey shale
Output_1_48	L1	36,26	395	2,3	0,171	67,5	0,0026	*Bdl*	3,63	29,8	*Bdl*	DI-1
Output_1_49	L1	36,66	45.6	2,53	2,165	389,8	0,093	0,0002	5,31	66	0,0031	DI-1
Output_1_50	L1	36,75	62.7	3,37	0,021	2,56	0,002	*Bdl*	*Bdl*	4,57	0,0004	DI-1
Output_1_51	L1	37,01	233.9	11,04	0,109	21,1	0,073	*Bdl*	1,42	109,3	0,0068	DI-3
Output_1_52	L1	37,26	60.6	3,85	0,642	206,1	0,061	*Bdl*	0,86	34,3	*Bdl*	DI-1
Output_1_53	L1	37,27	47.09	4,67	0,064	164,7	0,13	0,0015	1,01	114	0,0093	DI-1
Output_1_54	L1	37,37	35.13	10,14	0,926	631	0,064	*Bdl*	10,04	32,4	0,001	DI-1
Output_1_55	L1	37,41	59.1	3,17	1,138	751	0,136	*Bdl*	8,09	146,7	0,0062	DI-1
Output_1_56	L1	37,56	69.59	3,8	3,57	318,1	0,128	0,0023	13,71	85,5	0,0026	DI-1
Output_1_57	L1	37,58	54.8	2,54	3,36	226,3	0,114	*Bdl*	11,88	251,7	0,0094	DI-1
Output_1_58	L1	37,64	56.8	2,728	3,13	277,9	0,145	*Bdl*	17,91	331,4	0,0054	DI-4
Output_1_59	L1	37,73	91.1	0,588	0,381	39	0,053	0,0009	1,91	6,59	0,019	DI-4
Output_1_60	L1	38,66	3.3	0,527	0,498	33,3	0,054	0,0009	1,7	482	0,0033	DI-4
Output_1_61	L1	38,70	21.1	0,169	0,26	25,48	0,021	*Bdl*	3,9	404	0,03	DI-4
Output_1_62	L1	38,78	5.83	0,344	0,24	6,09	0,121	*Bdl*	2,65	165	0,146	DI-4
Output_1_63	L1	38,91	0.23	0,068	0,345	0,88	0,039	*Bdl*	4,05	99,5	0,0026	Grey shale
Output_1_64	L1	39,23	50.58	0,0308	0,024	97,4	0,11	*Bdl*	5,77	399,9	0,0045	DI-4

			Measured elements (ppm)									
Spot I.D	**Sample**	**Depth (m)**	**Mo**	**Ag**	**Cd**	**Sb**	**W**	**Ir**	**Hg**	**Pb**	**Bi**	**Bedrock**
Output_1_65	L1	39,60	68.69	2,862	0,05	187,5	0,113	*Bdl*	6,64	50,7	0,0018	DI-4
Output_1_66	L1	39,88	58.16	0,0357	0,068	143,4	0,125	0,0003	6,71	336,4	0,0001	DI-1
Output_1_67	L1	40,06	69.51	3,21	0,93	290,8	0,179	*Bdl*	4,23	141,6	0,0168	DI-1
Output_1_68	L1	40,40	63.5	5,25	0,81	21,69	0,062	0,0002	3,05	202,3	0,0189	DI-1
Output_1_69	L1	40,49	30.4	0,319	0,067	300,6	0,036	*Bdl*	3,6	14,6	0,0011	Limestone
Output_1_70	L1	40,71	1.295	0,171	0,177	6,02	0,091	*Bdl*	1,74	103,2	*Bdl*	DI-4
Output_1_71	L1	40,80	79.84	3,37	0,051	129,2	0,17	0,0017	9,34	26,5	*Bdl*	DI-4
Output_1_72	L1	40,87	48.3	3,6	1,84	164,8	0,124	*Bdl*	7,09	97,5	0,0152	DI-4
Output_1_73	L1	41,09	52.38	4,2	0,2	239,8	0,173	0,0053	13,8	11,06	*Bdl*	DI-4
Output_1_74	L1	41,13	61.5	1,34	0,043	37,68	0,14	0,0009	5,96	24,2	0,067	DI-4
Output_1_75	L1	41,20	28.23	6,17	0,055	3,82	0,066	0,0007	0,68	42,9	0,0114	DI-4
Output_1_76	L1	41,25	0.556	0,106	0,399	1,73	0,021	0,0027	2,81	49,3	0,0032	DI-4
Output_1_77	L1	41,34	52.66	5,88	0,203	401,2	0,196	*Bdl*	22,3	399	0,0235	DI-4
Output_1_78	L1	41,52	52.96	0,478	0,206	383,3	0,132	0,0003	10,93	228	*Bdl*	DI-4
Output_1_79	L1	41,57	66.7	0,112	0,225	155,9	0,103	*Bdl*	10,9	127,4	0,0113	DI-4
Output_1_80	L1	41,67	86.1	0,0481	0,126	99	0,068	0,0016	6,35	84,1	*Bdl*	DI-4
Output_1_81	L1	41,79	41.1	2,557	3,42	324,8	0,159	*Bdl*	11,27	57,6	0,0035	DI-4
Output_1_82	L1	42,68	47.12	4,63	1,95	170	0,142	0,001	22,7	53,5	0,0076	DI-4
Output_1_83	L1	42,71	49.6	3,05	0,139	52,6	0,05	0,001	2,64	54,3	0,0196	DI-4
Output_1_84	L1	42,98	46.03	3,51	0,056	329,7	0,08	0,0006	27,5	134,9	0,0135	DI-4
Output_1_85	L1	43,10	0.407	0,012	0,201	0,686	0,0014	0,0001	*Bdl*	17,67	0,0008	DI-4
Output_1_86	L1	43,15	33.51	2,86	0,133	73,6	0,062	*Bdl*	7,02	148,5	0,101	DI-4
Output_1_87	L1	43,24	52.49	3,71	0,069	104,2	0,099	0,0009	37,6	41,4	*Bdl*	DI-4
Output_1_88	L1	43,27	59.79	4,43	0,2	166,7	0,106	*Bdl*	39,1	84,9	0,0027	DI-4
Output_1_89	L1	43,31	51.95	0,0141	0,135	41,98	0,078	*Bdl*	20,6	289	0,001	DI-4
Output_1_90	L1	43,33	0.171	0,211	0,988	4,31	0,062	0,0025	5,54	72,4	0,0032	DI-4
Output_1_91	L1	43,82	49.17	1,163	0,15	160,9	0,064	0,0027	24,4	90,5	0,0041	DI-4
Output_1_92	L1	44,07	51.38	2,8	0,084	303,9	0,044	*Bdl*	36,1	149,2	*Bdl*	DI-4
Output_1_93	L1	44,14	89.6	2,242	0,041	28,71	0,039	*Bdl*	12,1	7,13	0,0507	DI-4
Output_1_94	L1	44,20	60.96	4,31	1,043	91,6	0,018	*Bdl*	12,9	22	0,0024	DI-4
Output_1_95	L1	44,50	2.17	0,163	0,136	4,13	0,0033	0,0007	2,39	77,5	0,0009	DI-1
Output_1_96	L1	44,57	51.3	1,543	0,042	168,6	0,063	*Bdl*	27,4	60,2	0,0001	Black shale
Output_1_97	L1	44,76	53.28	0,39	2,65	66,53	0,042	0,0007	17,2	137,5	0,0009	Black shale

			Measured elements (ppm)									
Spot I.D	**Sample**	**Depth (m)**	**Mo**	**Ag**	**Cd**	**Sb**	**W**	**Ir**	**Hg**	**Pb**	**Bi**	**Bedrock**
Output_1_98	L1	44,83	40.35	2,75	0,057	49,41	0,024	0,0032	37,6	76,2	*Bdl*	Black shale
Output_1_99	L1	45,06	39.36	1,903	0,833	8,84	0,039	*Bdl*	2,9	46,3	0,0111	Black shale
Output_1_100	L1	45,14	28.07	4,26	0,508	34,06	0,024	*Bdl*	37,5	9,77	0,0193	Black shale
Output_1_101	L1	45,43	20.19	0,548	0,438	114,2	*Bdl*	*Bdl*	17,3	17,66	0,0022	DI-3
Output_1_102	L1	45,53	169.1	0,0027	0,46	100,5	0,042	*Bdl*	40,7	370,7	*Bdl*	DI-3
Output_1_103	L1	45,63	51.47	0,348	0,069	0,923	0,239	0,0004	14,7	0,0105	*Bdl*	DI-4
Output_1_104	L1	45,78	225	0,421	*Bdl*	23,65	0,0149	*Bdl*	4,7	0,154	0,0004	DI-4
Output_1_105	L1	46,00	336	2,447	0,027	10,12	0,023	*Bdl*	10,3	21,7	*Bdl*	DI-4
Output_1_106	L1	46,10	55	0,0149	0,668	255	0,0087	*Bdl*	24,3	20,7	0,0006	Black shale
Output_1_107	L1	46,13	173.7	1,209	0,331	38,7	0,009	*Bdl*	9,7	11,68	*Bdl*	Black shale
Output_1_108	L1	46,29	154.2	0,092	0,789	95,3	0,034	*Bdl*	60,8	62,7	*Bdl*	Black shale
Output_1_109	L1	46,38	371.3	3,66	0,035	69,9	*Bdl*	*Bdl*	9,7	9,15	0,0033	Black shale
Output_1_110	L1	46,53	118.4	33,8	0,129	48,7	0,0011	*Bdl*	32,6	8,9	0,0057	Black shale
Output_1_111	L1	46,65	18.4	26	0,105	6,01	*Bdl*	*Bdl*	75	18,98	0,0162	DI-4
Output_1_112	L1	46,93	173.1	3,48	0,426	75,6	0,029	0,0029	7,3	19,1	0,0039	DI-4
Output_1_113	L1	47,00	134.9	1,595	0,132	13,41	0,0021	0,0018	4,7	19,75	*Bdl*	DI-4
Output_1_114	L1	47,15	732	8,89	0,209	51,2	0,011	0,0008	43,2	10,66	0,015	Black shale
Output_1_115	L1	47,25	660	6,86	0,083	13,07	0,0069	0,0004	13,7	30,3	0,0075	Black shale
Output_1_116	L1	47,36	165.3	0,0079	0,031	735	0,0051	*Bdl*	12,8	0,062	*Bdl*	DI-4
Output_1_117	L1	47,43	85.7	23,18	0,636	69,6	*Bdl*	*Bdl*	44,2	66,3	0,0153	DI-4
Output_1_118	L1	47,51	384	9,86	3,22	46,9	0,0015	*Bdl*	30,7	15,9	0,0047	DI-4
Output_1_119	L1	47,57	505	10,41	0,133	16,43	0,0045	*Bdl*	6,4	28,8	2,7	Grey shale
Output_1_120	L1	47,66	88.6	5,78	0,054	27,09	0,0056	*Bdl*	4,6	1,03	0,0291	Grey shale Grey
Output_1_121	L1	47,79	281.8	356	1,555	41,5	0,0008	*Bdl*	319	19,81	0,0139	shale
Output_1_122	L1	47,87	107.4	0,0158	1,18	708	0,017	0,0005	36,1	43	0,0023	DI-1
Output_1_123	L1	48,02	247.2	37,09	0,107	36,09	0,0009	0,0009	50,4	13,05	0,0312	DI-1
Output_1_124	L1	48,19	387.2	0,0516	0,319	135,1	0,0245	0,0012	39,1	30,09	0,0001	Black shale
Output_1_125	L1	48,61	274	2,255	0,265	35,1	*Bdl*	0,0002	25,8	22,6	0,0033	DI-4
Output_1_126	L1	48,80	0.338	0,118	0,529	9,84	0,032	0,0007	4,9	3,42	*Bdl*	Black shale
Output_1_127	L1	48,93	455.6	5,04	0,142	44,39	0,053	0,0008	17,8	75,9	0,0039	Black shale
Output_1_128	L1	49,02	896	1,67	0,049	150,7	0,0077	*Bdl*	3,8	4,66	0,0186	Black shale
Output_1_129	L1	49,32	480.1	0,0057	0,2	279	0,028	*Bdl*	38	8,24	0,0003	DI-4
Output_1_130	L1	49,50	307.2	0,0216	0,324	705,7	0,0111	*Bdl*	49,4	68,9	*Bdl*	DI-4

			Measured elements (ppm)									
Spot I.D	**Sample**	**Depth (m)**	**Mo**	**Ag**	**Cd**	**Sb**	**W**	**Ir**	**Hg**	**Pb**	**Bi**	**Bedrock**
Output_1_131	L1	49,58	143.8	5,26	0,327	31,68	0,124	*Bdl*	7,6	62,7	0,0071	DI-4
Output_1_132	L1	49,64	321.1	90,4	0,18	50,46	*Bdl*	*Bdl*	32,2	30,96	0,0144	DI-4
Output_1_133	L1	50,23	1299	154,9	0,412	104,4	*Bdl*	*Bdl*	162,8	58,8	0,0442	Black shale
Output_1_134	L1	50,60	211.9	0,026	0,181	321,7	0,0116	0,0026	44,5	24,82	0,0055	Black shale
Output_1_135	L1	51,25	32.42	1,318	0,148	65,8	0,0021	*Bdl*	89	71	0,0082	DI-1
Output_1_136	L1	52,44	26.06	4,15	0,101	24,36	*Bdl*	*Bdl*	25,5	61,6	0,0139	Black shale
Output_1_137	L1	53,70	397	0,85	0,021	8,08	*Bdl*	0,0008	5,4	0,041	*Bdl*	DI-4
Output_1_138	L1	54,98	220	0,565	0,044	1,9	0,0043	*Bdl*	3	4	0,0001	DI-4
Output_1_139	L1	55,74	72.2	0,196	0,006	1,08	*Bdl*	0,0003	3,7	2,15	0,0004	DI-4
Output_1_140	L1	56,63	207.9	0,487	0,018	13,35	0,0032	*Bdl*	18,1	2,49	0,041	DI-4
Output_1_141	L1	57,50	31.19	0,0144	0,021	22,42	0,0173	0,001	7,1	0,252	*Bdl*	Green shale
Output_1_142	L1	58,50	91.4	1,351	0,06	24,51	0,031	*Bdl*	35,9	100,4	0,0048	Green shale
Output_1_143	L1	59.44	145.3	0,733	0,039	17,01	0,0035	0,0004	27,9	0,404	0,001	Green shale
Output_1_144	L1	60.01	111.3	0,869	0,058	6,6	*Bdl*	*Bdl*	27,4	10,77	0,0169	DI-4
Output_1_35	L2	60.15	310.8	1,023	0,0308	16,04	*Nd*	*Nd*	3,7	6,81	*Nd*	DI-4
Output_1_145	L1	60.94	86.29	4,18	0,036	18,44	0,0035	*Bdl*	19,5	4,61	0,0042	DI-4
Output_1_36	L2	61.35	0.237	0,318	0,0144	0,346	*Nd*	*Nd*	*Bdl*	33,24	*Nd*	DI-4
Output_1_146	L1	61.84	0.049	0,0166	0,003	0,0432	0,0071	*Bdl*	1,5	0,404	0,0019	Green shale
Output_1_37	L2	62.04	99.5	12,7	0,0119	4,94	*Nd*	*Nd*	3,85	8,84	*Nd*	Green shale
Output_1_147	L1	62.57	3.53	0,0191	*Bdl*	0,168	0,0024	*Bdl*	*Bdl*	0,111	0,0001	Green shale
Output_1_148	L1	64.84	0.105	0,113	0,027	2,006	0,062	*Bdl*	12,7	17,26	0,0012	DI-2
Output_1_149	L1	65.80	74.3	*Bdl*	0,067	45,83	0,0046	*Bdl*	9,1	10,78	*Bdl*	Green shale
Output_1_150	L1	66.35	5.53	0,024	0,027	2,15	0,0014	0,0006	2,8	20,8	0,0049	DI-4
Output_1_151	L1	67.42	0.08	0,323	*Bdl*	0,522	*Bdl*	0,0007	9,4	12	*Bdl*	DI-4
Output_1_152	L1	68.05	285	1,846	0,009	4,7	*Bdl*	0,0004	7,1	6,65	0,0012	Black shale
Output_1_153	L1	69.40	5.48	0,128	0,144	30,9	0,0086	*Bdl*	7	287	0,0012	Black shale
Output_1_154	L1	70.37	321.9	0,0049	0,028	52,47	0,0065	*Bdl*	58,1	71,37	0,0027	Dark green shale
Output_1_155	L1	71.55	256.5	11,91	0,111	5,11	0,0077	*Bdl*	32,5	81	0,0052	Black shale
Output_1_38	L2	71.86	182.4	48,9	0,114	7,3	*Nd*	*Nd*	4,41	59,4	*Nd*	DI-4
Output_1_156	L1	72.68	47	0,96	0,032	1,46	*Bdl*	0,001	5,2	7,72	0,006	DI-4
Output_1_157	L1	73.71	26.6	*Bdl*	*Bdl*	8,54	0,0027	0,0001	16,1	30,69	*Bdl*	DI-4
Output_1_39	L2	74.16	4.34	18,5	0,0416	6,04	*Nd*	*Nd*	1,75	43	*Nd*	Black shale
Output_1_158	L1	74.94	119.7	2,07	0,081	7,33	0,0062	*Bdl*	7,7	28,77	0,0218	Black shale

Spot I.D	Sample	Depth (m)	Measured elements (ppm)									Bedrock
			Mo	Ag	Cd	Sb	W	Ir	Hg	Pb	Bi	
Output_1_159	L1	76.14	200.1	1,251	0,09	16,01	0,0017	*Bdl*	13,6	3,91	0,0035	Black shale
Output_1_40	L2	76.50	1.242	0,0297	1,708	26,02	*Nd*	*Nd*	2,269	187	*Nd*	DI-2
Output_1_160	L1	77.76	75.8	0,075	0,001	5,99	*Bdl*	*Bdl*	7,5	40,05	0,0001	DI-4
Output_1_161	L1	79.00	122.6	0,0289	0,03	6,91	*Bdl*	*Bdl*	10,3	48,2	0,018	DI-4
Output_1_41	L2	79.68	60.7	0,955	0,0111	5,22	*Nd*	*Nd*	0,678	40,7	*Nd*	Black shale

Appendix E

Table E1: Compilation of data from LA-ICP-MS analysis for Fågelsång-3 drill core. Isotopes analyzed include ^{33}S, ^{51}V, ^{52}Cr, ^{55}Mn, ^{59}Co, ^{65}Cu, ^{69}Ga, ^{75}As, ^{82}Se, ^{98}Mo, ^{107}Ag, ^{114}Cd, ^{121}Sb, ^{202}Hg and ^{208}Pb. Note, all concentrations are based on above mentioned isotopes and re-calculated after relative natural abundance for all isotopes for that particular element. *Bdl* = below detection limit, refers to isotopes that are not present in sufficient concentrations to be detected by the instrument. *DI* = darkness index, the darker the shale the higher the number.

			Measured elements (ppm)								
Spot I.D	**Sample**	**Depth (m)**	**As**	**S**	**V**	**Cr**	**Mn**	**Co**	**Cu**	**Ga**	**Bedrock**
Output_1_1	F1	6.57	1135	380000	5.04	1.77	0.06	72	62	8.18	DI-4
Output_1_2	F1	8.74	28	385000	0.335	1.11	55.5	14.72	*Bdl*	0.209	DI-3
Output_1_3	F1	10.28	25.61	385000	0.8	1.24	15.63	7.76	*Bdl*	0.134	DI-4
Output_1_4	F1	11.74	89.9	388000	2.808	1.64	50.89	5.13	9	0.48	DI-4
Output_1_5	F1	12.54	2.99	393000	0.29	1.53	0.419	5.27	*Bdl*	4.85	DI-4
Output_1_42	F2	15.33	14.44	387000	9.43	1.85	1280	12.5	124	1.749	Black shale
Output_1_6	F1	15.54	43.1	397000	6.78	1.35	228.7	6.2	50	2.76	Black shale
Output_1_7	F1	17.76	3.46	407000	0.341	1.39	1.954	0.849	*Bdl*	3.767	Black shale
Output_1_8	F1	21.20	535	411000	0.397	1.31	0.33	2.039	*Bdl*	2.732	Black shale
Output_1_9	F1	24.09	7	393000	0.263	1.32	284	1.318	87	1.371	Black shale
Output_1_10	F1	25.88	241	388000	0.0899	0.95	2	1.494	*Bdl*	0.787	Black shale
Output_1_11	F1	27.76	1.422	394000	0.322	1.19	223.5	0.282	*Bdl*	0.731	Black shale
Output_1_12	F1	31.11	384.8	386000	1.269	1.29	13.1	0.275	8.1	1.587	Black shale
Output_1_43	F2	34.52	93.8	390000	2.17	1.27	75.4	1.965	*Bdl*	0.565	Black shale
Output_1_13	F1	36.45	331.2	383000	0.066	0.82	*Bdl*	0.956	*Bdl*	0.0211	Black shale
Output_1_14	F1	37.00	474	405000	16.29	8.67	34.3	8.64	52	6.05	Black shale
Output_1_15	F1	38.31	1047	414000	21.62	13.4	14.5	24.17	130	6.9	DI-4
Output_1_16	F1	39.14	494	387000	1.415	1.82	1.45	1.02	*Bdl*	0.577	Black shale
Output_1_44	F2	42.30	629	396000	0.354	2.39	1180	4.19	21	0.174	Black shale
Output_1_17	F1	42.98	160.1	369000	0.454	1.62	33.5	59.7	62	0.294	Black shale
Output_1_18	F1	43.26	232.2	371000	0.28	1.44	4.03	17.12	27	0.0472	DI-4
Output_1_19	F1	43.36	54.3	365000	0.0529	1.11	80	0.232	157	0.0102	DI-4
Output_1_20	F1	44.05	50.4	371000	0.0446	1.16	74.7	0.27	194	0.0188	Black shale
Output_1_21	F1	44.23	405	372000	0.238	1.47	1646	5.86	*Bdl*	0.114	Black shale

			Measured elements (ppm)								
Spot I.D	**Sample**	**Depth (m)**	**As**	**S**	**V**	**Cr**	**Mn**	**Co**	**Cu**	**Ga**	**Bedrock**
Output_1_22	F1	44.68	81.7	388000	0.0525	0.86	294.4	6.44	184	0.028	Black shale
Output_1_23	F1	44.82	137	391000	0.046	1.55	124.2	0.331	179	0.0145	Black shale
Output_1_24	F1	44.90	5	403000	0.765	2.02	1180	40.8	46	1.466	Black shale
Output_1_45	F2	44.96	247.8	388000	0.322	2.05	38.5	35.28	193	0.154	Black shale
Output_1_25	F1	45.73	6.19	393000	0.241	1.23	1810	26	60	5.96	Black shale
Output_1_26	F1	45.92	3.33	389000	0.092	1.06	601	2.54	*Bdl*	1.121	Black shale
Output_1_27	F1	45.99	97.5	390000	0.0168	0.99	813	2.61	46	2.03	Black shale
Output_1_28	F1	45.99	2.101	381000	0.0658	0.91	57.2	32.1	65	0.512	Black shale
Output_1_29	F1	51.27	2.61	410000	0.0064	1.08	102.7	8.29	124	0.432	Limestone
Output_1_30	F1	58.95	2295	390000	0.0682	1.84	2.91	19.57	10.6	0.037	Black shale
Output_1_46	F2	58.95	0.236	477000	0.147	1.05	16	0.32	*Bdl*	0.2	Black shale
Output_1_31	F1	60.03	278.7	388000	0.0359	1.42	2.93	0.1336	74	0.0261	Black shale
Output_1_32	F1	61.78	480	396000	0.0899	1.36	24.63	3.42	82	0.0309	Black shale
Output_1_33	F1	62.89	0.076	406000	0.1228	0.62	211	0.0975	*Bdl*	0.0669	Black shale
Output_1_34	F1	64.56	320	388000	0.0446	0.47	152.6	0.066	13	0.0209	Black shale

(Cont. Appendix E)

Spot I.D	Sample	Depth (m)	Measured elements (ppm)							Bedrock
			Se	Mo	Ag	Cd	Sb	Hg	Pb	
Output_1_1	F1	6.57	24,05	586	0,1265	0,0424	18,04	0,529	37	DI-4
Output_1_2	F1	8.74	10,65	19,98	0,322	0,0081	1,102	0,239	5,71	DI-3
Output_1_3	F1	10.28	7,03	7,36	0,138	0,0081	0,455	0,18	3,55	DI-4
Output_1_4	F1	11.74	36,5	22,08	0,262	0,0273	5,14	0,545	13,44	DI-4
Output_1_5	F1	12.54	2,38	18,82	*Bdl*	0,014	0,0384	0,174	4,49	DI-4
Output_1_42	F2	15.33	18,44	2,838	0,289	0,0657	0,864	0,72	18,95	Black shale
Output_1_6	F1	15.54	23,9	6,31	0,149	0,2	2,811	0,448	12,61	Black shale
Output_1_7	F1	17.76	4,42	31,7	0,0004	0,003	0,0461	0,196	1,92	Black shale
Output_1_8	F1	21.20	5,12	823	*Bdl*	0,206	10,48	0,786	2,632	Black shale
Output_1_9	F1	24.09	38,1	23,4	0,0019	0,169	0,371	0,447	2,2	Black shale
Output_1_10	F1	25.88	2,58	828	0,0021	0,2	7,44	0,762	0,561	Black shale
Output_1_11	F1	27.76	3,48	0,863	0,0052	0,0239	0,0187	0,155	0,0498	Black shale
Output_1_12	F1	31.11	0,94	868	0,0112	0,323	5,2	0,884	2,089	Black shale
Output_1_43	F2	34.52	3,62	1,226	0,0093	0,343	5,95	0,009	57,8	Black shale
Output_1_13	F1	36.45	0,56	3,71	0,007	0,0312	17,57	0,282	74,6	Black shale
Output_1_14	F1	37.00	5,43	13,08	0,191	0,189	37,8	0,912	251,3	Black shale
Output_1_15	F1	38.31	18,83	19,66	0,269	0,398	83,5	1,808	667	DI-4
Output_1_16	F1	39.14	0,33	7,73	0,0088	0,0487	14,94	0,364	88,3	Black shale
Output_1_44	F2	42.30	22,92	119,9	0,212	0,0324	26,7	0,934	13,85	Black shale
Output_1_17	F1	42.98	1,79	61,7	0,0453	0,021	19,61	0,235	50,7	Black shale
Output_1_18	F1	43.26	0,21	29,68	0,1037	0,0354	67,7	0,289	7,84	DI-4
Output_1_19	F1	43.36	0,18	25,69	0,471	*Bdl*	1,953	0,116	0,45	DI-4
Output_1_20	F1	44.05	*Bdl*	24,81	0,1774	0,004	1,947	0,121	0,018	Black shale
Output_1_21	F1	44.23	39,8	110,8	0,285	0,0439	20	0,428	11,74	Black shale
Output_1_22	F1	44.68	1,2	37,9	0,207	0,0088	2,847	*Bdl*	0,465	Black shale
Output_1_23	F1	44.82	0,02	139	0,151	0,0058	0,395	0,059	0,892	Black shale
Output_1_24	F1	44.90	2,6	27,3	0,29	0,0461	1,37	0,339	20,2	Black shale
Output_1_45	F2	44.96	2,54	47,83	1,234	0,0091	52,38	0,434	2,64	Black shale
Output_1_25	F1	45.73	9,33	3,8	0,246	0,0176	0,989	0,187	23	Black shale
Output_1_26	F1	45.92	1,51	3,45	0,0547	0,0088	0,331	0,196	2,26	Black shale
Output_1_27	F1	45.99	7,85	19,2	0,381	0,002	2,691	0,176	5,08	Black shale

			Measured elements (ppm)							
Spot I.D	**Sample**	**Depth (m)**	**Se**	**Mo**	**Ag**	**Cd**	**Sb**	**Hg**	**Pb**	**Bedrock**
Output_1_28	F1	45.99	0,02	23,69	0,905	0,0004	0,195	0,175	3,17	Black shale
Output_1_29	F1	51.27	1,05	10,53	0,06	0,0049	0,866	*Bdl*	3,53	Limestone
Output_1_30	F1	58.95	0,42	10,61	0,573	0,275	176,8	0,218	9,4	Black shale
Output_1_46	F2	58.95	5,96	0,141	0,0113	0,0034	0,058	0,042	1,2	Black shale
Output_1_31	F1	60.03	0,28	13,18	0,0685	0,0008	21,24	0,116	0,0246	Black shale
Output_1_32	F1	61.78	0,46	58,5	0,364	0,0285	16,59	0,254	3,66	Black shale
Output_1_33	F1	62.89	3,9	0,1379	0,0005	0,007	0,006	0,229	0,1971	Black shale
Output_1_34	F1	64.56	0,02	88,9	0,0403	0,0081	0,247	0,097	0,827	Black shale

Tidigare skrifter i serien ”Examensarbeten i Geologi vid Lunds universitet”:

473. Jansson, Robin, 2016: Är ERT och Tidsdomän IP potentiella karteringsverktyg inom miljögeologi? (15 hp)
474. Heger, Katja, 2016: Makrofossilanalys av sediment från det tidig-holocena undervattenslandskapet vid Haväng, östra Skåne. (15 hp)
475. Swierz, Pia, 2016: Utvärdering av vattenkemisk data från Borgholm kommun och dess relation till geologiska förhållanden och markanvändning. (15 hp)
476. Mårdh, Joakim, 2016: WalkTEM-undersökning vid Revingehed provpumpningsanläggning. (15 hp)
477. Rydberg, Elaine, 2016: Gummigranulat - En litteraturstudie över miljö- och hälsopåverkan vid användandet av gummigranulat. (15 hp)
478. Björnfors, Mark, 2016: Kusterosion och äldre kustdyners morfologi i Skälderviken. (15 hp)
479. Ringholm, Martin, 2016: Klimatutlöst matbrist i tidiga medeltida Europa, en jämförande studie mellan historiska dokument och paleoklimatarkiv. (15 hp)
480. Teilmann, Kim, 2016: Paleomagnetic dating of a mysterious lake record from the Kerguelen archipelago by matching to paleomagnetic field models. (15 hp)
481. Schönström, Jonas, 2016: Resistivitets- och markradarmätning i Ängelholmsområdet - undersökning av korrosiva markstrukturer kring vattenledningar. (15 hp)
482. Martell, Josefin, 2016: A study of shock-metamorphic features in zircon from the Siljan impact structure, Sweden. (15 hp)
483. Rosvall, Markus, 2016: Spår av himlakroppskollisioner - bergarter i nedslagskratrar med fokus på Mien, Småland. (15 hp)
484. Olausson, My, 2016: Resistivitets- och IP -mätningar på den nedlagda deponin Gustavsfält i Halmstad. (30 hp)
485. Plan, Anders, 2016: Markradar- och resistivitetsmätningar – undersökningar utav korrosionsförhöjande markegenskaper kring fjärrvärmeledningar i Ängelholm. (15 hp)
486. Jennerheim, Jessica, 2016: Evaluation of methods to characterise the geochemistry of limestone and its fracturing in connection to heating. (45 hp)
487. Olsson, Pontus, 2016: Ekologiskt vatten från Lilla Klåveröd: en riskinventering för skydd av grundvatten. (15 hp)
488. Henriksson, Oskar, 2016: The Dynamics of Beryllium 10 transport and deposition in lake sediments. (15 hp)
489. Brådenmark, Niklas, 2016: Lower to Middle Ordovician carbonate sedimentology and stratigraphy of the Pakri peninsula, north-western Estonia. (45 hp)
490. Karlsson, Michelle, 2016: Utvärdering av metoderna DCIP och CSIA för identifiering av nedbrytningszoner för klorerade lösningsmedel: En studie av Färgaren 3 i Kristianstad. (45 hp)
491. Elali, Mohammed, 2016: Flygsanddyners inre uppbyggnad – georadarundersökning. (15 hp)
492. Preis-Bergdahl, Daniel, 2016: Evaluation of DC Resistivity and Time-Domain IP Tomography for Bedrock Characterisation at Önneslöv, Southern Sweden. (45 hp)
493. Kristensson, Johan, 2016: Formation evaluation of the Jurassic Stø and Nordmela formations in exploration well 7220/8-1, Barents Sea, Norway. (45 hp)
494. Larsson, Måns, 2016: TEM investigation on Challapampa aquifer, Oruro Bolivia. (45 hp)
495. Nylén, Fredrik, 2017: Utvärdering av borrhålskartering avseende kalksten för industriella ändamål, File Hajdarbrottet, Slite, Gotland. (45 hp)
496. Mårdh, Joakim, 2017: A geophysical survey (TEM; ERT) of the Punata alluvial fan, Bolivia. (45 hp)
497. Skoglund, Wiktor, 2017: Provenansstudie av detriala zirkoner från ett guldförande alluvium vid Ravlunda skjutfält, Skåne. (15 hp)
498. Bergcrantz, Jacob, 2017: Ett fönster till Kattegatts förflutna genom analys av bottenlevande foraminiferer. (15 hp)
499. O'Hare, Paschal, 2017: Multiradionuclide evidence for an extreme solar proton event around 2610 BP. (45 hp)
500. Goodship, Alastair, 2017: Dynamics of a retreating ice sheet: A LiDAR study in Värmland, SW Sweden. (45 hp)
501. Lindvall, Alma, 2017: Hur snabbt påverkas och nollställs luminiscenssignaler under naturliga ljusförhållanden? (15 hp)
502. Sköld, Carl, 2017: Analys av stabila isotoper med beräkning av blandningsförhållande i ett grundvattenmagasin i Älvkarleby-Skutskär. (15 hp)
503. Sällström, Oskar, 2017: Tolkning av geofysiska mätningar i hammarborrhål på södra Gotland. (15 hp)
504. Ahrenstedt, Viktor, 2017: Depositional history of the Neoproterozoic Visingsö Group, south-central Sweden. (15 hp)
505. Schou, Dagmar Juul, 2017: Geometry and faulting history of the Long Spur fault

zone, Castle Hill Basin, New Zealand. (15 hp)

506. Andersson, Setina, 2017: Skalbärande marina organismer och petrografi av tidigcampanska sediment i Kristianstadsbassängen – implikationer på paleomiljö. (15 hp)
507. Kempengren, Henrik, 2017: Föroreningsspridning från kustnära deponi: Applicering av Landsim 2.5 för modellering av lakvattentransport till Östersjön. (15 hp)
508. Ekborg, Charlotte, 2017: En studie på samband mellan jordmekaniska egenskaper och hydrodynamiska processer när erosion påverkar släntstabiliteten vid ökad nederbörd. (15 hp)
509. Silvén, Björn, 2017: LiDARstudie av glaciala landformer sydväst om Söderåsen, Skåne, Sverige. (15 hp)
510. Rönning, Lydia, 2017: Ceratopsida dinosauriers migrationsmönster under krittiden baserat på paleobiogeografi och fylogeni. (15 hp)
511. Engleson, Kristina, 2017: Miljökonsekvensbeskrivning Revinge brunnsfält. (15 hp)
512. Ingered, Mimmi, 2017: U-Pb datering av zirkon från migmatitisk gnejs i Delsjöområdet, Idefjordenterrängen. (15 hp)
513. Kervall, Hanna, 2017: EGS - framtidens geotermiska system. (15 hp)
514. Walheim, Karin, 2017: Kvartsmineralogins betydelse för en lyckad luminiscensdatering. (15 hp)
515. Aldenius, Erik, 2017: Lunds Geotermisystem, en utvärdering av 30 års drift. (15 hp)
516. Aulin, Linda, 2017: Constraining the duration of eruptions of the Rangitoto volcano, New Zealand, using paleomagnetism. (15 hp)
517. Hydén, Christina Engberg, 2017: Drumlinerna i Löberöd - Spår efter flera isrörelseriktningar i mellersta Skåne. (15 hp)
518. Svantesson, Fredrik, 2017: Metodik för kartläggning och klassificering av erosion och släntstabilitet i vattendrag. (45 hp)
519. Stjern, Rebecka, 2017: Hur påverkas luminiscenssignaler från kvarts under laboratorieförhållanden? (15 hp)
520. Karlstedt, Filippa, 2017: P-T estimation of the metamorphism of gabbro to garnet amphibolite at Herrestad, Eastern Segment of the Sveconorwegian orogen. (45 hp)
521. Önnervik, Oscar, 2017: Ooider som naturliga arkiv för förändringar i havens geokemi och jordens klimat. (15 hp)
522. Nilsson, Hanna, 2017: Kartläggning av sand och naturgrus med hjälp av resistivitetsmätning på Själland, Danmark. (15 hp)
523. Christensson, Lisa, 2017: Geofysisk undersökning av grundvattenskydd för planerad reservvattentäkt i Mjölkalånga, Hässleholms kommun. (15 hp)
524. Stamsnijder, Joaen, 2017: New geochronological constraints on the Klipriviersberg Group: defining a new Neoarchean large igneous province on the Kaapvaal Craton, South Africa. (45 hp)
525. Becker Jensen, Amanda, 2017: Den eocena Furformationen i Danmark: exceptionella bevaringstillstånd har bidragit till att djurs mjukdelar fossiliserats.(15 hp)
526. Radomski, Jan, 2018: Carbonate sedimentology and carbon isotope stratigraphy of the Tallbacken-1 core, early Wenlock Slite Group, Gotland, Sweden. (45 hp)
527. Pettersson, Johan, 2018: Ultrastructure and biomolecular composition of sea turtle epidermal remains from the Campanian (Upper Cretaceous) North Sulphur River of Texas. (45 hp)
528. Jansson, Robin, 2018: Multidisciplinary perspective on a natural attenuation zone in a PCE contaminated aquifer. (45 hp)
529. Larsson, Alfred, 2018: Rb-Sr sphalerite data and implications for the source and timing of Pb-Zn deposits at the Caledonian margin in Sweden. (45 hp)
530. Balija, Fisnik, 2018: Stratigraphy and pyrite geochemistry of the Lower–Upper Ordovician in the Lerhamn and Fågelsång -3 drill cores, Scania, Sweden. (45 hp)

LUNDS UNIVERSITET

Geologiska institutionen
Lunds universitet
Sölvegatan 12, 223 62 Lund